Modeling the development of tissue engineered cartilage

Document Version:
Publisher's PDF, also known as Version of Record (includes final page, issue and volume numbers)

Please check the document version of this publication:

• A submitted manuscript is the version of the article upon submission and before peer-review. There can be important differences between the submitted version and the official published version of record. People interested in the research are advised to contact the author for the final version of the publication, or visit the DOI to the publisher's website.
• The final author version and the galley proof are versions of the publication after peer review.
• The final published version features the final layout of the paper including the volume, issue and page numbers.
[Link to publication](#)

Modeling the development of tissue engineered cartilage

Modeling the development of tissue engineered cartilage

Proofschrift

ter verkrijging van de graad van doctor aan de
Technische Universiteit Eindhoven, op gezag van de
Rector Magnificus, prof.dr.ir. C.J. van Duijn, voor een
commissie aangewezen door het College voor
Promoties in het openbaar te verdedigen op
dinsdag 17 mei 2005 om 16.00 uur

door

Bram Gijsbert Sengers

geboren te Eindhoven

Dit proefschrift is goedgekeurd door de promotoren:

prof.dr.ir. F.P.T. Baaijens
en
prof.dr. D.L. Bader

Copromotor:
dr.ir. C.W.J. Oomens

Contents

Summary

The limited healing capacity of articular cartilage forms a major clinical problem. In general, current treatments of cartilage damage temporarily reliefs symptoms, but fail in the long term. Tissue engineering (TE) has been proposed as a more permanent repair strategy. Cartilage TE aims at cultivating suitable implant material for cartilage repair. This has to be achieved by providing a favorable environment for cartilage regeneration *in vitro* (Chapter 1).

The following phases can be distinguished: First, cells are isolated from the patient and expanded in culture to obtain sufficient numbers. Then the cells are seeded in a scaffold, i.e. a biodegradable three-dimensional structure that provides support for the cells. Subsequently, during culture in a bioreactor, the cells are conditioned to synthesize extracellular matrix components, resulting in neo-cartilage formation. Eventually, the newly formed cartilage construct has to acquire adequate mechanical properties, in order to be reimplanted into the patient.

However, in general the mechanical properties of TE cartilage do not meet these functional requirements. In addition there is a definite lack of control over the functional development of tissue engineered cartilage. Current research is mainly characterized by a strong experimental basis. The use of computational methods is relatively limited, while modeling can potentially provide an important contribution to the optimization of bioreactors and culture protocols. In addition, modeling can prove useful in the reduction of the number of experiments and the interpretation of the results.

In the present thesis, a computational approach is proposed that enables the modeling of the functional development of tissue engineered cartilage. The computational method is applied to establish relationships between mechanical stimulation of cartilage constructs by dynamic compression and transport of solutes, for example nutrients, within these constructs (Chapter 2). It is shown that compression-induced fluid flow can affect the transport of large solutes but not that of small solutes. This has implications for matrix synthesis.

A microstructural homogenization approach is used to determine how the synthesis of extracellular matrix at the cellular level, translates in the evolving mechanical properties of the newly formed cartilage as a whole (Chapter 3). The results indicate that the matrix distribution at the cellular level may be of less importance than its molecular organization.

With respect to the kinetics of cartilage formation, it is known that cellular energy

metabolism is closely associated with the synthesis of extracellular matrix. Therefore, using the model, the cellular uptake of glucose and oxygen and the production of lactate is characterized on the basis of experimental data (Chapter 4). It is shown that cellular uptake in the experiments was influenced by both the initial glucose concentration in the culture medium and the cell density in the construct.

Matrix synthesis and proliferation can be stimulated in an uncoupled manner, by applying different time intervals of dynamic compression. In order to interpret and predict cell behavior, models are developed for the temporal regulation of chondrocyte proliferation and biosynthesis, in response to varying dynamic compression regimens (Chapter 5). These models are able to provide a reasonable overall representation of experimental results for different loading regimens. However, for specific loading cases the predictive value is limited.

Subsequently, cellular uptake data is used to predict, numerically, the nutrient supply in different bioreactor setups and to evaluate the effect of mixing, perfusion and geometry (Chapter 6). The results indicate that transport limitations are not insurmountable, providing that the bioreactor environment is well homogenized and oxygenated.

It can be concluded that the proposed modeling approach can provide a valuable contribution in determining optimal culture conditions for cartilage tissue engineering (Chapter 7). At the present stage, additional identification and quantification of chondrocyte behavior is necessary, with respect to utilization, biosynthesis and mechanotransduction. In addition, criteria with respect to matrix synthesis have to be established.

Samenvatting

Gewrichtskraakbeen heeft slechts een beperkt vermogen om uit zichzelf te genezen. Behandeling van kraakbeenschade wordt hierdoor bemoeilijkt en is vaak niet succesvol op de lange termijn. Tissue engineering (TE) biedt mogelijk een meer permanente oplossing. Kraakbeen TE heeft als doel het kweken van geschikt implantatie materiaal voor kraakbeenreparatie. Dit moet worden bereikt door het bieden van gunstige voorwaarden voor kraakbeenregeneratie *in vitro* (Hoofdstuk 1).

De TE procedure bestaat uit een aantal stappen. Allereerst worden bij patiënten met kraakbeenschade cellen geïsoleerd. Deze cellen worden vervolgens opgekweekt om een voldoende aantal te verkrijgen en gezaaid in een scaffold, een driedimensionale poreuze structuur. Hierna worden de cellen in een bioreactor aangezet tot extracellulaire matrix productie, om zo nieuw kraakbeen te vormen. Dit moet uiteindelijk resulteren in een voldoende sterk geheel dat tenslotte in de patiënt kan worden geimplanteerd.

In het algemeen blijven de mechanische eigenschappen van "tissue engineered" kraakbeen echter nog achter bij de functionele eisen. Daarnaast is het ontwikkelingsproces dat moet leiden tot functionaliteit nog onvoldoende te sturen. TE onderzoek wordt gekenmerkt door een sterke experimentele basis. Modelvorming en het gebruik van numerieke methoden blijft hier in verhouding ver bij achter, terwijl deze technieken een belangrijke rol zouden kunnen spelen bij de optimalisatie van bioreactoren en kweekprotocollen. Ook kunnen modellen hun nut bewijzen in het terugbrengen van het aantal experimenten en het interpreteren van de resultaten.

In dit promotieonderzoek is een modelaanpak voorgesteld en uitgewerkt die het mogelijk maakt om de functionele ontwikkeling van TE kraakbeen te beschrijven. De methode is toegepast om de relaties vast te stellen tussen mechanische stimulatie van TE kraakbeen door middel van dynamische compressie en transport van opgeloste stoffen, bijvoorbeeld van voedingsstoffen, binnen dit kraakbeen (Hoofdstuk 2). De resultaten laten zien dat vloeistofstroming als gevolg van compressie wel het transport van grote opgeloste stoffen kan beinvloeden, maar niet dat van kleine. Dit heeft implicaties voor matrix aanmaak.

Met behulp van een microstructurele homogenisatie aanpak is bepaald hoe de extracellulaire matrix accumulatie op cel niveau zich vertaalt in de ontwikkeling van mechanische functionaliteit van het nieuwe kraakbeen als geheel (Hoofdstuk 3). De resultaten geven aan dat de moleculaire organisatie van het matrix materiaal belangrijker kan zijn dan de verdeling ervan op cel niveau.

Met betrekking tot kraakbeenvorming is bekend dat het energiemetabolisme van de cel nauw gerelateerd is aan de productie van extracellulaire matrix. Daarom is met behulp van de modelaanpak de opname van zuurstof en glucose en de productie van lactaat gekarakteriseerd op basis van experimentele gegevens (Hoofdstuk 4). Hieruit blijkt dat het opnamegedrag in de experimenten afhankelijk was van de initiële glucoseconcentratie in het kweekmedium en de celdichtheid in het TE kraakbeen.

Matrixproductie en celvermenigvuldiging kunnen onafhankelijk van elkaar gestimuleerd worden door het toepassen van verschillende intervallen van dynamische compressie. Om het celgedrag te voorspellen en interpreteren, zijn modellen ontwikkeld voor de regulatie van biosynthese en vermenigvuldiging door dynamische belasting in de tijd (Hoofdstuk 5). Deze modellen zijn in staat om een redelijke globale beschrijving te leveren van de experimentele resultaten voor de verschillende belastingsprotocollen. Voor specifieke belastingssituaties is de voorspellende waarde echter beperkt.

Gegevens over cellulaire consumptie zijn vervolgens gebruikt om met het model de voedingsstoffenvoorziening in verschillende bioreactor opstellingen te voorspellen en het effect van mixen, perfusie en de geometrie te evalueren (Hoofdstuk 6). De resultaten duiden er op dat transport beperkingen niet onoverkomelijk zijn, indien het medium in de bioreactor goed gehomogeniseerd wordt en van voldoende zuurstof is voorzien.

Geconcludeerd kan worden dat de voorgestelde modelaanpak een waardevolle bijdrage kan leveren aan het bepalen van optimale kweekomstandigheden voor kraakbeen tissue engineering (Hoofdstuk 7). In het huidige stadium is aanvullende identificatie en kwantificatie nodig van het gedrag van chondrocyten met betrekking tot verbruik, biosynthese en mechanotransductie. Ook moeten criteria voor matrixsynthese worden vastgesteld.

Chapter 1

Introduction

1.1   Problem definition

The high incidence of damage and disease of articular cartilage and its limited capacity to heal constitute a major clinical problem. During daily activities cartilage is subjected to severe dynamic loading conditions [66, 177]. Under these circumstances, healthy articular cartilage fulfils an essential role by distributing loads, dampening impact and providing lubrication to ensure smooth joint motion [75, 128]. Loss of articular cartilage, as in osteoarthritis, is therefore a disabling condition that can lead to joint pain, stiffness and reduced joint function. Articular cartilage damage can be the result of degenerative diseases, acute trauma or progressive wear [83]. Osteoarthritis affects an estimated 4% of the general population in the Netherlands (RIVM, Nationaal Kompas Volksgezondheid, Bilthoven, 2003). Predominantly the elderly are affected, but also 0.5% of the population between age 25-44. Current treatments of cartilage defects include chondral shaving, abrasion chondroplasty, subchondral drilling, microfracturing, allogeneic or autologous osteochondral transplantation and periosteum transplantation with or without injection of chondrocytes [83, 157, 179]. In general these procedures only temporarily relieve symptoms. Graft availability and survival is limited and the repair response induced by many techniques results in the formation of fibrocartilaginous tissue that is mechanically inferior to articular cartilage and degenerates in the long term. In addition, total joint replacement is not a suitable option for younger patients due to the limited lifespan of prostheses.

In order to obtain a more permanent repair and to overcome the inadequate healing capacity of cartilage under *in-vivo* conditions, a tissue engineering approach has been proposed, in which a favorable environment for cartilage regeneration can be provided *in-vitro* (Fig. 1.1) [22, 49, 96, 148]. Additionally, tissue engineering provides a well-controlled model system to study fundamental relationships in cartilage biology. The general procedure is that cells are harvested from the patient, expanded in culture and seeded in a three dimensional scaffold. Subsequently the cellular construct is cultured and conditioned in a bioreactor in order to promote new cartilage formation. Eventually, when a degree of functional properties have been attained, the autologous cartilage construct can be reimplanted into the patient to repair the cartilage defect. However, although promising results have been obtained, in general the mechanical properties of tissue engineered cartilage are presently insufficient for clinical applications [47, 118, 124]. In the next section a short literature review on current tissue engineering research will be given, followed by a section on the objectives of the present thesis.

1.2   Literature review

Every phase in the tissue engineering procedure (Fig. 1.1) is still subject to research and no definitive protocols have yet been established. Starting with the choice of cell source, availability and chondrogenic potential is important. For example, to date, primary chondrocytes have been most commonly used, although bone marrow stromal cells provide an alternative cell source [51]. The *in-vitro* cell expansion phase is associated with dedifferentiation, which can be influenced using scaffold
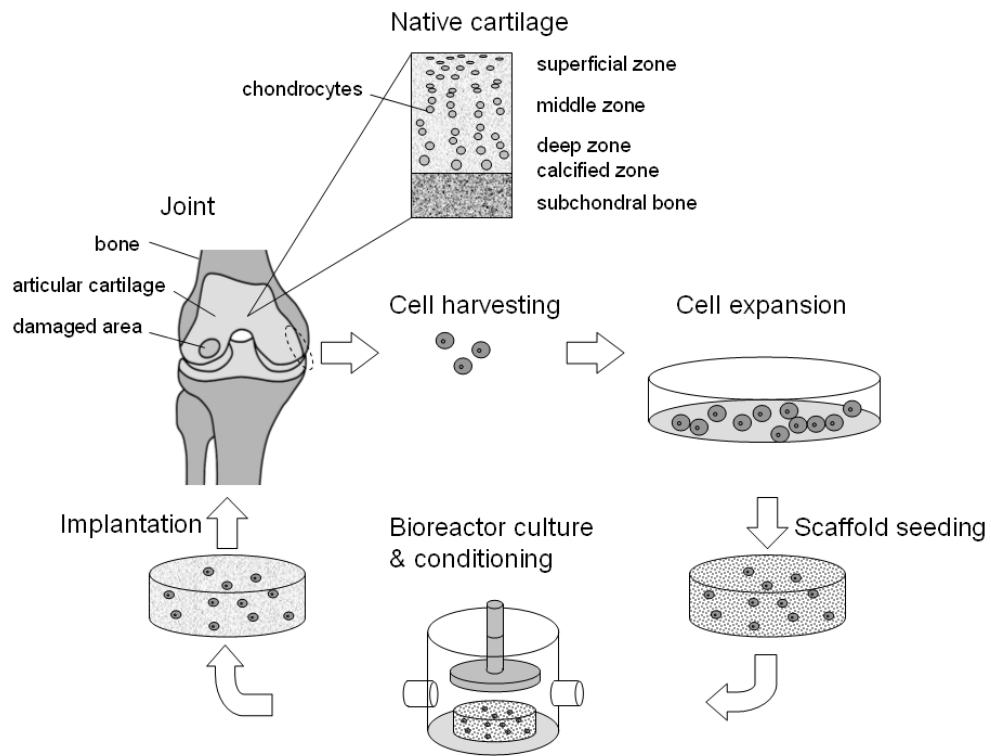
Figure 1.1: *The individual stages involved in developing tissue engineered implants intended for the repair of articular cartilage.*

materials and/or growth factors [11]. Critical parameters in scaffold design are the porosity, stiffness, cell attachment and biodegradability [84, 96]. Furthermore, depending on the scaffold, efficient cell seeding procedures are required [182]. For the bioreactor cultivation phase, different culture configurations have been employed, including static culture, perfusion bioreactors, mixed flasks and rotating bioreactors [38, 51]. It has been demonstrated that the bioreactor environment has a profound impact on tissue morphology and mechanical properties, associated with differences in mass transfer and hydrodynamic conditions [181]. Mechanical properties can be modulated by the biochemical composition of the culture medium, with respect to nutrient supply [125], but also for instance by using growth factors [138]. In addition, culture parameters like cell density and culture time need to be optimized [96]. Based on the sensitivity of mature cartilage to mechanical load [66, 72, 178], different mechanical stimulation protocols have been proposed to enhance matrix synthesis and mechanical functionality, incorporating dynamic compression [19, 82, 124], fluid shear stress [185] and hydrostatic pressure [26]. Furthermore, it has to be noted that the overall response to these stimuli will be influenced by the interaction between cell and scaffold material Finally, the difficulties encountered in the integration of implant and host tissue are an important issue [133, 157].

Relatively few computational studies have specifically addressed cartilage tissue engineering, despite widespread applications in related areas such as cartilage biomechanics and biochemical engineering. In recent years a number of studies have been published that can be roughly divided into two categories. The first category consists of elaborate finite element modeling of the physical environment in bioreactors, with little emphasis on cellular behavior. For example, computational fluid dynamics (CFD) models have been used to characterize the hydrodynamic environment in specific bioreactors, in order to determine the fluid shear stress on constructs [166, 185], as well as oxygen transport in the medium [185]. On a smaller scale, CFD models have been used to evaluate the local fluid shear stress on chondrocytes attached to fibers in a porous scaffold [145]. The second category comprises studies that focus on a more detailed exploration of cellular processes within constructs, using a relatively simple geometry. For instance, elaborate kinetic modeling of cell behavior has been used to study chondrocyte proliferation in scaffolds with relation to nutrient transport [56]. Oxygen diffusion and uptake were modeled to determine the oxygen utilization of chondrocytes in three-dimensional culture [111, 129]. A general model for scaffold degradation and matrix accumulation was shown to be capable of representing the evolving matrix content of cartilage constructs, for a large number of different experimental configurations [187]. Matrix deposition and synthesis based on oxygen availability were modeled to describe the inhomogeneous matrix distribution commonly found within engineered cartilage constructs [134].

It can be concluded that bioreactor cultivation offers a vast array of possibilities to enhance the functional properties of tissue engineered cartilage. Due to the large number of parameters, however, results are indeterminate beforehand and afterwards difficult to attribute to specific causes. Computational modeling can contribute to this process, but currently no models exist that are both generic enough for realistic,

clinical, bioreactor applications and incorporate a sufficient representation of cellular behavior.

1.3   Objectives

The focus of this thesis is on the bioreactor cultivation phase (Fig. 1.1). Current research is characterized by a strong empirical basis and there is a general lack of control over the functional development of tissue engineered constructs. Computational modeling can aid in a more structured approach. By attempting to establish quantitative relationships, experiments can be directed and reduced in number. In addition, modeling can contribute to the optimization of bioreactors and culture protocols. For this purpose, the eventual aim of computational modeling is to enable predictions on the functional development of tissue engineered cartilage, as a function of the physical and biochemical input parameters provided in the bioreactor environment. The following objectives were defined:

- The evolving nature and inherent coupling of solute transport, mechanics and cell behavior during bioreactor culture require an integrated approach. Therefore, the first objective was to establish a numerical framework that can describe the local spatial and temporal variations in solute concentrations within tissue-engineered constructs and the interrelated cell response. Specifically, the focus was on the interactions between mechanically induced fluid flow and the transport of bioactive solutes that can affect matrix synthesis.

- Although matrix accumulation is a prerequisite for mechanical functionality, there is no one-to-one relationship between composition and function. Possibly, this can be attributed to the microscopic matrix distribution. The second objective was therefore, to determine how the deposition of newly synthesized extracellular matrix at the cellular level translates into mechanical functionality of the construct as a whole.

- The kinetics of matrix synthesis are closely associated with chondrocyte energy metabolism. A quantified prediction of utilization is therefore important in optimizing culture conditions. Based on these considerations, the third objective was to characterize chondrocyte nutrient utilization under tissue engineering conditions. For this purpose, numerical modeling was employed in the analysis of experimental data, to account for spatial and temporal variations and to investigate metabolic relationships.

- Matrix synthesis and proliferation can be stimulated to a large extent independently, by applying different intervals of dynamic compression [33]. Therefore, potentially, mechanical loading protocols can be used to control tissue development. In order to interpret and predict cell behavior, the fourth objective was to establish a model for the temporal regulation of chondrocyte proliferation and biosynthesis, in response to varying dynamic compression protocols.

- Limitations in nutrient supply can lead to insufficient and inhomogeneous matrix deposition, in which the bioreactor configuration plays a crucial role. The fifth objective was therefore to determine under what conditions cellular utilization and restrictions in mass transfer can induce nutrient depletion, during bioreactor culture and to what extent transport can be enhanced by mixing and perfusion. Computational models developed for this purpose, may not only offer a large potential in bioreactor design and the optimization of culture protocols, but may also be employed in, possibly automated, bioreactor control applications.

In the following chapters, these objectives will be treated sequentially, concluding with the general discussion and future perspectives. The chapters were written in journal paper format and can be read independently. Chapter 7 summarizes the main results.

Chapter 2

An integrated finite element approach to mechanics, transport and biosynthesis in tissue engineering[1]

Abstract

A finite-element approach was formulated, aimed at enabling an integrated study of mechanical and biochemical factors that control the functional development of tissue engineered constructs. A nonlinear biphasic displacement-velocity-pressure description was combined with advective and diffusive solute transport, uptake and biosynthesis. To illustrate the approach we focused on the synthesis and transport of macromolecules under influence of fluid flow induced by cyclic compression. In order to produce net transport the effect of dispersion was investigated. An abstract representation of biosynthesis was employed, three cases were distinguished: Synthesis dependent on a limitedly available small solute, synthesis dependent on a limited large solute and synthesis independent of solute transport. Results show that a dispersion model can account for augmented solute transport by cyclic compression and indicate the different sensitivity to loading that can be expected depending on the size of the limiting solute.

7

2.1   Introduction

Tissue engineering aims at restoring tissue functionality by implanting neotissue obtained by in vitro cultivation of scaffolds seeded with autologous cells. In addition engineered tissue provides a well controlled experimental model for understanding in vivo processes [49, 51]. For some time the prospects of tissue engineered articular cartilage have attracted much attention. This interest is based on its large potential in clinical applications regarding the limited repair capacity of cartilage in-vivo, combined with its seemingly relatively simple structure, i.e. avascular and only one type of cell with low oxygen requirements [96, 148].

A rapidly increasing amount of experimental data is becoming available and results have been obtained that approximate some of the functional properties of natural articular cartilage [47, 118]. Despite these encouraging results there is still a long way to go before the process of engineering tissue to specific functional requirements can be controlled [22, 124]. Neotissue functionality can include factors like the ability of an implanted tissue engineered construct to adapt itself to the in-vivo conditions and integrate with the host tissue [49]. From a mechanical point of view tissue functionality is defined by parameters like permeability and stiffness, which can be related to tissue components such as glycosaminoglycan (GAG) and collagen II content. It has been shown that the bioreactor environment has a profound impact on the morphology, composition and mechanical properties of tissue engineered cartilage [181]. Freed and coworkers [49] have extensively investigated the effect of bioreactor systems with different hydrodynamic and mixing conditions, such as static flasks, mixed flasks with turbulent flow and rotating bioreactors with laminar flow. Static conditions resulted in fragile constructs with only peripheral matrix deposition. In constructs grown in mixed flasks more GAG is produced but also a larger amount is released into the culture medium [61]. Rotating vessels yielded a uniform cartilaginous matrix and superior mechanical properties. Mass transfer of biochemically functional solutes appears to be one of the main factors that determine the development of tissue engineered cartilage. This is also indicated by the fact that the averaged concentration of synthesized GAG, collagen and cells drops rapidly as the scaffold thickness increases [48, 52]. Oxygen uptake in the periphery may be one of the limiting factors since low oxygen levels associated with anaerobic cell metabolism have been found to suppress chondrogenesis [132]. The oxygen dependency of GAG synthesis rate has been demonstrated for dissected articular cartilage [103]. Also a significant drop in oxygen level has been observed for chondrocytes cultured in a hollow fiber bioreactor [44]. However high cell seeding concentrations favor chondrogenesis [182], despite the associated higher nutrient consumption rate. This could be partly related to cell-produced growth factors which have a large impact on chondrocyte matrix metabolism [60]. The use of supplemental growth factors and other regulatory factors has been shown to have a large impact on the growth of tissue engineered cartilage constructs, and potentially provides a valuable way of controlling the process of tissue formation: Insulin-like growth factor I (IGF-I), interleukin-4 and transforming growth factor-β1 increased construct wet weight by 1.5-2.9 fold [11]. Addition of IGF-I in combination with different mixing conditions

has been shown to produce engineered tissue superior to that obtained by each factor separately [59]. Also dynamic compression combined with supplemented IGF-I showed synergistic effects on protein and proteoglycan synthesis in explanted natural cartilage. IGF-I alone increased protein and proteoglycan synthesis by 90 % and 120 %, respectively. Dynamic compression by itself increased protein and proteoglycan synthesis 40 % and 90 %, respectively. Applied together protein and proteoglycan synthesis increased by 180 % and 290 %, respectively [13]. These results may be partially attributed to enhanced transport due to compression-induced convection. In natural cartilage this "pumping mechanism" will however only influence the transport of such large molecules and not that of low molecular weight solutes like glucose or oxygen. Due to the low permeability of natural cartilage the fluid velocities are so low that only transport of large molecules that have a very low diffusion rate is significantly affected by convection [17, 58, 65, 135]. Apart from such transport related effects, dynamic mechanical compression of natural cartilage gives rise to a complex interplay of various phenomena that are thought to stimulate chondrocyte biosynthesis, like fluid shear, streaming potentials, hydrostatic pressure, changes in the extracellular physiochemical environment and matrix mediated cellular deformation [19, 102, 178].

Mathematical modeling can provide a better understanding of the complex interplay between the array of factors that control the functional tissue development. Relatively few numerical modeling studies have addressed the bioreactor culture of cell seeded polymer constructs for tissue engineering. Diffusive oxygen transport and uptake in chondrocyte pellets has been described by Nehring [129]. Galban and Locke considered a system consisting of separate fluid and cell phases using a moving boundary approach to describe cell proliferation within a polymer scaffold [54]. They also developed a volume averaging approach accounting for diffusive transport and the effect of spatial variations of cells, nutrients and product concentrations on cell growth [55, 56]. These models gave a qualitative representation of cell growth trends when compared to experimental data, but could not provide a general quantitative fit. In the study by Obradovic [134] the deposition of GAG's throughout a scaffold was modeled based on computed oxygen profiles resulting from diffusion and uptake. The number of adjustable parameters was kept to a minimum by inserting detailed experimental data for cell concentrations and construct dimensions. Calculated GAG distribution profiles were in good quantitative agreement with experimental results, however at a lower oxygen concentration only qualitative resemblance was found. Outside the area of tissue engineering many modeling approaches can be found for related areas, such as for transport in tissues like natural cartilage [74], skin [12], blood vessel walls [163] and tumors [119, 130]. Models for cell growth and biosynthesis for organisms such as bacteria and yeast are common in the control and optimization of industrial bioreactors [6, 176]. Solute transport combined with cellular kinetics has been modeled extensively in areas like bioremediation and fixed bed bioreactors [29, 57, 170]. On the other side are biomechanical models like those used for describing tissue differentiation and bone adaptation, in which the local tissue type and mechanical properties are directly determined by the mechanical loading history and cells have only a conceptual role. [25, 140].

Summarizing, tissue function is determined by matrix components such as GAG's

and collagen II which are produced by cells in response to their local biochemical and mechanical environment which can be partially influenced via global bioreactor input parameters, like nutrient supply and mechanical stimulation. In order to reach the stage of clinical applicability a definite need arises for improved control over the functional properties and composition of tissue engineered constructs. Many tissue engineering experiments yield only qualitative histological data or quantitative data on a volume averaged basis. This provides valuable clues and indicates research directions, but is open to much speculation on possible mechanisms that govern tissue development. Mathematical models enable a further rationalization of experimental results and will be a key asset in controlling the development and thus the functionality of tissue engineered constructs. Since only a combination of a suitable biochemical and mechanical environment is likely to provide functional tissue engineered constructs, both aspects should be integrated in a numerical model. This requires a description of highly coupled phenomena such as solute transport, cell growth, matrix biosynthesis and mechanical adaptation. The objective of this study is to develop an integrated numerical framework for tissue engineering that is able to relate the evolution of local functional tissue components to both mechanical and biochemical global bioreactor input parameters. The modeling approach can eventually serve as an aid in tissue bioreactor design and the development of control strategies.

To illustrate the modeling approach we will focus on the interactions between mechanical loading and transport and synthesis of macromolecules. It is known that cyclic compression of cartilage explants can alter the synthesis rate of important tissue components such as proteoglycans [19, 102, 124, 178]. Based on these observations it has been proposed to use this mechanism to improve the functional properties of tissue engineered cartilage [22, 124]. However apart from stimulating GAG synthesis, cyclic compression can also increase the release of GAG's into the culture medium [151]. In this study, we will investigate the effect of cyclic compression on the distribution and loss of newly synthesized matrix components during the early stage of culture of a tissue engineered cartilage construct. For sake of clarity we will not assume a direct stimulation of biosynthesis by mechanical quantities such as local stress or strain. In addition we do not assume changes in material properties like permeability and stiffness due to matrix accumulation during the time of cultivation. The model however allows explicitly to investigate the effect of assumptions on these processes.

2.2   Methods

In Fig. 2.1, a schematic representation of the approach is given. The mechanical behavior of the fluid satured scaffold is represented by a biphasic mixture model consisting of a solid and a fluid phase. The effect of solute concentrations on the mechanical behavior is neglected. Mechanical output quantities like local deformation and fluid velocity can have a direct effect on cell behavior. The computed fluid velocity field is used to describe the advection and diffusion of an arbitrary number of solutes. On their turn solute concentrations will influence cell behavior. Nutrient uptake, cell growth and biosynthesis is taken into account using operator splitting. Finally the
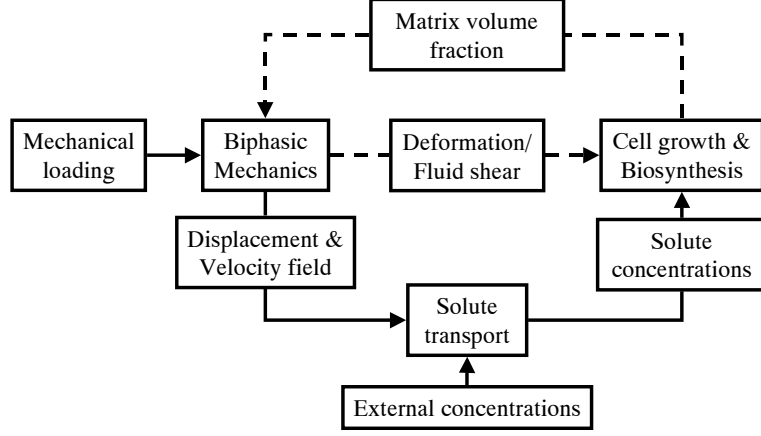
Figure 2.1: *Schematic representation of the modeling approach, showing the coupling between the different model components and the model inputs. Outputs are defined as the concentration of functional tissue components. Dashed routes will not be considered in the current study.*

amount of newly synthesized extracellular matrix can determine the permeability and stiffness of the tissue construct, as has been found experimentally [17, 182].

2.2.1   Conservation laws

In absence of inertia and body forces, the balance of momentum for phase α reads [3, 14, 53, 85, 169]:

$$\vec{\nabla} \cdot \boldsymbol{\sigma}^\alpha + \vec{\pi}^\alpha = \vec{0}, \qquad \alpha = s, f, \tag{2.1}$$

where σ is the partial Cauchy stress tensor for phase α and $\vec{\pi}^\alpha$ denotes the momentum interaction with phases other than α. The stress tensor for the solid and fluid phase, indicated by the superscript s and f respectively, is defined as:

$$\boldsymbol{\sigma}^s = -n^s p \boldsymbol{I} + \boldsymbol{\sigma}^e, \tag{2.2}$$
$$\boldsymbol{\sigma}^f = -n^f p \boldsymbol{I}, \tag{2.3}$$

where $\boldsymbol{\sigma}^e$ is the averaged effective stress tensor for the solid matrix, p is the hydrostatic pore pressure and $\boldsymbol{I}$ is the second order identity tensor. n^α is the volume fraction of component α defined as the volume occupied by phase α divided by the total mixture volume: $n^\alpha = V^\alpha / V^{tot}$. The momentum balance for the whole mixture is obtained

after the summation of Eq. (2.1) for the fluid and solid phase, in which the momentum interaction terms $\vec{\pi}^\alpha$ cancel out:

$$\vec{\nabla} \cdot \boldsymbol{\sigma} = \vec{\nabla} \cdot \boldsymbol{\sigma}^s + \vec{\nabla} \cdot \boldsymbol{\sigma}^f = \vec{\nabla} \cdot \boldsymbol{\sigma}^e - \vec{\nabla}p = \vec{0} \tag{2.4}$$

The mass balance for the solid and fluid phase, indicated by the superscript s and f respectively is:

$$\frac{\partial n^\alpha \rho^\alpha}{\partial t} + \vec{\nabla} \cdot (n^\alpha \rho^\alpha \vec{v}^\alpha) = 0, \qquad \alpha = s, f, \tag{2.5}$$

where ρ^α is the intrinsic mass density of phase α and $\vec{v}^\alpha$ is the velocity of phase α. The mass balances for solute species β is:

$$\frac{\partial n^f M^\beta c^\beta}{\partial t} + \vec{\nabla} \cdot (n^f M^\beta c^\beta \vec{v}^\beta) = M^\beta q^\beta(c^i, ..., c^n), \qquad \beta = 1, ..., n, \tag{2.6}$$

in which M^β is the molar mass of solute β and c^β denotes the concentration of solute β in mol per unit volume of fluid. q^β represents a source term, which can account for various interaction phenomena like (bio)chemical reactions or adsorption to the solid matrix. In general q^β can be a nonlinear function of the concentrations of all other solute species i, therefore coupling Eq. (2.6) for different solutes. Equation (2.6) assumes that the whole fluid space is accessible for a solute β, which may not be the case for large molecules due to pore size restrictions [139, 142].

The total mass balance of the mixture follows from the summation of the mass balances for the fluid and solid Eq. (2.5) and the saturation condition $n^s + n^f = 1$. The volume contribution of the solutes is assumed negligible and the fluid and solid phases are assumed to be intrinsically incompressible, i.e. ρ^α is constant:

$$\vec{\nabla} \cdot \vec{v}^s + \vec{\nabla} \cdot (n^f(\vec{v}^f - \vec{v}^s)) = 0. \tag{2.7}$$

The solute mass balance Eq. (2.6) is now rewritten with the solid matrix as reference. $\boldsymbol{F} = \vec{\nabla}_0 \vec{x}^s$ is introduced to denote the deformation gradient tensor with respect to the initial configuration of the solid phase. Using the determinant of the deformation tensor $J = det(\boldsymbol{F})$, which is the ratio between the current and initial volume, volume fractions per unit initial volume can be defined [85]:

$$N^\alpha = Jn^\alpha. \tag{2.8}$$

Making use of

$$\frac{D^s J}{Dt} = J\vec{\nabla} \cdot \vec{v}^s, \tag{2.9}$$

the mass balance for the solutes Eq. (2.6) can be written as [85]:

$$\frac{1}{J}\frac{D^s(N^f c^\beta)}{Dt} + \vec{\nabla} \cdot (n^f c^\beta(\vec{v}^\beta - \vec{v}^s)) = q^\beta, \tag{2.10}$$

where the constant molar mass M^β has been left out.

2.2.2   Constitutive equations

For the effective stress tensor in Eq. (2.4) a compressible hyperelastic neo-Hookean relation is used, assuming no intrinsic viscoelasticity of the solid material.

$$\boldsymbol{\sigma}^e = \kappa(J-1)\boldsymbol{I} + \frac{G}{J}\left(\boldsymbol{F}\cdot\boldsymbol{F}^T - J^{\frac{2}{3}}\boldsymbol{I}\right) \tag{2.11}$$

where κ is the bulk modulus and G the shear modulus.

The fluid velocity relative to the solid matrix in Eq. (2.7) is given by a standard Darcy law.

$$n^f(\vec{v}^f - \vec{v}^s) = -\boldsymbol{K}\cdot\vec{\nabla}p, \tag{2.12}$$

with the permeability tensor $\boldsymbol{K}$ defined as Eq. (2.13) [3, 85]. We restrict ourselves to isotropic permeability:

$$\boldsymbol{K} = (n^f)^2 C_F^{-1}\boldsymbol{I}. \tag{2.13}$$

Here C_F is the constant friction coefficient between the solid and fluid phase and n^f the current fluid volume fraction which is related to the initial fluid volume fraction n_0^f as follows:

$$n^f = \frac{V^f}{V^{tot}} = 1 - \left(\frac{1 - n_0^f}{J}\right) \tag{2.14}$$

Depending on the scaffold behavior exponential expressions for $\boldsymbol{K}$ in Eq. (2.12) can be employed, as are commonly used for cartilage [3]. Presently we do not assume such behavior.

The solute velocity with respect to the fluid is assumed to follow Fick's law for simple diffusion. Using Darcy's law Eq. (2.12) the relative solute velocity with respect to the solid matrix in Eq. (2.10) is given by:

$$\vec{v}^\beta - \vec{v}^s \quad = \quad (\vec{v}^f - \vec{v}^s) + (\vec{v}^\beta - \vec{v}^f), \tag{2.15}$$

$$= \quad -\frac{\boldsymbol{K}}{n^f}\cdot\vec{\nabla}p - \frac{\boldsymbol{D}}{c^\beta}\cdot\vec{\nabla}c^\beta, \tag{2.16}$$

where $\boldsymbol{D}$ is the diffusion tensor. In addition to pure molecular diffusion $\boldsymbol{D}$ can be extended by a mechanical dispersion term, which is a function of the relative fluid velocity. Note that Eq. (2.16) neglects the influence of matrix friction in restricting the convective and diffusive transport of large solutes [139].

The structure of the source term q^β in Eq. (2.10) depends entirely on the problem under consideration, see section 2.2.5 Model application.

2.2.3   Finite-element formulation

The biphasic mixture is described by the following set of coupled equations, Eq. (2.4, 2.12, 2.7):

$$\vec{\nabla}\cdot\boldsymbol{\sigma}^e - \vec{\nabla}p = \vec{0}, \tag{2.17}$$

$$\frac{1}{(n^f)^2} C_F \vec{v} + \vec{\nabla} p = \vec{0}, \tag{2.18}$$

$$\vec{\nabla} \cdot \vec{v}^s + \vec{\nabla} \cdot \vec{v} = 0, \tag{2.19}$$

in which the specific discharge, or apparent fluid flux, $\vec{v} = n^f(\vec{v}^f - \vec{v}^s)$ has been introduced. Several finite element formulations can be employed for solving this system in finite deformation as reviewed by Almeida [3]. We have adopted a u-v-p formulation as proposed by Levenston [106], considering the solid displacement, specific discharge and hydrostatic pressure as unknowns. The often used u-p formulation is computationally efficient [4], however the approximation of the fluid velocity field is poor, i.e. generally two orders lower then the displacement approximation and results in a fluid flux field that is discontinuous at the element boundaries. The u-v-p formulation computes the specific fluid velocity field simultaneously resulting in inter-element fluid fluxes which are continuous. Furthermore, the mass balance of the mixture is satisfied on a per element basis [53, 183].

Briefly, Eq. (2.17-2.19) are put in the weak form. The momentum balance and Darcy's law are integrated by parts and Gauss' theorem is applied. An updated Lagrange approach is followed. The mass balance is discretized in time by means of a Crank-Nicolson scheme. As the resulting system of equations is nonlinear with respect to the unknown position field $\vec{x}$ a Newton iteration procedure is employed. For simplicity and assembly speed terms arising from the linearization of the gradient operator and volume ratio J are only considered for the balance of momentum.

The finite element formulation for the advection-diffusion problem for solute transport can be derived in a similar way. Substitution of Fick's law Eq. (2.16) in the solute mass balance Eq. (2.10) gives:

$$\frac{1}{J} \frac{D^s(N^f c^\beta)}{Dt} + \vec{\nabla} \cdot (\vec{v} c^\beta - n^f \boldsymbol{D} \cdot \vec{\nabla} c^\beta) = 0. \tag{2.20}$$

The source term q^β has been omitted since this term will be included using operator splitting. $\vec{v}$ denotes again the specific discharge, which is computed in the biphasic finite element part, see Eq. (2.18). Equation (2.20) is written in the weak form, integrating over the domain Ω and partial integration and Gauss' theorem are applied. After time discretization by means of a Crank-Nicolson scheme and spatial discretization per element, the system of equations in matrix form becomes:

$$\left(\underline{M_t} + \theta \Delta t(-\underline{C} + \underline{K}) \right) \underline{c}_e^\beta = \left(\underline{M_{t_n}} + (1-\theta)\Delta t(\underline{C_n} - \underline{K_n}) \right) \underline{c}_{e_n}^\beta \tag{2.21}$$

where

$$
\begin{aligned}
\underline{M_t} &= \int_{\Omega_e} \underline{N} n^f \underline{N}^T d\Omega_e, & \underline{M_{t_n}} &= \int_{\Omega_e} \underline{N} \frac{n_n^f}{J_\Delta} \underline{N}^T d\Omega_e, \\
\underline{C} &= \int_{\Omega_e} \underline{B}^T \underline{v} \underline{N}^T d\Omega_e, & \underline{C_n} &= \int_{\Omega_e} \frac{1}{J_\Delta} \underline{B}^T \underline{F}_\Delta \underline{v}_n \underline{N}^T d\Omega_e, \\
\underline{K} &= \int_{\Omega_e} \underline{B}^T n^f \underline{D} \underline{B} d\Omega_e, & \underline{K_n} &= \int_{\Omega_e} \frac{1}{J_\Delta} \underline{B}^T \underline{F}_\Delta n_n^f \underline{D}_n \underline{F}_\Delta^T \underline{B} d\Omega_e
\end{aligned} \tag{2.22}
$$

Matrix $\underline{N}$ contains the shape or weighting functions, matrix $\underline{B}$ contains the spatial derivatives of the shape functions in the appropriate order and $\theta = 0.5$. $\underline{F}_\Delta$ is the incremental deformation tensor and $J_\Delta = det(\underline{F}_\Delta)$.

2.2.4   Numerical implementation

The biphasic finite-element formulation is implemented in the SEPRAN finite-element package [159]. A 2-D 9-node quadrilateral plane strain element with quadratic interpolation functions for the displacements and fluid velocity is used, yielding two unknowns in every node for both displacements and fluid velocity. The pressure interpolation functions are linear and discontinuous per element, with one pressure unknown and two pressure derivatives defined in the center node. The solute transport Eq. (2.21) is implemented using the input features of a standard advection-diffusion element for compressible flows, the same 9-node element shape is employed.

The biokinetic source term in Eq. (2.6) is implemented using an operator splitting technique, decoupling the computation of transport and source term. The second-order accurate Strang operator splitting scheme is used [81, 95, 127, 165]. The procedure consists of three parts, defined as follows: First, the coupled system of nonlinear biokinetic ordinary differential equations (ODE's) is solved per node for all species simultaneously, using a Crank-Nicolson scheme and Newton iteration, integrating over half a time step. In the second part, integration takes place over a full time step. The nonlinear biphasic system is solved once, after which the decoupled linear transport partial differential equations (PDE's) are solved per species separately. The third part is again equal to the first part.

The biokinetic part also describes the evolution of non-mobile species such as fixed cells or solutes adsorbed to the solid matrix. Concentrations defined per unit volume of mixture are corrected for changes in mixture volume. The biphasic finite-element method has been validated for the case of 1-D confined consolidation. For small deformations, the pressure response showed excellent agreement with the analytical solution. The operator splitting scheme has been validated for the case of diffusion in combination with a constant source term, without any deformation. Long-term results were found to match the steady state analytical solution.

2.2.5   Model application

As stated in the introduction, we will apply the model to investigate the effect of cyclic compression on the distribution and loss of newly synthesized matrix macromolecules during the early stage of culture of a tissue engineered cartilage construct. Throughout this study, we assume that the cell-scaffold system has enough mechanical integrity to withstand loading. The first case we consider is solute desorption without any cell activity during unconfined compression. We consider a 2-D plane strain problem, in which the construct size is 1 mm by 3 mm, see Fig. 2.2a. We assume no friction between the construct and the loading platens, since a detailed deformation field is not the primary objective of the present study and we want to provide a clear, 1-D, picture of solute transport.

Only half the scaffold needs to be modeled because of symmetry, see Fig. 2.2b. At the loading platens and the central edge zero flux boundary conditions are applied. At the peripheral edge, zero pressure is prescribed. The culture medium is assumed to be well mixed and continuously refreshed, therefore essential boundary conditions can be prescribed for the solute concentrations at the construct's peripheral edge. Horizontal
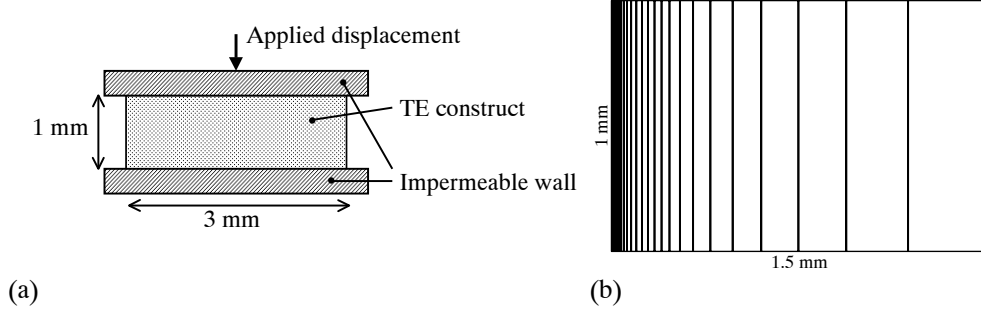
Figure 2.2: (a) Unconfined compression setup. (b) Finite element mesh containing 24 elements.

displacement is restricted for the central edge and vertical displacement for the lower loading platen. A cyclic vertical displacement is applied to the upper loading platen, resulting in a sinusoidal strain between 0% and 15%. It is assumed that the, possibly prestressed, construct remains in contact with the loading platens at all times. The following frequencies are applied: 0.001 Hz, 0.01 Hz, 0.1 Hz and 1 Hz. Also the case without loading is evaluated. The initial concentration is normalized to 1 and the evolution of the concentration is followed for a total time period of 4000 s.

Away from the construct edge cyclic fluid flow will only result in a net solute flux when mixing occurs. This is only the case for a nonuniform microscopic solute velocity distribution. Since computation of the velocity field produces only an averaged velocity, extra assumptions are necessary to describe transport phenomena due to cyclic fluid flow. Therefore a dispersion coefficient is introduced in Eq. (2.16). For istropic diffusion and since the fluid flux in the present problem is 1-D, $\boldsymbol{D}$ in Eq. (2.16) is given by [183]:

$$D = D^m + \frac{D^d}{n^f}|\vec{v}|, \tag{2.23}$$

where D^m is the molecular diffusion coefficient and $|\vec{v}|$ is the absolute value of the apparent fluid flux $\vec{v}$. D^d is the longitudinal dispersion coefficient, which is a measure of the solute spreading due to microscopic fluid velocity variations. D^d has dimension length and should be of similar order of magnitude as the pore size. As a representative value for the diffusion coefficient D^m of a matrix molecule we use the value for chondroitin sulfate in dilute solution: $D_{CS} = 4 \times 10^{-7}$ cm^2 s^{-1} [36]. The choice of the dispersion parameter D^d is less clear, therefore D^d is varied in the range from 1×10^{-6} mm to 1×10^{-1} mm. Also the case without dispersion is considered.

The fluid volume fraction is set to $n^f = 0.9$ based on the composition of a 4 day old tissue engineered cartilage construct [46]. This is a maximum value as no trapped water, for example in cells, has been taken into account. The mechanical material properties are based on the order of magnitude of the equilibrium modulus and permeability found in confined compression for three-day-old tissue engineered cartilage constructs [118]. A Poisson's ratio $\nu = 0.1$ is used in the light of the values 0.09 and 0.11 reported for fetal and calf cartilage [189]. The resulting bulk modulus
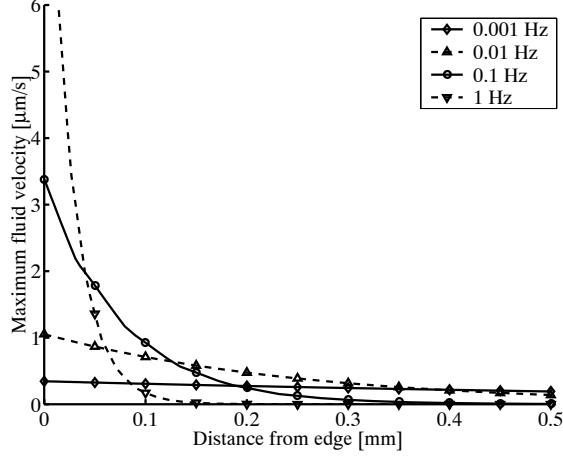
Figure 2.3: *Maximum local fluid velocity induced by dynamic loading in the last cycle before $t = 4000$ s, plotted in the undeformed geometry.*

$\kappa = 8.1$ kPa , the shear modulus $G = 8.9$ kPa and the friction coefficient $C_F = 8.1 \times 10^{12}$ N s m^{-4}, see Eq. (2.11,2.13).

Based on a fine initial mesh, the maximum local fluid velocity has been computed for the different frequencies, similar to Fig. 2.3. This velocity is used to select an element distribution that can be used for all frequencies under consideration, keeping the local element Peclet number $Pe = |\vec{v}|h/n^f D^m$, where h is the element size, lower than 2, see Fig. 2.2b. The time steps dt for the different frequencies have been selected to keep the maximum Courant number $Co = |\vec{v}|dt/n^f h$ lower than 1: $dt = 10$ s for 0.001 Hz, $dt = 2$ s for 0.01 Hz, $dt = 1$ s for 0.1 Hz and $dt = 0.1$ s for 1 Hz. $dt = 10$ s is used for the non-loaded case. The time step is always larger than the minimum time step required for the biphasic mechanics [4, 53].

In the second case, the problem is extended, taking into account matrix molecule synthesis. We distinguish three limiting cases: matrix synthesis limited by a small solute, matrix synthesis limited by a large solute and matrix synthesis independent of solute transport. A simple proportional relation for matrix molecule synthesis is employed:

$$q_p = k_p c^s \rho^{cell}. \tag{2.24}$$

Here, q_p is the matrix molecule synthesis rate, which is the source term in the transport equation Eq. (2.6). k_p is the synthesis rate constant, c^s is the concentration of the limiting solute and ρ^{cell} is the cell concentration. For the case in which matrix synthesis is independent of solute transport, c^s is left out of Eq. (2.24).

The concentration profile of the limiting solute is determined by diffusion and uptake. Michaelis-Menten kinetics are used for modeling uptake, which is taken to be independent of the synthesis rate:

$$q_s = \left(\frac{k_{max} c^s}{C_m + c^s} \right) \rho^{cell}. \tag{2.25}$$

q_s is the source term for solute uptake in Eq. (2.6). k_{max} is the maximum uptake rate and C_m the half maximum rate concentration. The cell concentration in the undeformed construct is assumed uniform. Since only relative changes are presently of interest, the values for the external solute concentration and cell concentration are chosen arbitrarily at 1 mol mm^{-3} and 1 cell mm^{-3}, respectively.

The diffusion coefficient D^m for the small solute is set to 1×10^{-5} cm^2 s^{-1}, the value for glucose in solution at 37° C [108]. Based on the assumption of a limited solute we chose the solute uptake time scale 10 times the diffusion time scale, which yields a k_{max} of 4×10^{-3} mol cell^{-1} s^{-1}. C_m is set to 0.1 mol mm^{-3} in order for the solute uptake rate to approach zero for low concentrations. Figure 2.5a shows the resulting steady-state solute concentration profile. For the large solute, D^m is set to 1×10^{-7} cm^2 s^{-1}, an order of magnitude representative for large molecules like serum albumin [135, 139]. Based on the same considerations, k_{max} is 4×10^{-5} mol cell^{-1} s^{-1} and C_m is set to 0.1 mol mm^{-3}. These values produce exactly the same steady-state concentration profile as for the small solute, see Fig. 2.5a.

For the case independent of solute transport, the matrix molecule production rate k_p is set to 7.66×10^{-6} mol cell^{-1} s^{-1} to produce a total matrix molecule content of 1 mol after 87000 s. For both the cases dependent on solute concentration, k_p is set to 3.99×10^{-5} mm^3 cell^{-1} s^{-1}, to produce the same 1 mol after 87000 s based on the steady-state solute concentration profile. Based on the results of the first desorption problem, dispersion parameters D^d of 0 mm, 0.01 mm and 0.1 mm are applied. The nonloaded case and frequencies of 0.001 Hz and 0.1 Hz are evaluated for 87000 s. For all problems, $dt = 1$ s is used. The initial condition for the limiting solutes is formed by the earlier computed steady state concentration profile. Matrix molecule concentration is initially zero.

2.3   Results

For the first problem the maximum fluid velocities during the last cycle are shown in Fig. 2.3. Low frequencies produce low velocities and a large fluid flow penetration depth, while for high frequencies the fluid velocity is much higher, however located only in a small peripheral zone.

Figure 2.4a shows the solute concentration profiles after 4000 s and Fig. 2.4b shows the evolution of the total solute content for the case without dispersion, $D^d = 0$. Different frequencies have little influence, indicating that the main effect for $D^d = 0$ is the size decrease due to consolidation of the construct. Figures 2.4c-2.4f show the results for $D^d = 1 \times 10^{-2}$ mm and $D^d = 1 \times 10^{-1}$ mm. Lower dispersion parameters, $D^d = 1 \times 10^{-6}$ mm and $D^d = 1 \times 10^{-4}$ mm, did not produce distinguishable results from $D^d = 0$ mm. Compared to the other dispersion parameters the total content decreases more rapidly for $D^d = 1 \times 10^{-1}$ mm. The decrease being largest for frequencies of 0.01 Hz and 0.1 Hz.

For the second problem Fig. 2.5a shows the steady state concentration profiles for both the small and large limiting solute, which are the same for the case without loading. In Fig. 2.5b, the concentration profiles of the large solute are shown
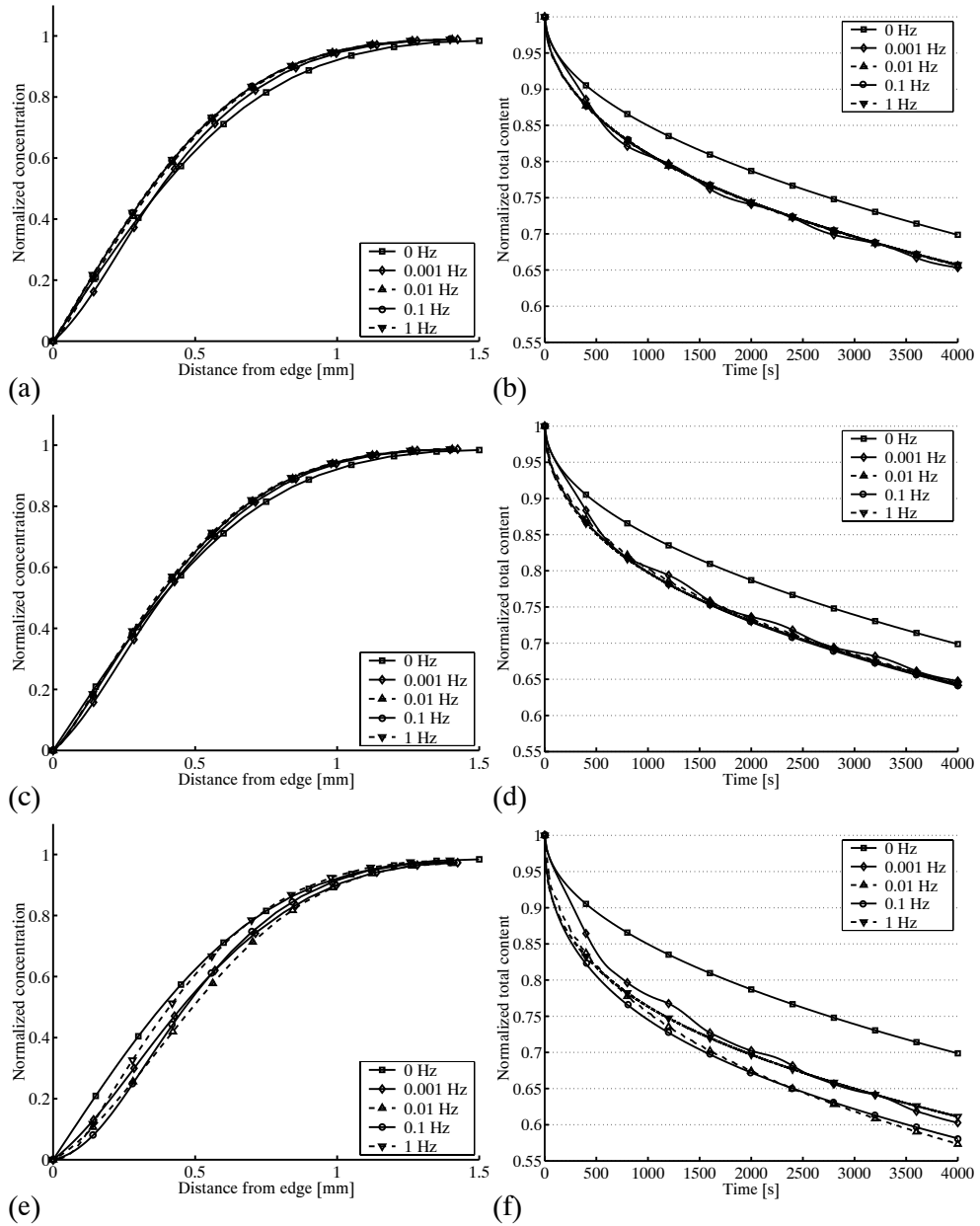
Figure 2.4: *Desorption of an initially homogeneous concentration for different loading conditions and dispersion parameters. (a), (b): $D^d = 0$ mm. (c), (d): $D^d = 0.01$ mm. (e), (f): $D^d = 0.1$ mm. Left: Matrix component concentration profiles after 4000 s. Right: Evolution of total matrix component content in time.*
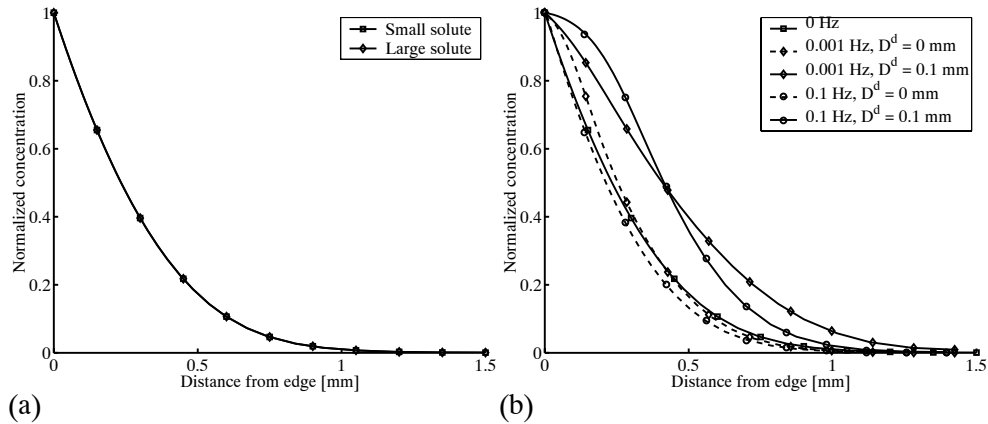
Figure 2.5: *(a) Steady state concentration profile resulting from diffusion and uptake for both the small and large solute. (b) Large solute concentration profiles at $t = 87000$ for different loading frequencies and dispersion parameters.*

after 87000 s for different loading and dispersion conditions. For high dispersion parameters, $D^d = 0.1$ mm transport into the construct is significantly enhanced by cyclic loading. In correspondence with the fluid velocity profiles in Fig. 2.3, the solute penetration depth is largest for 0.001 Hz, while for 0.1 Hz solute concentrations are higher in the periphery. Concentration profiles for the small limiting solute are hardly affected by different dispersion parameters and loading conditions.

In Fig. 2.6a-2.6c the matrix molecule profiles are given at 87000 s for the three limiting cases. In the case where matrix molecule synthesis is independent of solute transport, Fig. 2.6a shows that without dispersion concentrations are higher in the loaded situations due to consolidation, while for high dispersion $D^d = 0.1$ mm increased loss occurs. In Fig. 2.6b, it can be observed that for the case of a small limiting solute increased loss of matrix molecules dominates for high dispersion, while for the case of a large solute the increased production due to enhanced transport of the limiting solute dominates, see Fig. 2.6c.

To provide a clear overview, Figs. 2.7a-2.7c show the results for all loading cases and dispersion parameters considered. The white bar is the total amount of matrix molecule produced. The black bar represents the amount of matrix molecule retained in the construct.

2.4   Discussion

A model for the influence of mechanically induced fluid flow on the transport and distribution of macromolecules such as newly synthesized matrix components, important for tissue function, was studied. The model consists of a biphasic mechanical description of the tissue-engineered construct. The resulting fluid velocity field is used for evaluating solute transport. Solute concentrations determine
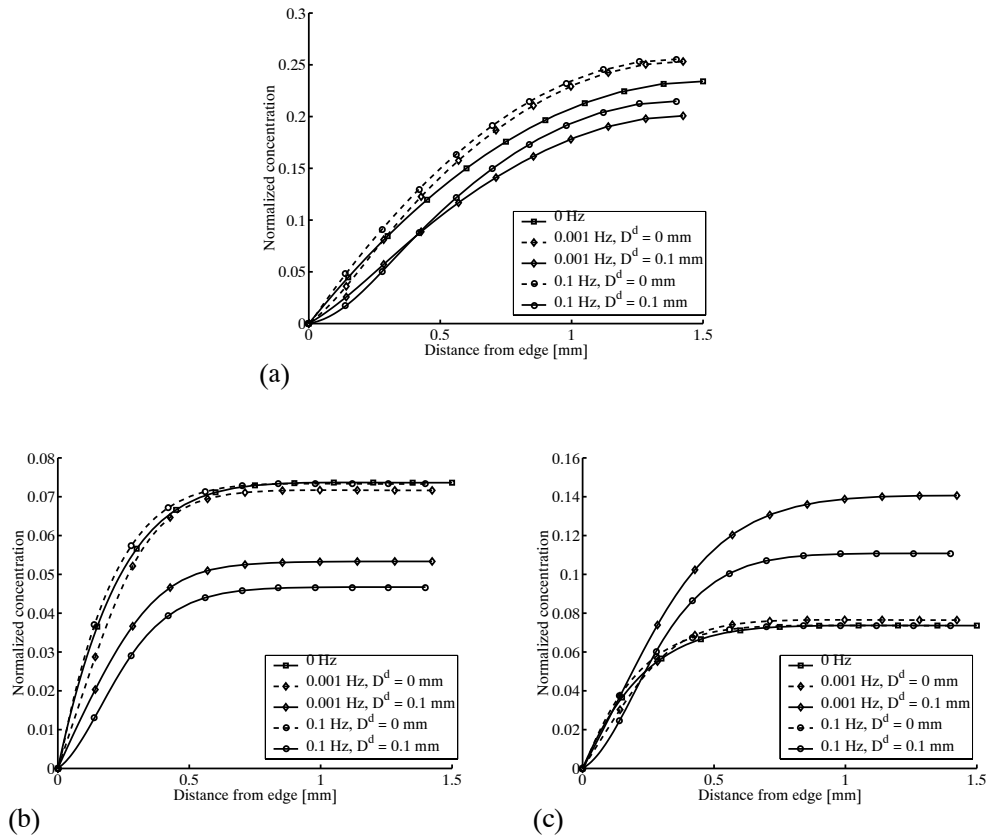
Figure 2.6: *Matrix component profiles at $t = 87000$ for different loading frequencies and dispersion parameters. (a) Synthesis independent of transport. (b) Synthesis limited by a small solute. (c) Synthesis limited by a large solute.*

(a)

(b)   (c)
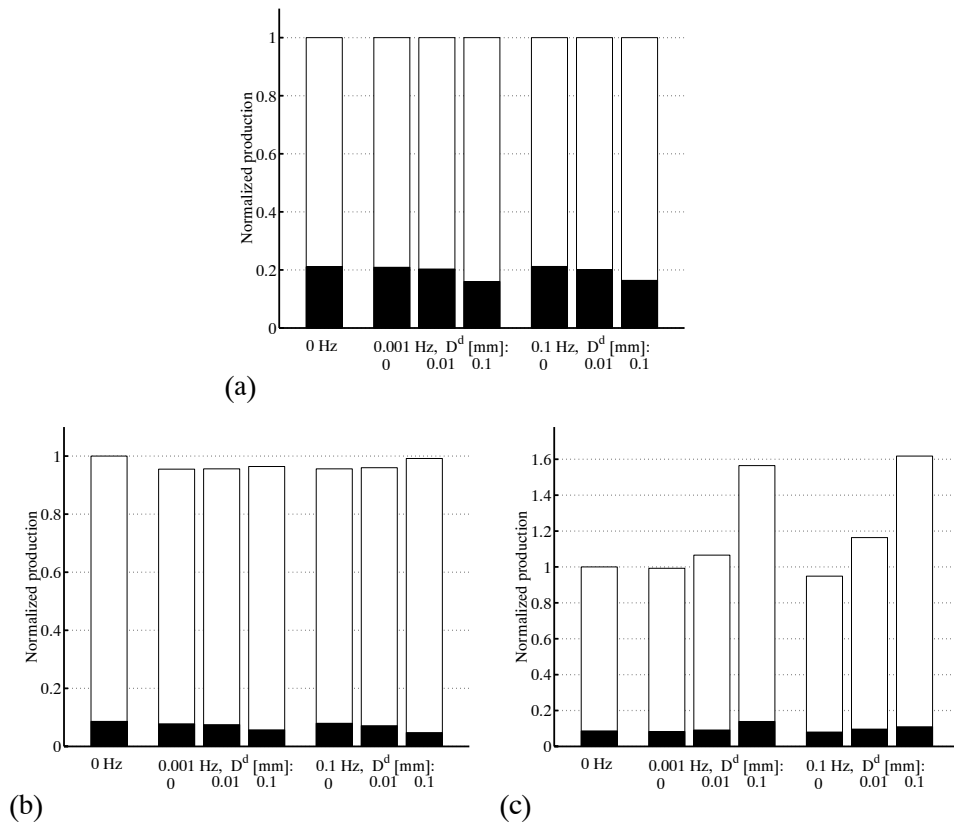
Figure 2.7: *Integrated effect of different loading frequencies and dispersion parameters on total biosynthesis at $t = 87000$. The white bar represents the total synthesis. The black bar represents the fraction retained in the construct. (a) Synthesis independent of transport. (b) Synthesis limited by a small solute. (c) Synthesis limited by a large solute.*

biosynthetic behavior.

Plane strain unconfined compression of a tissue engineered construct was considered, although an axisymmetric configuration may be more appropriate for most current tissue engineering model systems. A physiologically relevant strain of 15 % at frequencies ranging from 0.001 Hz to 1 Hz was applied, [39, 102]. The frequency dependency of the fluid velocity profile found in Fig. 2.3 was consistent with the numerical results of Suh [167, 168].

The first case investigated was redistribution and desorption of an initially uniform macromolecule concentration with and without cyclic compression. After an initial time phase of solute expression due to deformation and consolidation, the total solute content decreased at approximately the same rate as for simple diffusion for all frequencies, see Fig. 2.4b, indicating a simple shift in the diffusion process from a constantly refreshed zone. Within the short time span of the first study, 4000 s, effects of augmented transport by cyclic fluid flow were only observed for relatively high dispersion parameters. A mixing length of $D^d = 0.1$ mm will only be realistic for highly porous constructs with large pores in the same order of magnitude. The effect of enhanced transport was largest for frequencies of 0.01 and 0.1 Hz, which combine an averaged fluid flow penetration depth and fluid velocity, see Fig. 2.3. In an experimental desorption study, the concentration profile of 3kDa dextran showed a concave shape qualitatively similar to those in Fig. 2.4e for the case of natural cartilage after one hour of unconfined compression at a loading frequency of 0.001 Hz. In that study, it was also shown that the same concave shape could be modeled using a position dependent diffusion parameter [144].

In the second problem, a time period of 87000 s was considered and the model was extended with biosynthesis. Three cases were distinguished: Synthesis dependent on a limited small solute, synthesis dependent on a limited large solute and synthesis independent of solute transport. As expected, transport of small solutes was not significantly affected by cyclic loading while transport of large molecules was enhanced when dispersion was taken into account, see Fig. 2.5b. These results are in agreement with literature: For natural cartilage in unconfined compression, it was reported that a cyclic load at 1 Hz increased the desorption rate of serum albumin by 30%-100%, while smaller molecules like urea and NaI were not affected [135]. Figure 2.5b shows that for the case of large solutes low frequencies yielded a large solute penetration depth, while for higher frequencies the solute concentration was higher in the periphery. The integrated effect of cyclic loading on total synthesis in Fig. 2.7 shows the different sensitivity to loading that can be expected for the cases of limiting large and small solutes.

In a dynamic confined compression study of three-week polyglycolic acid (PGA) constructs at 0.001 Hz and 0.1 Hz, the increase in protein and GAG synthesis was of similar order of magnitude as the 60% reported here for the case of large molecules and $D^d = 0.1$ mm [39]. In another study, it was found that unconfined dynamic compression of chondrocytes in agarose yielded only a small increase in synthesis at early times, while at later times the effect of loading was increased. Based on these results among others it was concluded that flow induced streaming potentials associated with the presence of more extra cellular matrix at later times may be more

important than augmented solute transport [19]. Whether solute transport will be a limiting factor in a particular tissue engineering application will depend on cell activity and the cell concentrations used. The cases investigated in the present study served the purpose of demonstrating the influence of mechanically induced convection on the transport of solutes that have been assumed limited a priori and cannot be expected to give a complete representation of actual cell behavior. We have adopted only a basic, abstract, description of cell behavior. Michaelis-Menten kinetics were used for modeling solute uptake, as reported for oxygen uptake in mini-pig articular cartilage [129], chick growthplate [74] and bovine intervertebral disk [86]. Although in reality especially growth factor utilization may be much more complicated, we have employed this type of relation for both small and large solutes [65]. The relation for matrix component synthesis used was simply proportional in the limiting solute as in the model employed by Obradovic [134], although we did not include the effect of product inhibition since it does not become relevant at the early times considered in the present study. Since we primarily focused on transport, we did not assume a direct stimulation of cell biosynthesis by mechanical quantities such as strain and local fluid velocity [102]. We also did not include the adaptation of material properties such as permeability and stiffness as a consequence of matrix deposition. However, models for these processes can be included in a straightforward manner.

The percentage of synthesized matrix components that is retained in the construct is relatively low compared to literature, 20% is retained for homogeneous production and even less for inhomogeneous production, see Fig. 2.7. During a six-week culture period 42% of the synthesized GAG has been retained for the static case and 25%-29% for various mixing conditions [61]. Figure 2.7a shows that cyclic deformation resulted in a slightly lower percentage of matrix molecules retained. Experimentally, the percentage retention was only affected significantly by cyclic loading at a high offset strain of 50% for three-week constructs in confined compression at 0.001 Hz and 0.1 Hz [39]. Even for the cases of inhomogeneous production the matrix component profiles in Fig. 2.6b-c do not show a dip in the center as experimentally found for GAG in six-week-old constructs [117]. The reason behind this as well as behind the low retention fraction is the value for the diffusion coefficient used for the matrix components $D_{CS} = 4 \times 10^{-7}$ cm^2 s^{-1}, while aggregation of GAG's over longer culture periods will result in proteoglycan aggregates which can have a much lower diffusion coefficient of order 10^{-9} cm^2 s^{-1} [36]. Another reason for the relatively fast transport of matrix components is that Eq. (2.16) assumes that the whole fluid phase is accessible for the solute and neglects the influence of matrix friction in restricting the convective and diffusive transport of large solutes [139]. In a typical highly porous PGA scaffold inter fiber spacing is in the order of tenths of micrometers [51]. For 2 % agarose the averaged pore size has been determined between $124 - 206$ nm, while the hydrodynamic radius of a large molecule like bovine serum albumin 68 kDa is in the order of $3 - 4$ nm [139]. However, as tissue formation continues this space is filled with extra cellular matrix. In natural cartilage, the partition coefficients and diffusivity of 3 and 40 kDa dextran have been shown to be significantly reduced by compression [142]. To account for some of these matrix related effects, the use of an effective fluid volume fraction and the introduction of a friction factor in Eq. (2.16)

may be considered.

A finite deformation biphasic u-v-p formulation has been implemented in order to produce an accurate specific fluid velocity field, in spite of higher computational costs compared to other (u-p) formulations. As a first approximation osmotic and electric effects are not taken into account, based on the assumption that there is no electrical charge and solute concentrations are low. This assumption can prove invalid for charged hydrogels like alginate, or constructs in a later development stage when large quantities of proteoglycans have accumulated, since it is well known that the osmotic pressure caused by the highly charged proteoglycans has a major contribution to the mechanical properties of mature cartilage [53]. Although commonly applied for modeling cartilage, a biphasic model may thus be inappropriate for describing the process of tissue formation and a multiphase modeling approach that accounts for phenomena like swelling and (electro)-osmosis may be required [53, 67, 85, 169]. Including osmosis implies that solute transport and mechanics are no longer decoupled, it will be necessary to include the total operator splitting scheme (solute transport and solute source term) in the iterative mechanical loop.

Strang operator splitting is used to solve the nonlinear biokinetic source terms in the solute transport equations separately. This renders the transport equations linear and adds to flexibility by decoupling transport of different solutes which can thus be solved separately. Although splitting will inevitably lead to loss of accuracy compared to the fully coupled case, numerical tests indicate that this error is negligible for time steps that are small with respect to both the time scale of transport and the time scale of consumption. Although in literature more elaborate iterative splitting schemes have been used, Strang-splitting has been found competitive in the trade-off between computational time and accuracy [109, 158].

Summarizing, numerical models can help to clarify experimental observations and provide a higher level of control over the development of tissue-engineered constructs during bioreactor culture. Apart from biochemical factors it is generally believed that some sort of mechanical conditioning may be important to obtain neotissue that can withstand or adapt to in vivo conditions post implantation. Based on the high level of coupling between mechanical and nonmechanical factors that influence cell behavior it has been argued that an integrated approach is necessary for modeling the development of functional tissue engineered constructs during bioreactor cultivation. For this purpose, a modeling framework has been proposed that enables an integrated study of combined effects between mechanical loading and the transport of biochemical important solutes and their influence on cell behavior. Despite their large potential contribution, numerical models involving cell behavior will only be useful when properly validated. This requires a large amount of systematic experimental data with respect to the same reference system. Focusing not only on trends or extremes in cell behavior, but providing complete quantitative relations of cell growth and biosynthesis as a function of different concentrations of solutes, cells and matrix and local mechanical quantities. In determining such relations use of thin scaffolds or small beads is advantageous since cell behavior can be regarded as uniform without further assumptions, while providing a 3-D structure which is necessary for conservation of phenotype.

Chapter 3

The local matrix distribution and the functional development of tissue engineered cartilage, a finite element study[1]

Abstract

Assessment of the functionality of tissue engineered cartilage constructs is hampered by the lack of correlation between global measurements of extra cellular matrix constituents and the global mechanical properties. Based on patterns of matrix deposition around individual cells, it has been hypothesized previously, that mechanical functionality arises when contact occurs between zones of matrix associated with individual cells. The objective of this study is to determine whether the local distribution of newly synthesized extracellular matrix components contributes to the evolution of the mechanical properties of tissue engineered cartilage constructs. A computational homogenization approach was adopted, based on the concept of a periodic representative volume element. Local transport and immobilization of newly synthesized matrix components were described. Mechanical properties were taken dependent on the local matrix concentration and subsequently the global aggregate modulus and hydraulic permeability were derived. The transport parameters were varied to assess the effect of the evolving matrix distribution during culture. The results indicate that the overall stiffness and permeability are to a large extent insensitive to differences in local matrix distribution. This emphasizes the need for caution in the visual interpretation of tissue functionality from histology and underlines the importance of complementary measurements of the matrix's intrinsic molecular organization.

3.1   Introduction

Articular cartilage has only a limited capacity for repair after damage. Current therapies aimed at aiding the natural repair process yield inconsistent, often unsatisfactory long-term results [96]. Tissue engineering of cartilage can be used to study the process of cartilage formation in a controlled *in-vitro* environment and can potentially provide transplant material for cartilage reconstruction [49]. A prerequisite for clinical use is that a cultured cartilage construct meets, or has the capacity to adapt to, *in-vivo* functional requirements [22]. The construct's mechanical properties can be modulated by adjusting the parameters that define the culture environment, such as scaffold material [84], hydrodynamic conditions [118, 181], mechanical loading [19, 122, 124], addition of growthfactors [122, 138], cell seeding density and nutrition [125]. Although it has been shown that mechanical properties which approach those of natural cartilage can be obtained after long term culture [47], there is still a lack of control over the functional development of tissue engineered constructs.

The general concept is that natural cartilage derives its resistance to mechanical loading from a fibrous network consisting mainly of collagen type II, which is prestressed due to the osmotic or electrostatic swelling pressure exerted by a high concentration of negatively charged glycosaminoglycans (GAG's), immobilized in the form of large proteoglycan (PG) aggregates [7, 20, 75, 128]. Based on this relation between the molecular composition and function of natural cartilage, the most frequently measured quantities in tissue engineering experiments are the collagen and GAG content. However, even though the presence of these molecular components is prerequisite, their amount does not fully determine the construct's global mechanical properties. Besides collagen and PG's, cartilage contains also noncollagenous proteins such as for example link protein which play a role in the functional assembly of the extracellular matrix [75, 128]. Significant differences in the Poisson's ratio have been found between calf and adult bovine cartilage, which had equal collagen content. This discrepancy could be attributed to the difference in crosslink density, which determines to a large extent the functionality of the collagen network [189]. Moreover natural cartilage displays a highly organized zonal structure with different molecular composition, fibril diameter and organization. The anisotropic collagen fiber orientation ranges from perpendicular at the bone interface to parallel to the cartilage surface near the joint cavity. Within these zones a structural distinction can be made between a thin layer of pericellular matrix surrounding the cells, the territorial matrix farther away and the interterritorial matrix, which connects the regions of cell associated matrix [75].

In cartilage tissue engineering the extracellular matrix (ECM) formed by chondrocytes within an artificial scaffold is initially less organized. Newly synthesized matrix molecules like procollagen and PG's are secreted by the cells and transported away while undergoing an assembly process to form fibers and large immobilized molecular aggregates [41, 128, 143, 152, 164]. In addition the thus formed extracellular matrix is also subject to physical, chemical and chondrocyte mediated degradation, leading to a constant matrix remodeling [27, 151, 156]. In the course of time the construct's

collagen and proteoglycan content can approach a steady state [46], resulting from a balance between synthesis, incorporation and degradation and/or product inhibited synthesis [73, 134, 187].

The relation between the content of extracellular matrix constituents and biomechanical function has been investigated in various studies. For mature natural cartilage the aggregate modulus has been correlated to GAG content primarily [31, 128, 175] and to both GAG and collagen density [150]. For the hydraulic permeability an inverse relationship with fixed charge density, i.e. PG content, has been demonstrated [115], on the other hand also no significant dependence has been found [150]. For developing articular cartilage, relationships for the aggregate modulus and permeability as a function of GAG and collagen concentration have been established [186]. It was concluded that changes in biomechanical properties during development were primarily associated with the increase in collagen content. In tissue engineering studies the aggregate -and Young's moduli and permeability of chondrocyte seeded constructs have been correlated with the amount of GAG, collagen and water present [26, 123, 181]. A strong dependence of the stiffness on either collagen [123] or GAG was observed [26, 181].

Although the relations between tissue averaged ECM content and mechanical properties are highly instructive, the introduction of additional parameters is necessary to account for the variability in regression slope and large amount of scatter in the data. Besides difference in the molecular organization such as crosslinking, part of this variability may arise from the fact that only tissue averaged quantities were considered, while clear gradients in matrix deposition can occur between the construct's periphery and center [117]. Another factor, which has received relatively little attention, is that also the local, cell scale, matrix distribution potentially plays an important role. Patterns of matrix deposition around individual cells in agarose have been quantified and observed to spread outwards in time [19, 122, 143]. It has been hypothesized that mechanical functionality arises when contact occurs between zones of matrix associated with individual cells [19, 122, 125, 143]. In addition it has been speculated that one of the mechanisms by which dynamic loading could contribute to improved mechanical functionality is the dispersion of matrix constituents by compression induced fluid flow, leading to a local matrix redistribution [122, 141].

The main question is whether assessment of tissue functionality from the main ECM constituents requires in the first place additional information about the local matrix distribution from histology, or complementary global measurements of molecular organization. Therefore the objective of this study is to determine whether the local distribution of newly synthesized extracellular matrix contributes to the evolution of the global mechanical properties of tissue engineered cartilage constructs, in particular the aggregate modulus Ha and hydraulic permeability K. More specifically, if mechanical functionality arises as a result of contact between zones of cell associated matrix, a relatively sudden increase in stiffness at a certain point in time during culture is to be expected. Also, if mechanically induced matrix redistribution can improve tissue functionality, the same amount of matrix with the same properties, only distributed more homogeneously, should give rise to a significant improvement of the mechanical properties. To answer these questions a computational

(a)   (b)
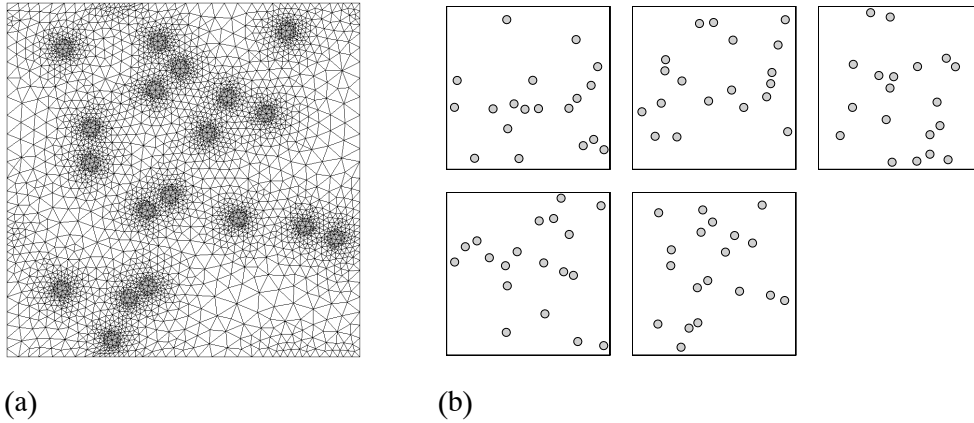
Figure 3.1: *(a) Finite element mesh of a representative volume element (RVE), consisting of randomly distributed cells embedded in a hydrogel, modeled as a porous medium. (b) The homogenized Ha and K were derived for 5 different RVE's in two directions.*

approach is particularly useful, since it enables to distinguish matrix distribution from other important factors that affect functionality, such as for example in the case of dynamic compression, an increase in the amount of matrix synthesized and the production of more link molecules [21, 39, 98, 122].

3.2   Methods

A finite element homogenization approach based on the concept of a periodic representative volume element (RVE) was adopted [15, 93, 162]. The global material behavior can be captured by modeling only a limited, but sufficiently large part of an inhomogeneous microstructure, in which the microstructural components can be considered as a continuum. Local cellular ECM synthesis and passive transport were modeled. The local stiffness and permeability were adjusted according to the amount of ECM present. Subsequently the averaged, global, material properties Ha and K were derived. The transport parameters were varied to assess the effect of the evolving matrix distribution during culture.

The RVE geometry is based on the case of 2% agarose seeded with 10 million cells cm^{-3} [122]. To allow for representative cellular structures, a two dimensional cross sectional area of 200 μm squared is considered. Assuming the cells are stacked in the in-plane dimension, the rounded number of cells in this area is 19 and the interlayer spacing is 46.4 μm. Cells are randomly placed and the cell size is set to 10 μm [71, 100]. An example of an RVE is shown in Fig. 3.1a. The mesh was generated using the MATLAB PDE toolbox v1.0.3.

To describe the process of tissue formation at the cellular scale, a model was adopted which was initially proposed by Dimicco to interpret the spatially varying

matrix distribution in articular cartilage at the tissue scale [41]. It is assumed that transport of newly synthesized matrix components can be described by a process of diffusion, binding and degradation [41]. No distinction is made between collagen and proteoglycans. Only a mobile matrix component c_m and an immobilized, bound, matrix component c_b are distinguished. Transport of the mobile ECM concentration c_m [g cm^{-3}] is described by Eq. (3.1):

$$\frac{\partial c_m}{\partial t} - \vec{\nabla} \cdot (D\vec{\nabla} c_m) = q - k_b c_m, \tag{3.1}$$

where D [cm^2 s^{-1}] is the diffusion coefficient, q [g cm^{-3} s^{-1}] the matrix synthesis rate and k_b [s^{-1}] the first order binding constant. k_b Controls the speed at which the newly synthesized matrix components become immobilized and assembled into a functional matrix. The immobilized matrix concentration c_b [g cm^{-3}] is described by Eq. (3.2):

$$\frac{\partial c_b}{\partial t} = k_b c_m - k_d c_b, \tag{3.2}$$

in which the first term in the right hand side is the matrix assembly term from Eq. (3.1). The second term accounts for matrix catabolism, where k_d [s^{-1}] is the degradation constant which determines the matrix turnover speed. It was assumed that degraded matrix molecules are no longer able to bind again. In case of proteoglycan aggregates, cleavage by matrix metalloproteinases and aggrecanases results in aggrecan fragments that cannot reattach due to the missing link protein [27, 41, 151].

For the reference binding k_b^{ref} and degradation rate k_d^{ref} the same parameters as in the work of Dimicco [41] were adopted, which were derived based on proteoglycans in cartilage: $k_b^{ref} = 1.2 \times 10^{-5}$ s^{-1} [41, 155], $k_d^{ref} = 3.7 \times 10^{-7}$ s^{-1} [41, 156]. To evaluate the sensitivity, also variations of these parameters were carried out. The diffusion coefficient D of aggregating proteoglycans in solution lies in the order of 10^{-8}-10^{-9} cm^2 s^{-1} [36, 62, 63]. The reference diffusion coefficient D_{ref} was set to 10^{-10} cm^2 s^{-1} since molecular movement will be severely hindered by the gel, given the hydrodynamic radius of a proteoglycan subunit of 54-80 nm [36] and the estimated pore size of 2% agarose 124-206 nm [139]. To investigate the influence of matrix distribution D has been varied to $D_{ref} \times 10$ and $D_{ref}/10$. The matrix production rate per cell q^{cell} was set to 3×10^{-12} g cell^{-1} h^{-1}. This value for q^{cell} was derived based on the case of an initial cell seeding density of 10 million cells cm^{-3}, free swelling culture in 2% agarose with medium containing 10% serum, where matrix accumulation showed a linear increase in time over 42 days [125], the percentage wet weight GAG and collagen were pooled and a construct density of 1 g cm^{-3} was assumed (natural cartilage: 1.15 g cm^{-3} [46]). Note that the value for q^{cell} is an underestimate, since it was based on matrix accumulation data in the construct and did not account for matrix molecules lost to the medium.

To evaluate the functional properties resulting from matrix accumulation, the chondrocyte seeded construct was modeled as a porous medium, assuming linear elasticity. Hooke's law in confined compression is given by Eq. (3.3):

$$\sigma_e = Ha\,\varepsilon_z, \tag{3.3}$$

where σ_e [Pa] is the effective stress, Ha [Pa] the aggregate modulus and ε_z [-] the engineering strain. Darcy's law is given by Eq. (3.4):

$$Q = -K\vec{\nabla}p, \tag{3.4}$$

where Q [m s^{-1}] is the specific discharge, or apparent fluid flux, K [m^4 N^{-1} s^{-1}] the hydraulic permeability and p [Pa] the fluid pressure. It was assumed that only the bound matrix component c_b contributes to the construct's mechanical properties and that the matrix is immediately functional upon immobilization. Based on global, i.e. tissue scale, correlations, expressions of the following form were selected for the local mechanical properties as a function of c_b, Eqs. (3.5,3.6) [123, 181, 186]:

$$Ha = Ha_0 + A_{Ha}c_b, \tag{3.5}$$

where Ha_0 is the scaffold aggregate modulus and A_{Ha} the proportionality constant with c_b.

$$log_{10}\left(\frac{K}{K_0}\right) = -A_K c_b, \tag{3.6}$$

where K_0 is the scaffold permeability and A_K the proportionality constant with c_b. Values for A_{Ha} ranging from 2.2 MPa cm^3 g^{-1} to 10 MPa cm^3 g^{-1} can be derived based on global correlation relations [123, 150, 181, 186] and the GAG to collagen synthesis ratio from the case considered for q, see above [125]. The lower value of $A_{Ha} = 2.2$ MPa cm^3 g^{-1} was used, which was derived for agarose culture [123], reflecting a lower degree of molecular ECM organization than mature tissue. Since the global effective stiffness can underestimate the local stiffness, depending on the local distribution, also $A_{Ha} = 5$ MPa cm^3 g^{-1} was considered. In a similar manner $A_K = 19$ cm^3 g^{-1} was derived [186], which was also varied to $A_K = 50$ cm^3 g^{-1}.

The aggregate modulus Ha of the cell free 2% agarose gel was set to 6 kPa [122, 124] and the permeability K to 6.61×10^{-13} m^4 N^{-1} s^{-1} [69]. For the Poisson's ratio ν of the matrix and scaffold a value of 0.1 was used, based on fetal and calf cartilage [189]. The experimental variability in cell properties has only a limited effect on the effective global modulus and permeability [190]. Therefore the cell properties were kept constant at the following values: $Ha = 1$ kPa , $K = 10^{-15}$ m^4 N^{-1} s^{-1} and $\nu = 0.4$ [71, 88].

The finite element package SEPRAN was employed for the numerical implementation [159]. The transport problem Eq. (3.1,3.2) was solved for a period of 56 days. Matrix synthesis was prescribed as a line-source on the cell edge, assuming an RVE thickness equal to the in-plane cell stacking distance. No transport within the cells was considered. Periodical boundary conditions were applied for the concentration on the RVE edges. 6-Node triangular elements and Crank-Nicholson time integration with a time step of 8 h were used. For the elasticity problem plane strain, linear elastic, 3-node triangular elements were used. The Darcy problem was solved employing lowest-order Raviart-Thomas mixed finite elements [90, 172], for the resulting system of equations an iterative solver (BiCGstab) was used. Coefficients were taken constant per element and adjusted according to the element-averaged bound concentration c_b.

To determine the RVE-averaged aggregate modulus a homogenization technique was adopted, which was developed by Smit in the context of a micro-macro multilevel finite element approach [15, 93, 162]. Briefly, periodical boundary conditions for the RVE edge displacements are applied. Because of these periodical boundary conditions the averaged RVE stress and deformation can be described by the displacements and forces in three RVE corner points. The averaged stiffness can then be determined via a variation expression of the averaged RVE stress, which involves the static condensation of the full RVE stiffness matrix in order to determine the relation between corner point force and displacement. The RVE averaged hydraulic permeability in the undeformed state was evaluated using Darcy's law by applying an arbitrary pressure gradient over the RVE and monitoring the resulting total edge flux. Periodical boundary conditions were prescribed for the fluid flux through the RVE edges. To account for different patterns of cell distribution, the averaged aggregate modulus and permeability were determined every two days for 5 different cell distributions in two directions (Fig. 3.1b). Unless explicitly stated otherwise, the reference parameters have been used.

3.3   Results

A representative distribution of the bound matrix c_b at $t = 56$ days is depicted in Fig. 3.2a-c, for the different PG diffusion coefficients considered (D_{ref}, $D_{ref} \times 10$, $D_{ref}/10$). Fig. 3.3 shows the resulting global aggregate modulus and permeability as a function of culture time. The standard deviations in Fig. 3.3, 3.5 and 3.6 are due to the averaging over the different microstructures (Fig. 3.1b). The homogeneous matrix distribution (Fig. 3.2a) results in approximately the same global functional properties (Fig. 3.3) as the same amount of matrix distributed more inhomogeneously (Fig. 3.2b). Only for the case with very localized pericellular matrix deposition (Fig. 3.2c), the global aggregate modulus is significantly lower (Fig. 3.3a). In addition the standard deviation increases, which is a measure of the influence of the microstructure. The global permeability however is not affected (Fig. 3.3b). This is an unexpected result since the local flow pattern is clearly altered by zones of more intense matrix accumulation (Fig. 3.4).

Increasing the influence of the bound matrix concentration on the aggregate modulus and permeability (higher A_{Ha} and A_K) leads to generally the same observations. The global permeability however, shows more variation as a function of matrix distribution (Fig. 3.5). The effect of varying the binding coefficient k_b and degradation coefficient k_d can be seen in Fig. 3.6a-b and Fig. 3.6c respectively. Since the effective transport distance is determined by a combination of diffusion and binding, k_b has been varied to a faster binding rate of 3.4×10^{-5} s^{-1}, a value corresponding to a lowest half-time of 5.7 h reported for the conversion of low-affinity proteoglycan monomers to a form with a high binding affinity [152], which has been assumed to be rate limiting [41]. Comparing Fig. 3.3a with Fig. 3.6a, the faster binding results in a larger standard deviation for the reference diffusion coefficient and produces a small difference between D_{ref} and $D_{ref} \times 10$. Thus the faster binding rate extents the influence of the microstructure to higher diffusion coefficients, due to

Concentration: min = 0.018, max = 0.024

(a)

Concentration: min = 0.0092, max = 0.049

(b)

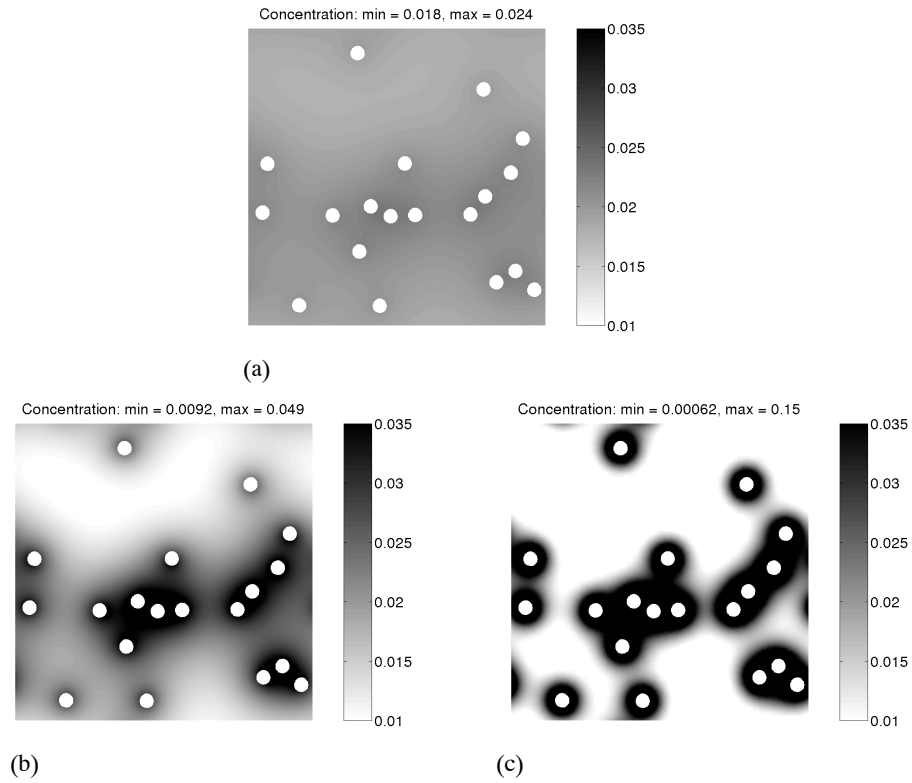Concentration: min = 0.00062, max = 0.15

(c)

Figure 3.2: *Concentration of immobilized extracellular matrix components, c_b [g cm^{-3}], at $t = 56$ days for different diffusion coefficients, (a); $D_{ref} \times 10$, (b); D_{ref}, (c); $D_{ref}/10$. Periodical boundary conditions were applied at the RVE edges. Note that the colorbar limits do not represent the full concentration range.*
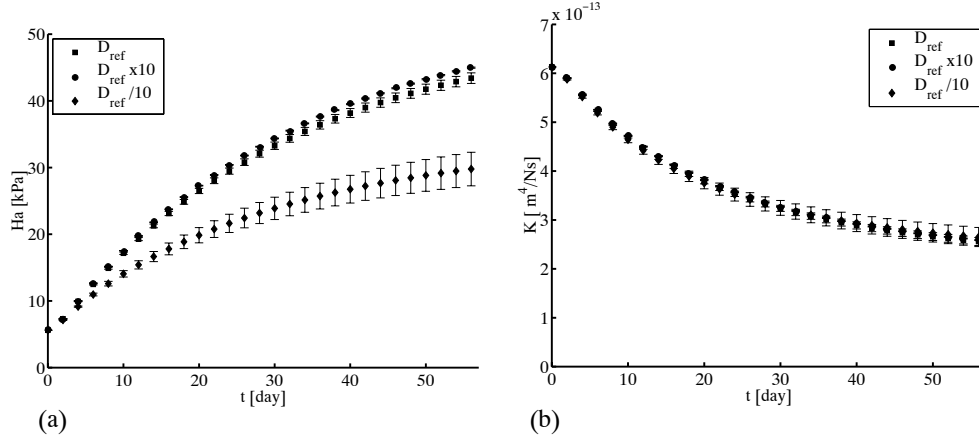
Figure 3.3: *Evolution of the overall aggregate modulus Ha (a) and hydraulic permeability K (b) as a function of time, for different diffusion coefficients. Results were averaged over 5 RVE's in two directions.*

more localized matrix deposition. As can be observed in Fig. 3.6b, a slower binding rate $k_b^{ref}/10$ results in an initial delay and eliminates any diffusion dependence. Even slower binding increases the delay and reduces the absolute value of Ha reached within the computed time-scale (data not shown). For a slower degradation rate $k_d^{ref}/10$, Ha does not level off as a function of time (Fig. 3.6c). The dependence on the local matrix distribution remains the same however (Fig. 3.3a, 3.6c). In general, differences in averaged permeability between the cases with different diffusion coefficients tend to be less pronounced than differences in the aggregate modulus (data not shown).

3.4   Discussion

A computational homogenization approach was adopted to determine to which extent the evolution of the functional properties of tissue engineered cartilage constructs can be attributed to the microscopic distribution of newly synthesized matrix components. To assess the influence of the extracellular matrix distribution, different local distributions were considered from which global mechanical properties were derived.

The computed ECM patterns for the lower diffusion coefficients (D_{ref}, $D_{ref}/10$) were qualitatively similar to experimental distributions of proteoglycans found in agarose culture, with newly synthesized proteoglycans located primarily in the pericellular region (Fig. 3.2b, 3.2c) [19, 122, 143]. The collagen deposition on the other hand tends to be more homogeneous, which correspond with the $D_{ref} \times 10$ case (Fig. 3.2a) [122, 143]. Pericellular GAG profiles in agarose, determined by quantitative autoradiography, were of similar shape as those computed in the model [143]. Moving outwards from the cell, the sharp drop in matrix concentration found experimentally, is in accordance with a diffusion-binding model as employed in this

(a)

(b)

(c)
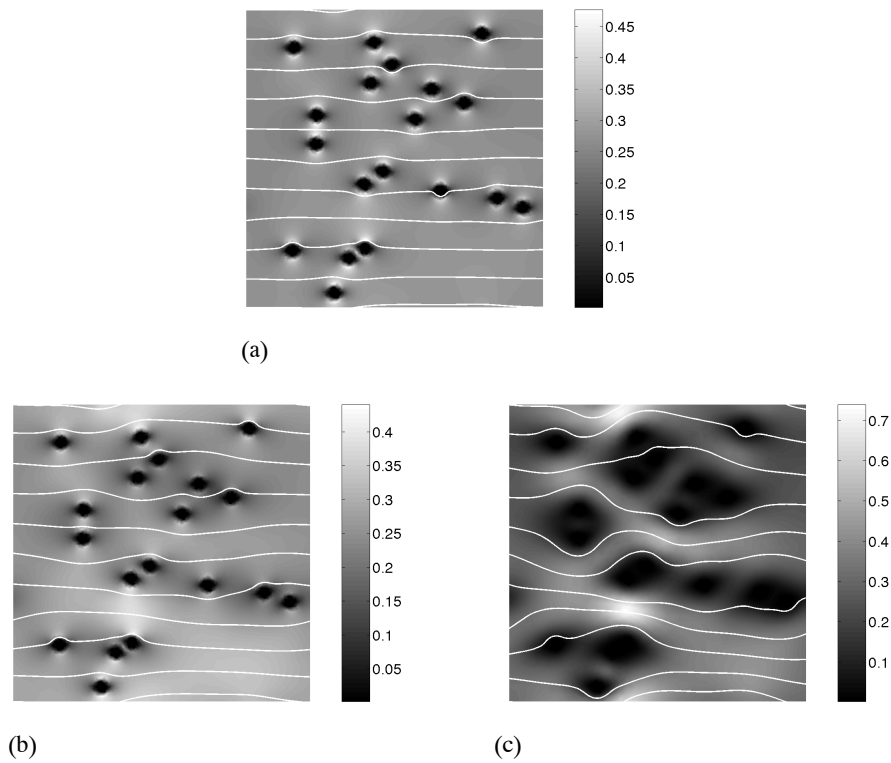
Figure 3.4: *Visualization of the fluid flux patterns resulting from microscopic inhomogeneity at $t = 56$ days, (a); $D_{ref} \times 10$, (b); D_{ref}, (c); $D_{ref}/10$. A negative pressure gradient was applied from left to right, the fluid flux was subjected to periodical boundary conditions and deformation was suppressed. Gray values indicate the absolute value of the local Darcy flux. Given values provide only a relative comparison. Depicted streamlines contain equal mass flux. Note that streamlines on the left and right edge do not necessarily coincide.*

study. Also the experimental finding that the main PG deposition occurred within 10 μm from the cell membrane corresponds very well with the reference case in Fig. 3.2b, where this distance is determined by diffusion and binding. The time course of matrix formation has been studied in alginate culture, where it has been observed that by 6 weeks multiple islands of matrix have joined together as can be seen in Fig. 3.2b for the model at 56 days [28]. At 12 weeks homogeneous GAG staining was observed which was attributed to alginate degradation. Related to this, the importance of matrix diffusivity has been demonstrated by modulating the degradation behavior of PEG hydrogels [16]. It was found that collagen II was either localized in the pericellular region or became distributed throughout the construct as a function of the hydrogel degradation properties.

In general the calculated increase in aggregate modulus Ha and decrease in permeability K are well within the range found for cartilage tissue engineering, considering the major differences in culture conditions [19, 118, 122–125, 181]. Based on the distinct matrix distributions in Fig. 3.2a-b and the similar resulting mechanical properties in Fig. 3.3, it can be concluded that the overall stiffness and permeability are to a large extent insensitive to differences in local matrix distribution. From the parameter variations in binding and degradation rate, it appears that the amount of matrix and the intrinsic assembly and turnover time of the matrix components are more important in determining the evolution of the functional properties. Therefore the redistribution of matrix components by dynamic mechanical compression may play only a limited role. Alternatively, for the same ECM content compression may also passively increase tissue properties by altering the functional organization and entanglement of the ECM network. A continuous increase in stiffness with time has been observed in several studies [19, 28, 118], while others have found an initial increase followed by a plateau [122, 123, 125, 149]. As shown in Fig. 3.6c a continuous increase in stiffness can simply be the result of a lack of degradation. A sudden rise in stiffness due to contact between cell associated matrix zones cannot be observed for the diffusion-binding model, indicating an important role of progressing ECM molecular organization. The results in Fig. 3.6b show that an initial lag time, followed by an increase in stiffness which gradually levels off, can be explained from a binding and degradation process without the need for a distribution related effect. However this does not mean that the diffusion of ECM does not need to be considered for cartilage tissue engineering. As shown in this study, the importance of matrix distribution will depend to a large extent on the diffusive properties of the construct. The $D_{ref} \times 10$ corresponds in fact to the situation in which the gel is absent, while for $D_{ref}/10$ the mechanical properties are affected considerably by distribution as the matrix is very localized (Fig. 3.2c, Fig. 3.3a).

In general, the model assumption to apply global relations between tissue constituents and stiffness at the local level will underpredict global stiffness, in case the local matrix distribution plays a role. To have an indication of the predictive value of the model, the increase in Young's modulus over 56 days ($\Delta E \sim 40$ kPa) in the case from which the matrix synthesis rate was derived [125], was compared with the model predictions, which use a relation based on the correlation between global matrix content and aggregate modulus established in a separate study by the
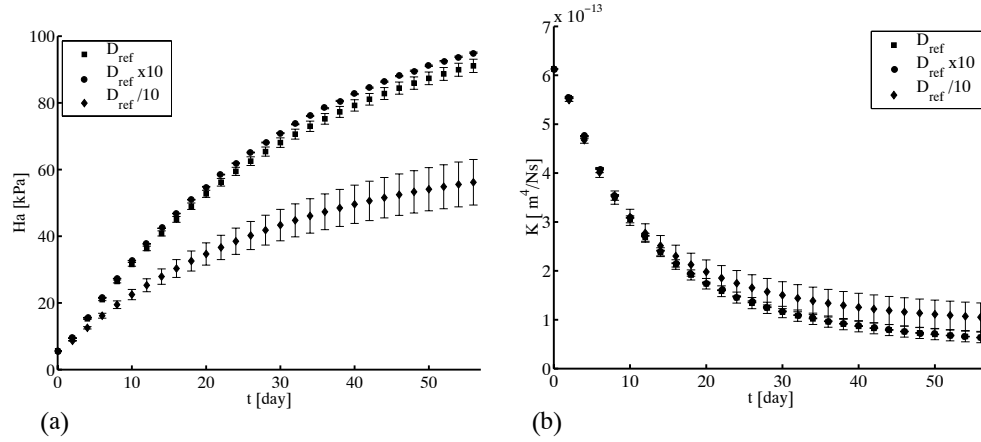
Figure 3.5: *Parameter variation assuming a greater influence of the bound matrix concentration on the local mechanical properties, Eq.(3.5,3.6); $A_{Ha} = 5$ MPa cm^3 g^{-1}, $A_K = 50$ cm^3 g^{-1}. (a); Global aggregate modulus Ha, (b); Hydraulic permeability K.*

same group [123]. Although the predicted values ($\Delta E = 39$ kPa, $\Delta E = 37$ kPa) for $D_{ref} \times 10$ and D_{ref} corresponded very well for this specific case, no general agreement could be observed for different culture conditions and in the absence of a distribution related effect the model reduces to the global relations.

The primary objective of this study however, was not to give an accurate prediction of the evolution of the mechanical properties of a tissue engineered construct, but to isolate and assess the effect of matrix distribution. Therefore, as a clear reference, simple assumptions were made for the dependence of the functional properties on the matrix concentration and a constant matrix synthesis was assumed, neglecting any cellular regulation mechanisms. A model aiming at predicting the temporal development of the mechanical properties more precisely should include the functional interactions between the separate PG and collagen components and should take into account the time course of the synthesis of specific matrix components, which is affected by factors like mechanical stimulation, growth factors, the amount of matrix present, nutrient availability and cell proliferation [19, 122, 125, 134, 182]. For example, in contrast to the constant matrix synthesis rate assumed here, it has been demonstrated in several studies that GAG synthesis decreased as a function of time [19, 122], while collagen production can also increase in later stages of culture [122].

To provide a clear comparison between the different matrix distribution cases only the initial, linear elastic, stiffness and undeformed permeability were compared. The relation between the local aggregate modulus Ha and the amount of ECM present was assumed to be linear based on global correlations, while for example the proteoglycan swelling pressure as a function of PG concentration and the collagen network tensile behavior are known to be highly nonlinear [7, 20]. A nonlinear increase in local stiffness as a function of ECM concentration would increase the
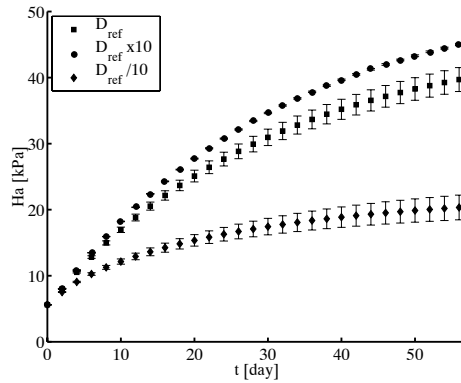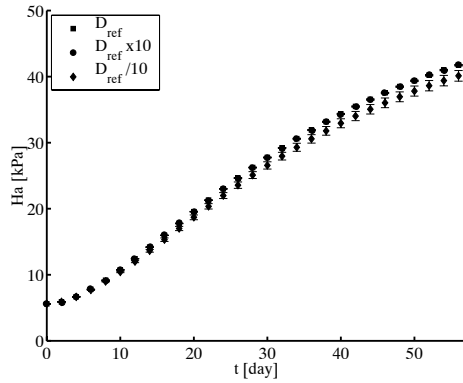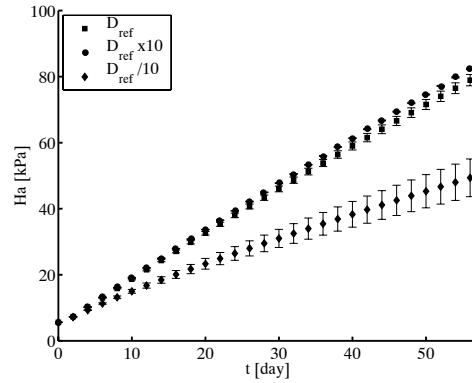
Figure 3.6: *Parameter variation of matrix assembly and turnover time, Eq. (3.1,3.2). Global aggregate modulus, (a); $k_b = 3.4 \times 10^{-5}\ s^{-1}$, (b); $k_b = k_b^{ref}/10$, (c); $k_d = k_d^{ref}/10$. Differences in permeability are much less pronounced, data not shown.*

sensitivity to the microscopic matrix distribution. The matrix distribution may also have more effect on the averaged stiffness at lower cell concentrations, since transport distances are longer. At higher cell concentrations the matrix distribution will be more homogeneous. Although the basic mechanisms remain the same, the results may be affected by the fact that only a two-dimensional RVE has been considered. In general, contact between homogeneous cylindrical zones will be stiffer than in case of spheres. In addition the probability of aligned contact is higher. On the other hand, since the same amount of matrix is distributed by diffusion in a cylindrical, respectively spherical manner, the gradients in local stiffness will be sharper for the spherical case.

In the present study it has been assumed that the diffusion coefficients remain constant during the culture period, while in reality the accumulation of ECM components can also progressively decrease the diffusivity [17, 97, 131], leading to a more localized matrix distribution. In addition it has been shown that diffusion of proteoglycans is highly dependent on concentration [36]. The concentration consists of both mobile newly synthesized matrix molecules as well as degraded matrix molecules. However, in the model we have, as a first estimate, considered the diffusion of matrix molecules to be independent of concentration (constant D). Nonbinding degraded matrix molecules can therefore be considered as a seperate species which does not influence the transport of mobile newly synthesized matrix molecules. For this reason, transport of degraded matrix molecules was not further considered in this study. When such concentration dependency is introduced in the model also the transport of degraded matrix molecules must be included. In agarose culture it has been observed that at high concentrations matrix components not only diffuse through the gel, but that newly formed matrix which is immobilized pericellularly, can also push away the gel material [19]. To account for this the modeling approach should be extended to include volumetric growth, possibly stress free, or the results of PG swelling, in which case separate PG and collagen components need to be distinguished [7, 92].

It can be concluded that the evolution of the global permeability and aggregate modulus of tissue engineered cartilage constructs appears to a large extent insensitive to the microscopic matrix distribution. Based on this low sensitivity it is also unlikely that dispersion of matrix components by mechanical compression alone, can significantly enhance tissue properties. It has been shown however that the global stiffness can be significantly reduced in case the microscopic matrix distribution is very localized, which can occur when matrix accumulation poses increasingly severe restrictions on transport. In addition a larger sensitivity to matrix distribution cannot be excluded in case of a non-linear dependence of the local stiffness on matrix constituents. For cartilage tissue engineering the results imply that the diffusive properties of the construct will determine to a large extent whether matrix distribution becomes important. Modeling matrix deposition as a simple diffusion, binding and degradation process does not result in a sudden increase in global stiffness as a result of contact between cell associated matrix, instead the time evolution of the global aggregate modulus is dominated by the matrix's binding and degradation behavior. The present results emphasize the need for caution in the visual interpretation of tissue functionality from histology. Also, since the matrix distribution itself cannot

fully explain the lack of correlation between global measurements of collagen and PG content and the mechanical properties of tissue engineered constructs, complementary global measurements of intrinsic matrix properties like crosslink density remain essential [92]. Apart from molecular organization and matrix distribution on the microscopic scale, measurements of mechanical properties may be complicated by tissue scale inhomogeneities in matrix distribution, which may be dominating measured mechanical properties.

Microscopic computational models can be used for the optimization of bioreactor culture conditions and protocols, with respect to functionality and culture time, as a function of the initial cell seeding density. Since, in principle, the time evolution of matrix deposition in relation to tissue functionality can be predicted, also the effectiveness of stimulating matrix synthesis, by growth factors and/or mechanical compression, at different times in culture can be assessed. It is also known that the presence of a pericellular matrix plays an important role in mediating the cell response to mechanical stimulation. On the other hand, the development of a pericellular matrix during culture, will gradually shield cells from externally applied deformation [19], possibly reducing the effect of mechanical stimulation protocols. Model predictions of the local cell deformation can be used to adjust the level of global deformation necessary to achieve optimal stimulation. Apart from tissue engineering protocols, model applications lie also in the optimization of, possibly larger pore, scaffolds in relation to matrix deposition. In cartilage explants compression has been shown to introduce direction dependent matrix deposition at the cellular level [141]. Since effects of compression induced direction dependent diffusion, convective transport and cell alignment may be readily incorporated, the computational approach adopted in the present study may prove especially useful to study and modulate the development of anisotropy in tissue engineered constructs.

Chapter 4

Nutrient utilization by bovine articular chondrocytes: a combined experimental and theoretical approach[1]

Abstract

A combined experimental-numerical approach was adopted to characterize glucose and oxygen uptake and lactate production by bovine articular chondrocytes in a model system. For a wide range of cell concentrations, cells in agarose were supplemented with either low- or high glucose medium. During an initial culture phase of 48 h, oxygen was monitored non-invasively using a biosensor system. Glucose and lactate were determined by medium sampling. In order to quantify glucose and oxygen uptake, a finite element approach was adopted to describe diffusion and uptake in the experimental model. Numerical predictions of lactate, based on simple relations for cell metabolism, were found to agree well for low glucose, but not for high glucose medium. Oxygen did not play a role in either case. Given the close association between chondrocyte energy metabolism and matrix synthesis, a quantifiable prediction of utilization can present a valuable contribution in the optimization of tissue engineering conditions.

---

[1]The contents of this chapter have been submitted for publication: B.G. Sengers, H.K. Heywood, D.A. Lee, C.W.J. Oomens, D.L. Bader, *J. Biomech. Eng.*

4.1   Introduction

In-vitro tissue engineering is considered a promising strategy in articular cartilage repair. After chondrocyte isolation and expansion, the cells are seeded in a three dimensional scaffold, which is gradually replaced by newly formed extra cellular matrix (ECM). Eventually, the cartilage construct is required to possess mechanical functionality that enables it to withstand *in-vivo* loading conditions post implantation. Therefore, in order to promote matrix synthesis and to obtain sufficient quantities of organized ECM, a high cell density combined with a high cellular activity is advantageous [48, 49]. The high rate of nutrient utilization associated with these conditions, combined with the inherent limitations in diffusive transport in constructs of clinically relevant dimensions, raises the issue of adequate nutrient supply [111, 125]. Depending on the culture conditions, large gradients in cell viability and/or matrix deposition can arise between the periphery and center of the construct, leading to inferior functional properties, such as stiffness and permeability [117, 181].

Numerous experimental studies have demonstrated the close relationship that exists between matrix synthesis and energy metabolism of chondrocytes [64, 87, 104, 105, 173]. Proteoglycan synthesis has been shown to be affected by nutrition [125], pH [147] and oxygen [34, 80, 86, 94, 103, 113, 132, 153]. Quantification of the uptake and production of basic metabolites, such as glucose, oxygen and lactate, is therefore important in order to evaluate whether a favorable environment for chondrogenesis exists within constructs and to optimize and design culture conditions and protocols. An additional issue is to what extent measured values are representative of specific culture conditions, given the large variability in metabolic rates and the dependence of cell source, culture conditions and differentiation state [164]. A complicating factor is the involvement of cellular regulation mechanisms resulting in large concentration dependencies of nutrient utilization. For example, the dependency of glucose uptake and lactate production on the oxygen concentration has been investigated in various studies. Depending on the culture conditions, a low oxygen level has been shown to increase [94, 113, 132, 146], or decrease [64, 103, 104] glycolysis in articular chondrocytes. An alternative question, whether oxygen consumption is a function of glucose concentration, again revealed the dependence on the initial glucose concentrations [136]. However, a conflict can arise between an accurate measurement of changes in concentration and constant culture conditions. As the composition of the culture medium changes over time, it is important not to rely solely on initial and end point measurements, but to determine concentrations to which cells are actually exposed and respond.

The objective of the present study is to characterize chondrocyte nutrient utilization under tissue engineering conditions by frequent, simultaneous, measurements of multiple metabolites. This approach could examine the relationship between the different metabolites and more specifically, to what extent cellular uptake and production is dependent on medium glucose level and cell concentration. A numerical model was developed based on diffusive transport and simple relationships for chondrocyte metabolism. The model was evaluated using experimental data for glucose, lactate and oxygen concentrations which had been measured simultaneous
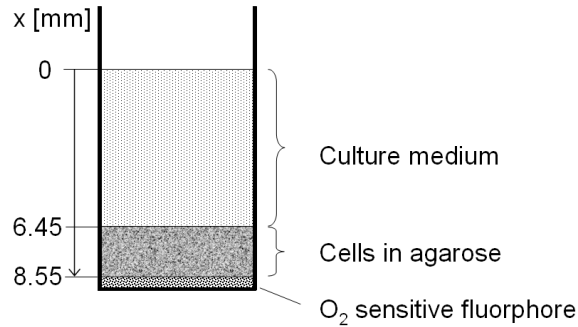
Figure 4.1: *Geometry of an individual well of the 96-well plate set-up. An oxygen sensitive fluorphore is immobilized in a silicon matrix at the well base. 65 μL of cells embedded in 4% agarose was added and supplemented with 200 μL culture medium, giving a total diffusion distance of 8.55 mm from the free surface to the oxygen sensor.*

during the early phase of culture. The numerical model provides an estimation of the spatial profile of glucose, lactate and oxygen which is not provided during experimental monitoring.

4.2 Methods

The experimental protocols have been described in detail by Heywood [76]. Briefly, the experimental setup, as shown in Fig. 4.1, is based on a 96-well plate with an oxygen sensitive fluorphore embedded in a gas permeable matrix at the base of each well (Becton Dickinson Biosciences, Oxford, UK). The cell-seeded agarose constructs were formed by adding 65 μL of 4% ultralow gelling agarose (type IX, SIGMA, Poole, UK), containing bovine articular chondrocytes at concentrations of 1.25, 2.5, 5, 10, 20 and 40×10^6 cell·cm^{-3}, into individual wells. After the agarose had gelled, 200 μL of either low glucose (LG) medium or high glucose (HG) medium was added to each well. The medium consisted of DMEM containing 5.55 mM glucose in case of LG and 22.2 mM glucose in case of HG, supplemented with 16% (v/v) fetal calf serum, 2 μM L-glutamine, penicillin (5 μg·mL^{-1}), streptomycin (5 μg·mL^{-1}), 20 μM HEPES buffer and 0.85 μM L-ascorbic acid (all from SIGMA, Poole, UK). The glucose concentrations in the supplemented media were 5.1 mM and 22 mM, based on experimental measurement. The well plates were placed in a standard humidified incubator at 5% CO$_2$ and 37 °C. At 0.5, 1, 2, 4, 8, 12, 18, 24, 36 and 48 hours of incubation, 3 wells for both high and low glucose medium were sacrificed and glucose and lactate assays were performed, according to Heywood [76]. In parallel, using a separate plate prepared using the same cell isolation, the fluorescence intensity of each well was measured at the same time points to determine oxygen concentration.

Theoretically, the experimental setup in Fig. 4.1 can be represented as a one-dimensional diffusion-uptake problem, in which a medium zone and an agarose zone containing the cells can be distinguished. The metabolite concentrations are governed

by the solute mass balance including Fick's law for diffusion:

$$\frac{\partial n^f c^\beta}{\partial t} - D\frac{\partial^2 c^\beta}{\partial x^2} = q^\beta, \tag{4.1}$$

where c^β [mol·m^{-3}] is the solute concentration in the fluid phase, n^f is the fluid volume fraction [-] ($n^f = 1$ in the medium), D [m^2·s^{-1}] is the effective diffusion coefficient and q^β [mol·m^{-3}·s^{-1}] is a source term that represents cellular utilization or production. The number of different solutes taken into account was limited to the measured metabolites, glucose, lactate and oxygen. To model the experimental data the following procedure was adopted: First, the glucose uptake was determined by fitting the experimental data, based on a simple relation for cellular uptake. Subsequently, the lactate concentrations were predicted based on the glucose uptake alone and compared with the values measured in the experiments. Next it was evaluated whether lactate estimation could be improved by extending the model structure to take into account oxygen. For this purpose uptake relations for oxygen were proposed, based on the experimental results and fitted to the data. To represent glucose uptake, a Michaelis-Menten relation was assumed for q^{glc} in Eq. (4.1).

$$q^{glc} = -\frac{V^{glc}c^{glc}}{K_m^{glc} + c^{glc}}\rho^{cell}, \tag{4.2}$$

where V^{glc} [mol·cell^{-1}·s^{-1}] is the maximum uptake rate, K_m^{glc} [mol·m^{-3}] is the half maximum rate concentration and ρ^{cell} [cell·m^{-3}] is the cell density. It has been found that articular chondrocytes display a ratio of lactate production to glucose uptake close to 2:1, even under aerobic conditions [103, 104]. Therefore, in order to predict lactate, the following expression for the lactate production term q^{lac} in Eq. (4.1) was used as a first estimate:

$$q^{lac} = -2q^{glc}. \tag{4.3}$$

However, lower lactate to glucose ratios, approximately 1.6 - 1.7, have been found in bioreactor studies and it is well established that in principle chondrocytes can use both anaerobic and aerobic metabolic pathways [132, 153, 173]. Therefore, as opposed to the purely anaerobic case in Eq. (4.3), an alternative approach was considered, in which it is assumed that all oxygen uptake is fully used to break down glucose aerobically [1]:

$$q^{lac} = -2q^{glc} + \frac{1}{3}q^{ox}, \tag{4.4}$$

where q^{ox} is the oxygen uptake rate. For this purpose the oxygen uptake rate has to be determined. As a first step a Michaelis-Menten relation was assumed for q^{ox}:

$$q^{ox} = -\frac{V^{ox}c^{ox}}{K_m^{ox} + c^{ox}}\rho^{cell}, \tag{4.5}$$

where V^{ox} [mol·cell^{-1}·s^{-1}] is the maximum oxygen uptake rate and K_m^{ox} [mol·m^{-3}] is the half maximum rate concentration. However, simple uptake and diffusion alone

cannot account for the time course of the measured oxygen level (Results section). Therefore V^{ox} was assumed to be a function of time. A phenomenological time-dependent relation for oxygen consumption was introduced:

For $t < t_m$:

$$V^{ox} = V^{ox}_{max}(1 - e^{-K_t t}) \tag{4.6}$$

and for $t >= t_m$:

$$V^{ox} = V^{ox}_{max}((1 - e^{-K_t t}) - A^{ox}(1 - e^{-K_{t2}(t - t_m)})). \tag{4.7}$$

In Eq. (4.6), V^{ox} increases as a function of time, with time constant K_t, to V^{ox}_{max}. Above a critical time t_m, the second negative term in Eq. 4.7 increases, with time constant K_{t2}, until V^{ox} is reduced with a fraction A^{ox} for large t.

For the parameter estimation of glucose, K^{glc}_m in Eq. (4.2) was fixed at 0.35 mM [188]. Only V^{glc} was fitted based on a least squares criterion. For this purpose, the experimental glucose values at all time points were compared to the computed mean glucose concentration in the medium zone of the model. V^{glc} was determined for LG and HG medium and for every cell concentration separately. For oxygen K^{ox}_m in Eq. (4.5) was set at 6 μM [74]. The parameters V^{ox}_{max} and K_t in Eq. (4.6) and when appropriate, t_m, K_{t2} and A^{ox} in Eq. (4.7), were fitted simultaneously, on a least squares basis, by comparing the measured and computed oxygen concentrations at the base of the well for all time points. In Eq. (4.1) the diffusion coefficient D_{medium} in the medium was set at $D^{ox}_0 = 3.0 \times 10^{-5}$ cm$^2 \cdot$s^{-1} for oxygen [74, 107], $D^{glc}_0 = 9.2 \times 10^{-6}$ cm$^2 \cdot$s^{-1} for glucose [2, 174] and $D^{lac}_0 = 1.4 \times 10^{-5}$ cm$^2 \cdot$s^{-1} for lactate [79], which represent values for water at 37 $°C$. From these values the diffusion coefficients in the construct were estimated based on the Mackie and Meares relation: $D_{constr}/D_0 = (n^f)^2/(2 - n^f)^2$ [18, 116], $n^f = 0.96$ for 4% agarose gives $D_{constr}/D_0 = 0.85$ for all solutes [69, 70]. To determine the sensitivity of the model and to assess the influence of the assumed transport parameters on the fitted uptake rates, a parameter variation study was carried out. Based on measurements, the initial glucose values were set at 5.1 mM and 22 mM for LG and HG medium, respectively. The agarose construct was prepared from equal volumes of LG medium containing the cells and an 8% solution of agarose in Earle's balanced salt solution (SIGMA, Poole, UK), containing 5.5 mM glucose. Therefore the initial value for glucose in the agarose zone was set at 5.3 mM (Fig. 4.1). The initial value for oxygen was set at 205 μM in both the medium and agarose zone. An essential boundary condition of 205 μM was applied at the well surface. In the medium zone, the initial value for lactate was set to the measured medium value of 2.3 mM. In the agarose zone the initial lactate value was set at 1.2 mM.

A finite element approach was adopted to solve Eq. (4.1) numerically [160]. Briefly, the experimental setup can be represented by one-dimensional finite elements. For this purpose a standard Galerkin linear diffusion element was implemented in Matlab (version 6.5). The transport and source term equations were solved separately using Strang operator splitting [81]. Crank-Nicholson time integration was used for the transport term and Runge-Kutta time integration for the biokinetic source term. The number of elements used was 47. The element size was refined around the transition from medium to agarose and a time step ranging from 0.01 h to 0.1 h was employed.

Table 4.1: *Maximum rates of glucose uptake by chondrocytes at different cell densities, cultured in medium at two glucose levels.*

Cell densities [$\times 10^6$ cell$\cdot$cm^{-3}]	LG: V^{glc} [$\times 10^{-13}$ mol$\cdot$cell$^{-1}\cdot$h^{-1}]	HG: V^{glc} [$\times 10^{-13}$ mol$\cdot$cell$^{-1}\cdot$h^{-1}]
40	1.4	0.65
20	1.0	0.80
10	1.1	1.1
5	1.3	1.2
2.5	1.3	2.0
1.25	1.3	3.1

4.3   Results

For the case of LG medium, the glucose measurements and the computed mean medium glucose, as a function of time, are shown in Fig. 4.2a, for six separate cell densities. The computed spatial distribution of glucose throughout the well is most distinct at high cell densities, therefore the results for 40×10^6 cell$\cdot$cm^{-3} are shown in Fig. 4.2b, with 1 h intervals. The corresponding results for HG medium are shown in Fig. 4.3. The experimental data show that for LG medium almost all glucose is consumed within 48 h for 5, 10, 20 and 40×10^6 cell$\cdot$cm^{-3}, while for HG medium some glucose remains, even at high cell densities. From the numerical results in Fig. 4.2b it can be observed, that for LG medium glucose is consumed rapidly by the cells in the agarose construct and that, as glucose diffuses inwards, large gradients develop. For HG medium in Fig. 4.3b the situation is somewhat different. A large difference in initial glucose between the medium and the construct exists, leading to an initial rise in the concentration within the construct, due to diffusion inwards from the surrounding medium and then, in the course of time, the glucose level reduces due to cellular uptake. The values determined for the maximum glucose uptake rate, V^{glc}, are given in Table 4.1. For LG medium the uptake rates are fairly constant over the different cell densities, while for HG large differences exist, with increasing uptake associated with the low cell densities. The experimental values and the computed lactate prediction based on a simple 2:1 ratio between lactate production and glucose uptake are shown in Figs. 4.4a and 4.5a, for LG and HG respectively. In general, the numerical results for the LG case correspond well to the experimental data, whereas for HG medium, lactate production is considerably overpredicted by the model. Nonetheless a small underprediction is evident in the final lactate for LG medium and 40×10^6 cell$\cdot$cm^{-3}. For LG at low cell densities of 1.25, 2.5 and 5×10^6 cell$\cdot$cm^{-3}, the experimental data show a decline in lactate compared to the numerical predictions, although the end value at $t = 48$ h is represented correctly. The computed spatial lactate distributions in Figs. 4.4b and 4.5b show that the lactate levels within the construct increase sharply, while lactate diffuses outwards into the surrounding medium.

The measured and numerically calculated oxygen levels at the base of the well are presented in Fig. 4.6a for LG medium. The computed spatial oxygen profiles for 40×10^6 cell$\cdot$cm^{-3} are illustrated in Fig. 4.6b, with 1h intervals. Similarly for HG
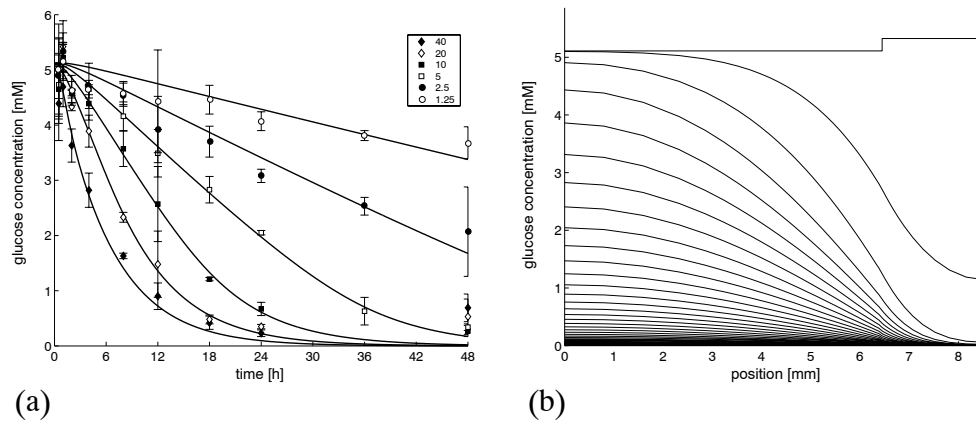
Figure 4.2: *Low glucose. (a): Glucose measurements and the computed mean medium glucose concentration, as a function of time, for 1.25 - 40 $\times 10^6$ cell·cm^{-3}. (b): Computed spatial glucose distribution in the well for 40 $\times 10^6$ cell·cm^{-3}, at 1 h intervals. The free surface is located to the left and the well base to the right. The medium zone extents from 0 - 6.45 mm and the agarose zone from 6.45 - 8.55 mm.*
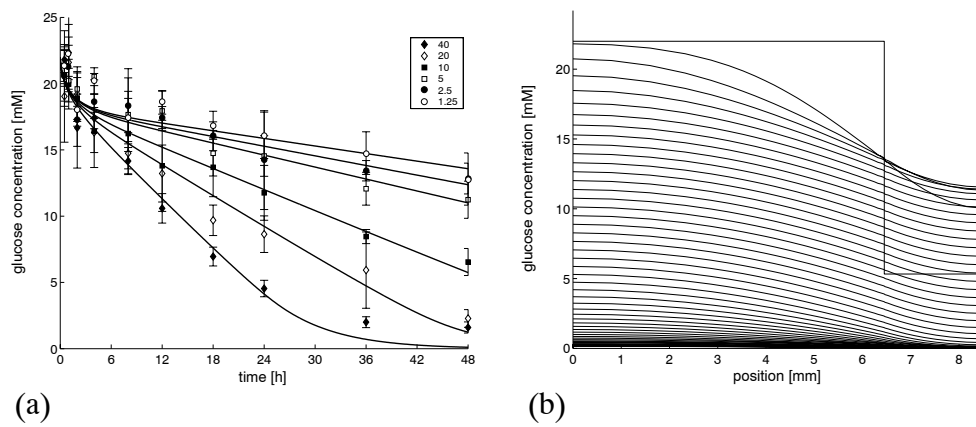
Figure 4.3: *High glucose. (a): Glucose measurements and the computed mean medium glucose concentration, as a function of time, for 1.25 - 40$\times 10^6$ cell·cm^{-3}. (b): Computed spatial glucose distribution in the well for 40$\times 10^6$ cell·cm^{-3}, at 1 h intervals. The free surface is located to the left and the well base to the right. The medium zone extents from 0 - 6.45 mm and the agarose zone from 6.45 - 8.55 mm.*
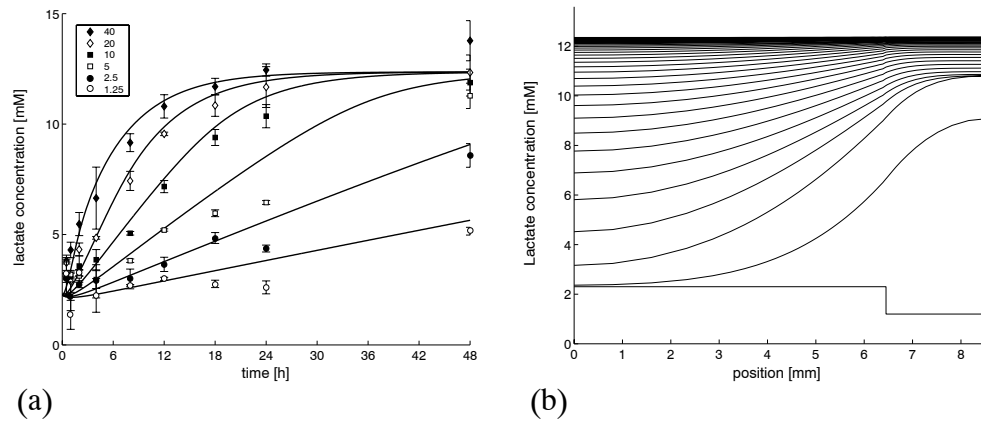
Figure 4.4: *Low glucose. (a): Lactate measurements and the predicted mean medium lactate concentration based on glucose alone Eq. (4.3), 1.25 - 40×10^6 cell·cm^{-3}. (b): Computed spatial lactate distribution in the well for 40×10^6 cell·cm^{-3}, at 1 h intervals. The free surface is located to the left and the well base to the right.*

Figure 4.5: *High glucose. (a): High glucose. (a): Lactate measurements and the predicted mean medium lactate concentration based on glucose alone, Eq. (4.3), 1.25 - 40×10^6 cell·cm^{-3}. (b): Computed spatial lactate distribution in the well for 40×10^6 cell·cm^{-3}, at 1 h intervals. The free surface is located to the left and the well base to the right.*

Table 4.2: *Maximum rates of oxygen uptake by chondrocytes at different cell densities, cultured in medium at two glucose levels.*

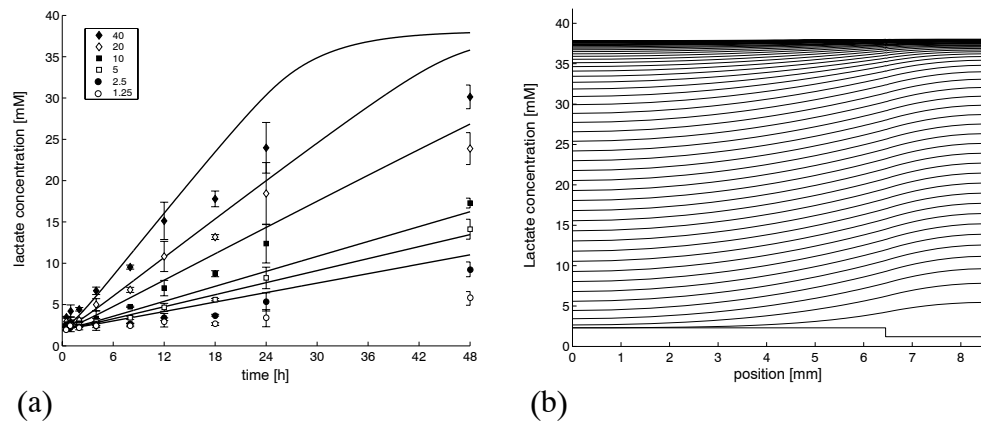| Cell densities [$\times 10^6$ cell·cm^{-3}]	LG: V^{ox}(t = 48h) [$\times 10^{-15}$ mol·cell^{-1}·h^{-1}]	HG: V^{ox}(t = 48h) [$\times 10^{-15}$ mol·cell^{-1}·h^{-1}]
40	4.0	1.7
20	6.7	1.7
10	9.8	2.8
5	6.1	5.6
2.5	7.8	6.3
1.25	7.1	5.7

medium in Fig. 4.7. It was observed that the oxygen level at the base of the well decreases gradually as a function of time, at a rate approximately proportional to cell concentration, until a steady state is reached. A qualitatively different behavior is displayed by the HG case at high cell concentrations of 10, 20 and 40×10^6 cell·cm^{-3}, where at a certain point in time the oxygen concentration starts to increase again. From the computational results in Fig. 4.6b it can be seen that, due to cellular uptake, a linear steady state profile develops, in which oxygen diffuses at a steady rate from the free surface of the well to the construct. Therefore a constant low oxygen level at the base of the well, in Figs. 4.6a and 4.7a, represents a high ongoing uptake. However, it was found that a diffusive lag time alone cannot account for the initial gradual decrease in base oxygen level as a function of time in Figs. 4.6a and 4.7a. An increase in cellular oxygen consumption must play a role, since for the case of constant oxygen utilization a steady state would already be obtained within the characteristic diffusion time scale $t_d = l^2/D = 6.7$ h, where l is the diffusion distance, for all cell concentrations in Figs. 4.6a and 4.7a. Since V^{ox} was considered to increase as a function of time, only the value of V^{ox} at t = 48 h is reported in Table 4.2. The oxygen uptake rate per cell was found to be of the same order for most cases, although for HG at high cell densities the oxygen uptake was clearly reduced (Table 4.2, row 1 - 3, column 2). The numerical lactate predictions based on both oxygen and glucose uptake, Eq. (4.4), are illustrated in Fig. 4.8. The results are similar to the lactate predictions based on glucose alone, as presented in Figs. 4.4a and 4.5a.

The effects of parameter variation on the fitting procedure for the uptake rates are summarized in Tables 4.3 and 4.4, for glucose and oxygen respectively. First the sensitivity of the glucose uptake rate to the precise value of the diffusion coefficient was assessed. A 50% higher (Table 4.3, row 1) and 50% lower (row 2) value for D_0^{glc} were evaluated to cover the range in literature [2, 18, 108, 121, 174]. It was found that the glucose uptake rate was especially sensitive to the diffusion coefficient for LG medium at high cell concentrations (row 1 and 2, column 1). In this case diffusion is limiting and a high uptake rate is required to overcome the transport restrictions and produce the rapid decrease in mean medium glucose found experimentally. The best fit of the experimental data was however obtained for the reference diffusion coefficient (comparison not shown). Since the numerical model was based on the assumption of a perfectly static medium, it was assessed to what extent the results
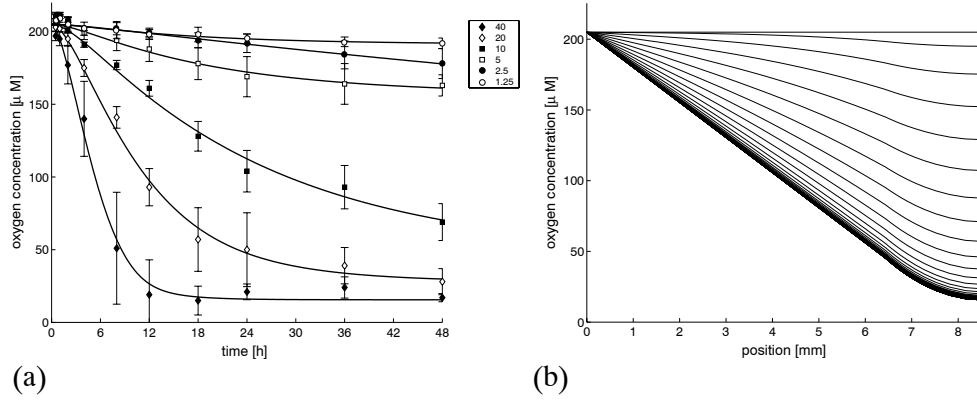
Figure 4.6: *Low glucose. (a): Measured and computed base well oxygen concentration, 1.25 - 40×10⁶ cell·cm⁻³. (b): Computed spatial oxygen distribution in the well for 40×10⁶ cell·cm⁻³, at 1 h intervals. The free surface is located to the left and the well base to the right.*
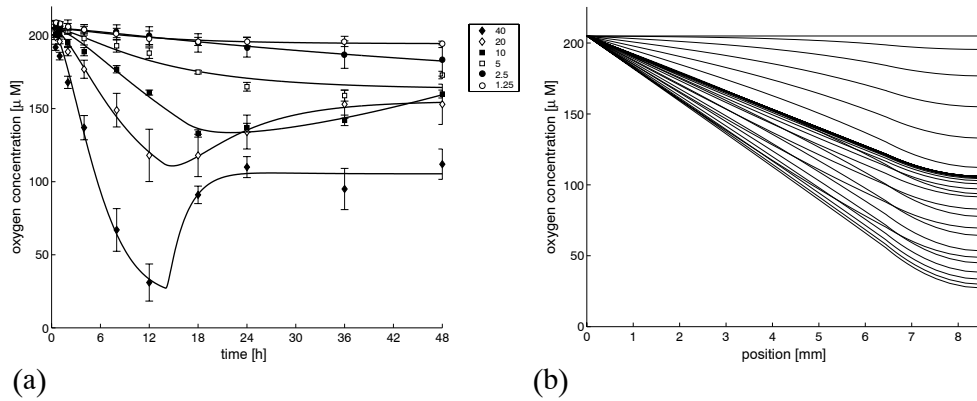
Figure 4.7: *High glucose. (a): Measured and computed base well oxygen concentration, 1.25 - 40×10⁶ cell·cm⁻³. (b): Computed spatial oxygen distribution in the well for 40×10⁶ cell·cm⁻³, at 1 h intervals. The free surface is located to the left and the well base to the right.*
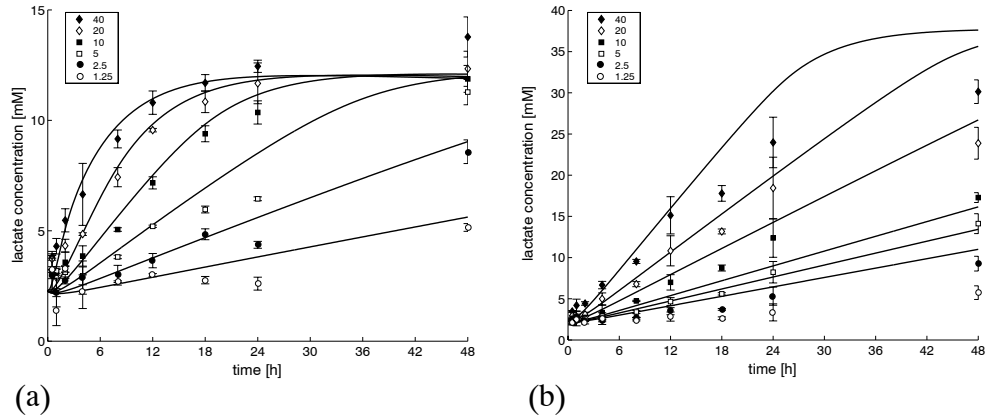
Figure 4.8: *Lactate measurements and the predicted mean medium lactate concentration based on glucose and oxygen, Eq. (4.4), 1.25 - 40×10^6 cell·cm^{-3}. (a): Low glucose. (b): High glucose.*

could be affected by possible mixing of the medium. For this purpose the diffusion coefficient in the medium zone alone was increased by a factor of 10 (Table 4.3, row 3), resulting in a relatively flat spatial concentration profile in the medium. Again the sensitivity was the largest for LG at high cell densities (row 3, column 1) and the reference fit provided a better match for the measurements. Next the assumption on the reduction in diffusivity within the agarose construct was tested. $D_{constr}^{glc}/D_0^{glc}$ was set at 1 (row 4) and at 0.35 (row 5), corresponding to the case in which the construct is completely absent and the case of mature cartilage respectively [18, 115]. Only the lower diffusivity for LG at high cell concentrations was found to affect the uptake rate significantly (row 5, column 1). The Michaelis Menten constant K_m^{glc} was varied to a lower value of 0.1 mM (row 6) and a higher value of 3.5 mM (row 7), which is 10 times the reference value. The relatively low sensitivity for a lower value of K_m^{glc} (row 6) indicates that the constant uptake regime of the Michaelis Menten relation dominated the fit in the reference situation. For a high value of K_m^{glc} the fitted V^{glc} was affected considerably in the LG case for both cell densities (row 7, column 1 and 2), since the glucose concentrations were within the linear Michaelis Menten regime. From the HG results it can be seen that this influence extends up to high glucose concentrations (row 7, column 3 and 4).

For oxygen uptake the LG case was varied alone, since HG takes place in the same concentration range. From Table 4.4 (row 1 and 2) it evident that V^{ox} at t = 48 h is directly proportional to the oxygen diffusion coefficient D_0^{ox}, as the results are dominated by the linear steady state concentration profile in the medium (Fig. 4.6b). The diffusion coefficient of oxygen within the construct was varied from the medium value (row 3) to the value for cartilage [111] (row 4) and no significant influence was revealed. In addition a constant, i.e. concentration independent, oxygen uptake was evaluated by setting K_m^{ox} to zero (row 5). Due to the low value of K_m^{ox} in the reference case, the oxygen uptake was already largely concentration independent and

Table 4.3: *Sensitivity of estimated maximum glucose uptake rate to model parameters.*

Parameter variation	LG 40×10^6 cell·cm^{-3}: % change V^{glc}	LG 1.25×10^6 cell·cm^{-3}: % change V^{glc}	HG 40×10^6 cell·cm^{-3}: % change V^{glc}	HG 1.25×10^6 cell·cm^{-3}: % change V^{glc}
$D_0^{glc*} = D_0^{glc} \times 1.5$	-39 *	-1.3	-4.2	-2.3
$D_0^{glc*} = D_0^{glc} \times 0.5$	+185 *	+4.0	+25 *	+7.0
$D_{medium}^{glc*} = D_0^{glc} \times 10$	-58 *	-2.4	-7.4	-4.5
$D_{constr}^{glc*}/D_0^{glc} = 1$	-4.6	-0.2	-0.6	-0.3
$D_{constr}^{glc*}/D_0^{glc} = 0.35$	+48 *	+1.5	+6.8	+2.7
$K_m^{glc*} = 0.1$ mM	-15 *	-5.6	-3.4	-1.6
$K_m^{glc*} = 3.5$ mM	+146 *	+70 *	+37 *	+20 *

* Indicates changes larger than 10%.

only a moderate effect on $V^{ox}(t = 48h)$ was seen for high cell concentrations (row 5, column 1), where low oxygen levels were attained.

4.4   Discussion

A combined experimental-numerical approach was adopted to characterize glucose and oxygen uptake and lactate production by bovine articular chondrocytes in a model system. It was shown that the use of low glucose compared to high glucose medium resulted in marked differences in oxygen uptake as well as glucose utilization and lactate production. Basic metabolic relationships were evaluated using the computational model. The maximum glucose uptake rates of 0.65 - 3.1×10^{-13} mol·cell^{-1}·h^{-1} found in the present study, corresponded very well with the range reported in literature for chondrocytes in general: 0.56 - 4.0×10^{-13} mol·cell^{-1}·h^{-1} (Converted using 7.7 pg DNA·cell^{-1} [91]) [113, 132, 173, 188]. Although when extreme values are omitted and the comparison is restricted to bovine articular chondrocytes, representative uptake values of the order of 1.0 - 1.4×10^{-13} mol·cell^{-1}·h^{-1} determined in the current study, are twice as high as the values of 0.557 and 0.612×10^{-13} mol·cell^{-1}·h^{-1} reported previously [132, 188]. This may be related to differences in serum content. Depending on the cell source and culture conditions a wide range of oxygen uptake rates have been found in earlier studies: 7.2×10^{-16} - 1×10^{-13} mol·cell^{-1}·h^{-1}. [74, 87, 111, 113, 129, 134, 164, 173]. The oxygen uptake rates in the range of 1.7 - 9.8×10^{-15} mol·cell^{-1}·h^{-1}, determined in the present study, are of the same order as the value of 6.70×10^{-15} mol·cell^{-1}·h^{-1} found for bovine articular chondrocytes in 3D culture [134]. Notably the low cell densities showed a close correspondence.

For LG medium, it was found that the experimental glucose and lactate data could be adequately represented over a wide range of cell concentrations. By contrast, for HG medium lactate predictions based on the experimental glucose uptake led to a considerable overestimation. With respect to the model system, it was shown that no

Table 4.4: *Sensitivity of estimated maximum oxygen uptake rate to model parameters.*

Parameter variation	LG 40×10^6 cell·cm^{-3}: % change V^{ox}(t=48h)	LG 1.25×10^6 cell·cm^{-3}: % change V^{ox}(t=48h)
$D_0^{ox*} = D_0^{ox} \times 1.5$	+54 *	+51 *
$D_0^{ox*} = D_0^{ox} \times 0.5$	-49 *	-51 *
$D_{constr}^{ox*}/D_0^{ox} = 1$	+3.1	+2.4
$D_{constr}^{ox*}/D_0^{ox} = 0.7$	-4.0	-3.3
$K_m^{ox*} = 0 \ \mu$M	-21 *	-3.0

* Indicates changes larger than 10%.

significant differences in lactate prediction occurred whether or not oxygen was taken into account, since the oxygen uptake rate was an order of magnitude lower than the rate of glucose uptake. Therefore, the aerobic consumption of glucose could not account for the overprediction of lactate in the HG case. The glucose missing from the carbon balance could indicate a role for intermediate metabolites, for example glucose-6-phosphate and pyruvate, which were not included in the model. In addition glucose can be stored in the form of glycogen and used for the synthesis of extracellular matrix components [104]. In other studies lactate to glucose ratios varying from 1.3 to 3.9 have been found, depending on the involvement of either oxygen or glycogen supplies respectively [103, 132]. For the cell concentrations employed in the current study, diffusion restrictions in the experimental setup did not fully limit oxygen uptake. Nonetheless, low oxygen levels were reached, which may invoke metabolic regulation mechanisms such as a (negative) Pasteur effect [64, 94, 103, 104, 113, 132, 146]. The glucose and lactate measurements in the present study did not present clear indications regarding the involvement of such mechanisms.

For both LG and HG, a definite upregulation of cellular oxygen uptake as a function of culture time was demonstrated. Remarkably, in case of HG medium the oxygen uptake was shown to decrease again after a certain point in time. In the model the upregulation of the oxygen uptake was represented by a phenomenological time dependent relation. The mechanism behind this increase in oxygen uptake is unknown and could represent an internal cellular mechanism, such as a gradual adaptation to the culture environment after being isolated from the joint. A direct regulation by an external solute concentration, such as glucose or lactate, seems less likely. With respect to glucose, the oxygen levels for LG and HG medium coincide exactly in the initial phase (0 - 12 h), independent of the glucose level. It can also be seen that the decrease in oxygen concentration with time is roughly linearly proportional to cell density (Fig. 4.6a), while if the increase in oxygen uptake was regulated by increasing lactate one would expect a quadratic dependency, since in a first order approximation both the lactate production and oxygen uptake would be linearly proportional with cell density. On the other hand, lactate may provide a mechanistic explanation for the sudden drop in oxygen uptake for HG medium. High lactate levels are reached in the HG case at high cell densities. Although it has been observed that at high lactate concentrations chondrocytes can utilize lactate [136], which would be associated with

an increased oxygen uptake, it has also been shown that lactate inhibits proteoglycan synthesis [147], which can potentially decrease the demand for oxygen [132, 173]. The latter mechanism is not likely however, since measured end point GAG quantities show greater than two times higher GAG content in constructs maintained in HG medium compared to LG medium [76]. Lactate accumulation can also be related to reduced viability [80], resulting in a decrease in overall oxygen uptake, although this was not considered appropriate during the limited time period of the present experiment. Apart from this, the glucose concentration may directly affect the oxygen uptake, as the highest oxygen uptake rates were found for LG compared to HG medium. Therefore, in response to a glucose shortage, the available glucose or glycogen supplies may be used more efficiently by upregulating oxygen consumption, given the much higher energy yield from aerobic, compared to anaerobic, metabolism. For porcine articular cartilage it has been shown that the oxygen uptake was up to 2.35 times higher for zero compared to higher initial glucose values [136]. Although in the current study the time point, at which the oxygen consumption for the LG and HG case start to deviate, corresponds roughly to the depletion of glucose in the LG case, this effect can provide only a partial explanation, since it does not fully explain the behavior in the HG case.

With respect to the model, an important assumption was that the medium was considered to be completely static and transport was considered to be governed solely by diffusion. From the parameter variation it is clear that disturbances causing mixing can affect the estimated uptake values for high cell densities, but not those for low cell densities, where uptake is slow compared to diffusion and no transport restrictions apply. For LG and high cell densities, however, assuming a further homogenization of the medium concentration resulted in a poor fit of the experimental data, indicating that a model based on a well-mixed bulk medium would not have been appropriate. Another issue that can affect the accuracy of the estimated uptake rates are the initial conditions in the construct adopted in the model. Cellular uptake during preparation may have lowered the initial glucose levels in the construct. With respect to the estimated uptake rates it is also important to note that, especially for low cell densities, the measurement variability can be relatively large with respect to the measured differences. In principle, computed concentration profiles can also be affected by an inhomogeneous cell distribution. For the agarose construct, however, the cell distribution is approximately uniform. In addition, based on the relatively slow proliferation rate of chondrocytes, the cell density was considered to be constant within the time span of the current study [102].

The experimental setup employed in the current study enables the screening of large numbers of samples, under 3D culture conditions representative of tissue engineering. In addition, oxygen within the construct can be monitored non-invasively in a straightforward manner. The relatively simple experimental model system can therefore represent a valuable addition to studies using full scale bioreactors, involving a more complicated geometry, fluid dynamic and mechanical loading conditions, which generally can not be operated in large numbers. Numerical modeling is an essential part of the approach and has been found to be valuable in the interpretation of measurements under inhomogeneous, time varying conditions. The key benefit of

the numerical approach is that spatial concentration profiles can be estimated that are not easily available experimentally. Indispensable for this approach, however, is that diffusion coefficients need to be determined accurately. In order to form a real asset for tissue engineering, the eventual goal of computational modeling is to quantitatively correlate culture parameters to the synthesis of functionally important matrix components such as proteoglycans and collagen. The numerical model enables a rapid assessment of various hypotheses on chondrocyte behavior for consistency with the experimental data, in a quantitative manner. Furthermore relationships established in the model system can be used to predict the situation in real bioreactors, as the finite element approach adopted in the current study can be readily extended to multiple dimensions and arbitrary geometry.

Chapter 5

A computational model for the temporal regulation of chondrocyte proliferation and biosynthesis in response to varying dynamic compression regimens[1]

Abstract

Based on previously published experimental work, a computational model was developed for the effect of different dynamic compression regimens on chondrocyte activity. In particular, the balance between proliferation and matrix synthesis can be adjusted by applying different intervals of continuous, or intermittent, mechanical compression. The model can prove a valuable predictor of optimized compression regimens, with respect to the desired cell response and, hence, could be used to exert control over the development of tissue engineered constructs during bioreactor culture. In addition, a cell cycle based model has been proposed to further explore the mechanisms of chondrocyte proliferation, in response to different dynamic loading regimens.

5.1   Introduction

In-vitro mechanical stimulation by dynamic compression has great potential in improving the functional properties of tissue engineered constructs intended for the repair of cartilage defects [82]. Depending on the magnitude of the load, in general, high frequencies are associated with an increase in biosynthetic activity, while static compression, or low frequencies, result in decreased synthesis [19, 39, 98, 101, 124]. Chondrocytes embedded in agarose have been shown to demonstrate a frequency dependent response in both proliferation and proteoglycan (GAG) synthesis, with optimal proteoglycan synthesis at 1 Hz [101]. In various studies, different loading regimens have been employed, in which the dynamic load was applied continuously, or for limited durations during a day [82, 101]. To evaluate the effect of the loading protocol, a systematic study has been carried out, in which chondrocytes embedded in agarose were subjected to different durations of 1 Hz compression within a 48 h culture period (Figs. 5.1a, 5.2a) [33]. It was found that, compared to unstrained controls, GAG synthesis and proliferation were upregulated for each of the loading regimens (Figs. 5.1 and 5.2). Furthermore, a small number of consecutive cycles was associated with the largest increase in proliferation (Fig. 5.1b) and the lowest increase in GAG synthesis (Fig. 5.1c). By contrast, a large number of consecutive cycles yielded the smallest increase in proliferation and the highest increase in GAG synthesis. It was demonstrated that apart from the total number of cycles within the culture period, the intervals over which these cycles were distributed had an even more profound effect. For the same total number of cycles, short intervals were more stimulative for proliferation (Fig. 5.2b), while longer intervals were optimal for enhanced GAG synthesis (Fig. 5.2c).

The apparent balance between the extent to which proliferation and GAG can be stimulated has important implications for tissue engineering. The ability of influencing chondrocyte activity, more or less independently, towards either proliferation or matrix synthesis, provides a direct means of controlling the development of tissue engineered constructs for cartilage repair in different phases of culture. Potentially, computational modeling can be valuable in applying different loading combinations in a predictive and controlable manner. The objective of the present study is to establish a model for the temporal regulation of chondrocyte proliferation and biosynthesis in response to varying dynamic compression protocols. Two modeling approaches will be presented. In the first, both proliferation and GAG synthesis were represented using a largely phenomenological approach. In the second model a more mechanistic approach to cell proliferation was explored.

5.2   Model 1: biosynthesis and proliferation

The model was developed based on the assumption that the cell population can be divided in three compartments: A quiescent fraction C_r, a fraction committed to proliferation C_p and a fraction committed to proteoglycan production C_g (Fig. 5.3). Based on the duration of chondrocyte cell division, which may take several days, proliferation during the time scale of the experiment is a unique event [33]. Therefore

(a)

(b)

(c)

Figure 5.1: *Experimental results adapted from Chowdhury [33]. (a): Continuous 'C' loading regimens. During strained periods the agarose construct is loaded with a 15% cyclic deformation of 1Hz. (b): Experimental stimulation of proliferation synthesis by different mechanical loading regimens. (c): Stimulation of GAG synthesis.*
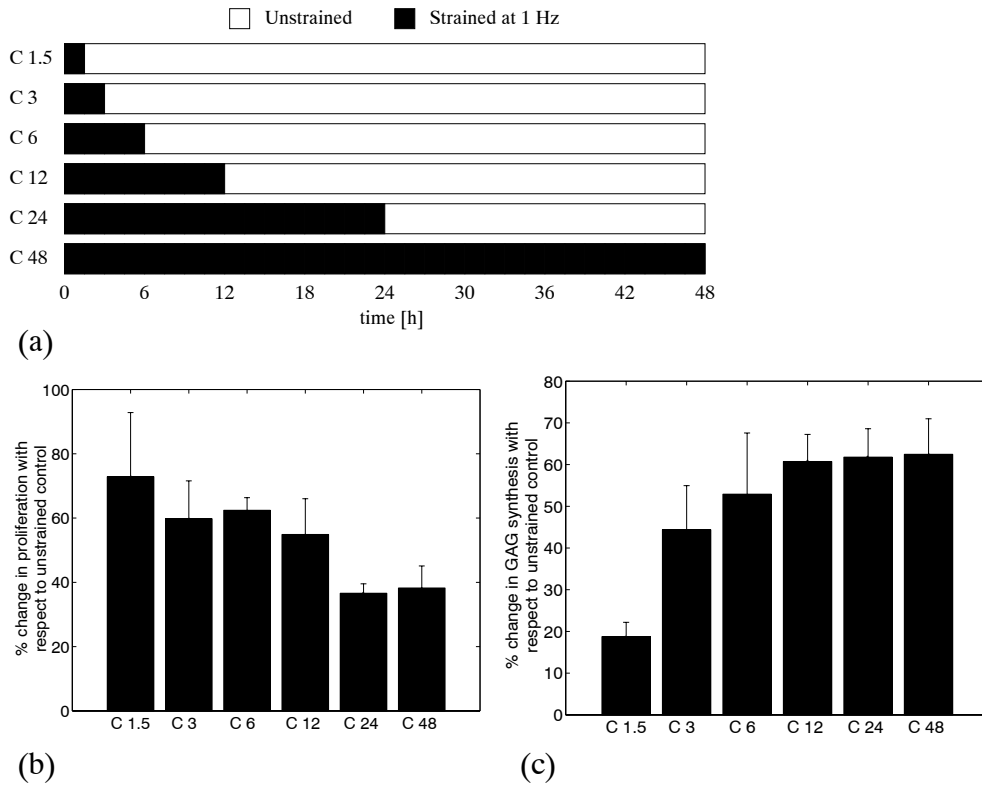
Figure 5.2: *Experimental results adapted from Chowdhury [33]. (a): intermittent 'I' loading protocols. During strained periods the agarose construct is loaded with a 15% cyclic deformation of 1Hz. (b): Experimental stimulation of proliferation synthesis by different mechanical loading regimens. (c): Stimulation of GAG synthesis.*
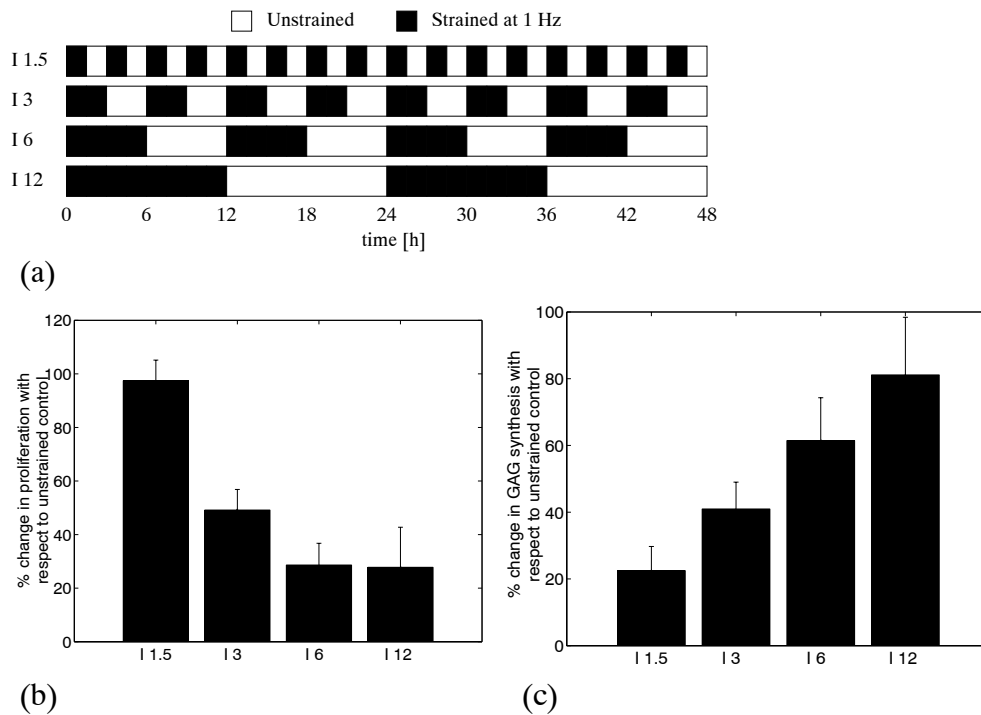
the normalized total number of cells was kept constant: $C_r + C_p + C_g = 1$. It was also assumed that there is a constant exchange of cells between the compartments, which is in equilibrium in the unstimulated state. Furthermore it was assumed that this balance can be adjusted by mechanical loading in the following manner: Start of a loading period temporarily shifts the balance to the proliferative compartment by increasing the cell flux from the quiescent to the proliferative compartment. When loading is continued, proliferation is inhibited by increasing the cell flux from the proliferative back to the quiescent compartment. At the same time the cell flux from the quiescent to the GAG producing compartment increases temporarily. In the experiments, cell proliferation and GAG synthesis were measured by [³H]thymidine and ³⁵SO₄ incorporation respectively. In the model it was assumed that, at any time, the [³H]thymidine and ³⁵SO₄ incorporation rates are proportional to the number of cells in the proliferative and GAG producing compartment, respectively. Therefore, the total [³H]thymidine and ³⁵SO₄ incorporation, P_{Tdr} and P_{SO_4} respectively, during the culture period is governed by Eqs. (5.1, 5.2):

$$\frac{dP_{Tdr}}{dt} = K_p C_p, \tag{5.1}$$

$$\frac{dP_{SO_4}}{dt} = K_g C_g, \tag{5.2}$$

in which K_p and K_g are the [³H]thymidine and ³⁵SO₄ incorporation rate constants, respectively. The exchange between the three compartments is governed by the following expressions (Eqs. 5.3-5.5):

$$\frac{dC_r}{dt} = Q_{p2r} - Q_{r2p} + Q_{g2r} - Q_{r2g}, \tag{5.3}$$

$$\frac{dC_p}{dt} = -Q_{p2r} + Q_{r2p}, \tag{5.4}$$

$$\frac{dC_g}{dt} = -Q_{g2r} + Q_{r2g}, \tag{5.5}$$

where Q_{A2B} is the exchange rate from a compartment A to a compartment B. The pair Q_{A2B} and Q_{B2A} takes the form of:

$$Q_{A2B} = (R_{A2B}^s + R_{A2B}^a)C_A, \tag{5.6}$$

$$Q_{B2A} = (R_{B2A}^s + R_{B2A}^a)C_B. \tag{5.7}$$

The first terms R_{A2B}^s and R_{B2A}^s establish a steady state equilibrium between A and B in the absence of loading and are defined as:

$$R_{A2B}^s = V_{A\&B}^s / C_A^0, \tag{5.8}$$

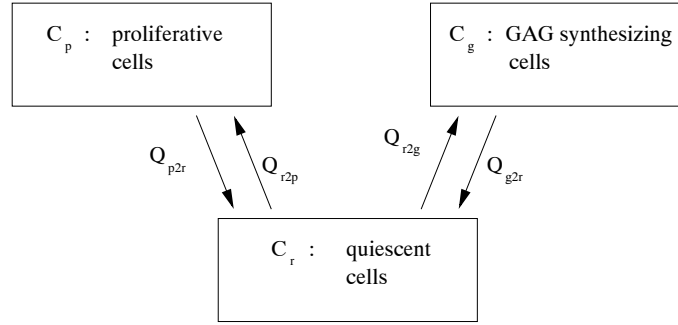$$R_{B2A}^s = V_{A\&B}^s / C_B^0. \tag{5.9}$$

Figure 5.3: *Schematic model representation, showing the conceptual cell compartments and exchange pathways.*

$V_{A\&B}^s$ is the steady state exchange rate and C_A^0 and C_B^0 are the initial values for C_A and C_B. The term R_{A2B}^a in Eq. 5.6 is associated with the presence of cyclic loading, analogously for R_{B2A}^a in Eq. 5.7:

$$R_{A2B}^a = V_{A2B}^a f_{A2B}^a, \tag{5.10}$$

where V_{A2B}^a is the maximum rate constant due to cyclic loading and f_{A2B}^a is a function of the time t^l elapsed since the start of a period of cyclic loading: Eq. 5.11. Therefore f_{A2B}^a is completely reset each time a new loading interval starts.

$$
\begin{aligned}
f_{A2B}^a &= exp(-(t^l - t_{A2B}^m)^2/a_{A2B}) &&\text{, during a period of cyclic loading,}\\
&= \qquad\qquad 0 &&\text{, between periods of cyclic loading.}
\end{aligned}
\tag{5.11}
$$

t_{A2B}^m is the time at which the maximum function value occurs and a_{A2B} determines the duration of activation.

To yield the total [³H]thymidine and $^{35}SO_4$ incorporation, Eqs. (5.1 - 5.5) were solved for the 48 h culture period (Matlab, ode45). The total incorporation in the dynamically loaded cases was compared to the total incorporation in the unloaded case to determine the percentage change due to stimulation. It has to be noted, however, that in the experiments the total incorporation was normalized with the end value for DNA, rather than the initial value. Therefore the model slightly overestimates incorporation at high proliferation rates.

5.3   Results 1: biosynthesis and proliferation

The model was subjected to the different loading protocols displayed in Figs. 5.1a and 5.2a. The model parameters were manually adjusted to provide a close match to the experimental data (Table 5.1). The functions f_{r2p}^a and f_{p2r}^a which determine the activation and inhibition of proliferation due to loading, respectively, have been visualized in Fig. 5.4a. For GAG synthesis, the activation function f_{r2g}^a is presented in Fig. 5.4b. The active inhibition of GAG synthesis due to prolonged loading was not necessary to represent the experimental results, therefore f_{g2r}^a was kept at zero.

(a)   (b)
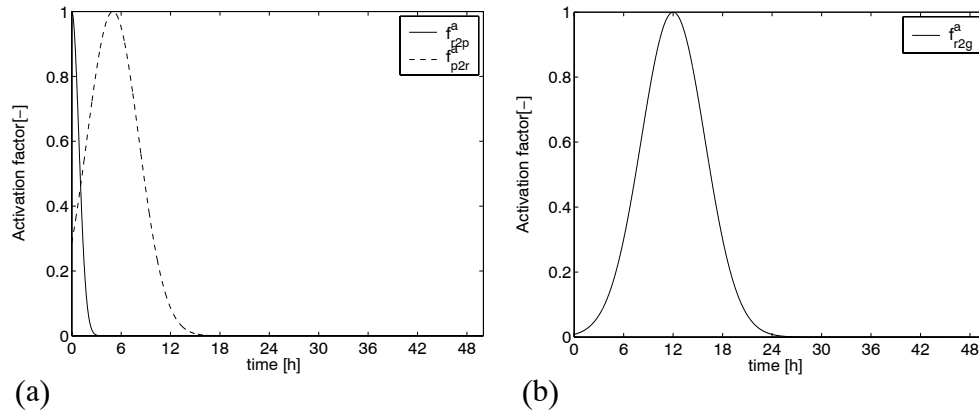
Figure 5.4: *(a): Visualization of the cell flux factors due to loading, f_{r2p}^a and f_{p2r}^a in Eq. (5.10), as a function of the time since the start of the current loading period. f_{r2p}^a promotes the flux from the quiescent to the proliferative compartment, f_{p2r}^a from the proliferative to the quiescent compartment. (b): Visualization of f_{r2g}^a in Eq. (5.10), cell flux factor from the quiescent to the GAG synthesizing compartment. The reverse flux factor f_{g2r}^a is zero.*

The comparison between the model output and experimental data is presented in Fig. 5.5, for all loading protocols. The results show the percentage change with respect to unstimulated controls in cumulative proliferation and GAG synthesis at 48 h. It is clear that qualitative trends in proliferation and GAG synthesis were represented correctly, as a function of the different continuous and intermittent compression regimens.

5.4   Discussion 1: biosynthesis and proliferation

A model has been proposed for chondrocyte proliferation and biosynthesis in response to varying dynamic compression regimens. The model can provide a reasonable overall description of the experimental data, although for specific loading protocols the predictive value is limited.

In the model, an active increase in cell flux from the proliferative to the resting compartment was required to represent the inhibitory effect of prolonged loading. For this purpose, it was assumed that cells can switch back and forth into proliferative phase at any time. However, in reality, once a cell enters the division process, the complete cell cycle has to be completed. This is particularly relevant, since the chondrocyte cell cycle can take several days [33, 101] and the experimental time scale is 48 h. By stimulating proliferation, mechanical loading may induce a synchronization in cell cycle phase within the cell population, which can modulate the effect of subsequent loading. Only the predicted end values at 48 h have been compared to the experimental data and whether the time course of [3H]thymidine incorporation corresponds is questionable. Indeed in the unloaded situation, a large increase in
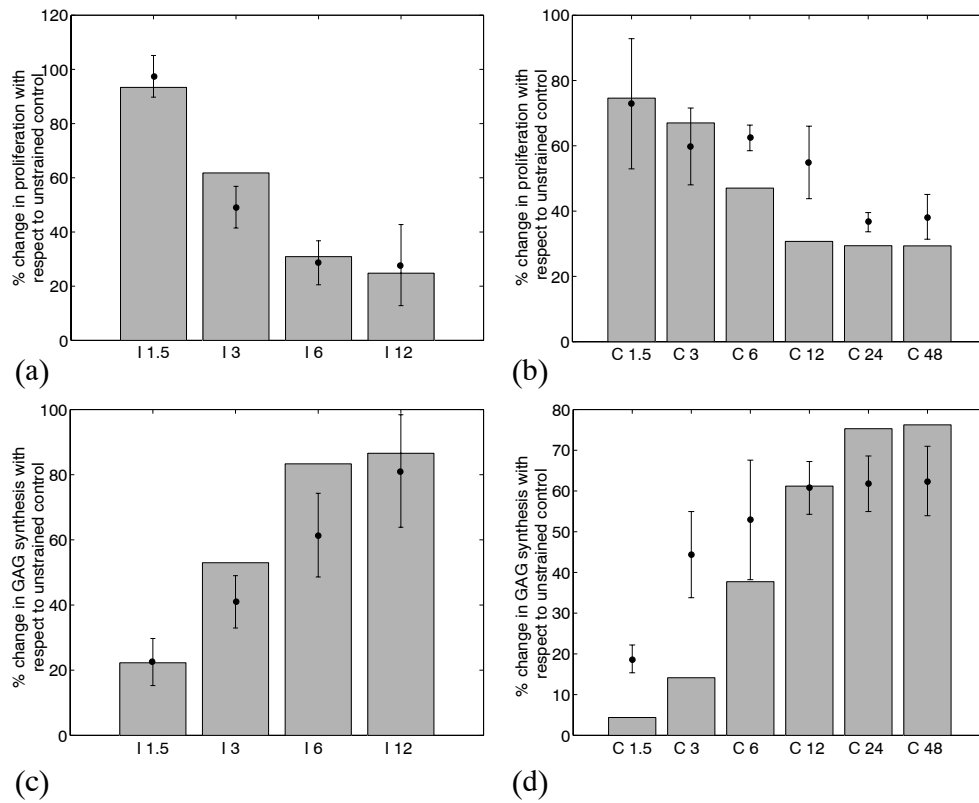
Figure 5.5: *The effect of different intermittent 'I' and continuous 'C' loading regimens (Figs. 5.1a, 5.2a) on stimulating cell proliferation (a,b) and GAG synthesis (c,d). The gray bars represent the numerical results from the present study. Errorbars indicate the experimental data, adapted from Chowdhury [33].*

Table 5.1: *Model parameter values used to obtain the numerical results (Fig. 5.5). The parameters were tuned to provide the closest overall match to the experimental data for proliferation and GAG synthesis, for the different continuous and intermittent loading regimens.*

C_r^0	0.38	[-]
C_p^0	0.31	[-]
C_g^0	0.31	[-]
K_p	$1/(48\ C_p^0)$	[h^{-1}]
K_g	$1/(48\ C_g^0)$	[h^{-1}]
P_{Tdr}^0	0	[-]
$P_{SO_4}^0$	0	[-]
$V_{r\&p}^s$	0.005	[h^{-1}]
$V_{r\&g}^s$	0.01	[h^{-1}]
V_{r2p}^a	3	[h^{-1}]
V_{p2r}^a	0.05	[h^{-1}]
V_{r2g}^a	60	[h^{-1}]
V_{g2r}^a	0	[h^{-1}]
t_{r2p}^m	0	[h]
t_{p2r}^m	5	[h]
t_{r2g}^m	12	[h]
a_{r2p}	1.5	[h^2]
a_{p2r}	20	[h^2]
a_{r2g}	30	[h^2]

proliferation was demonstrated between 24 - 48 h of cultivation compared to 0 - 24 h [102], with maximum values being attained at 72 - 96 h of cultivation, after which incorporation decreased again [32]. Such a peak in proliferation cannot be accounted for by the present model, but is consistent with a cell cycle based mechanism. The measured [3H]thymidine is incorporated into DNA in the S-phase of the cell cycle. Therefore, to explain the maximum effect of short intervals of dynamic loading on proliferation, it has been hypothesized that a small number of loading cycles is enough to rapidly stimulate cells to enter S-phase, while further loading cycles reduce the probability of cells entering S-phase [33]. This reasoning prompts the adoption of a more mechanistic model to determine whether a cell cycle based approach can account for the effect of different dynamic loading protocols on chondrocyte proliferation.

5.5   Model 2: cell cycle based proliferation

The cell cycle consists of a number of specific phases which a cell must pass through in order to divide [1]. The following phases can be distinguished: the G_1 (gap 1), S (DNA synthesis), G_2 (gap 2) and M (mitosis) phase. In addition, non-dividing cells that have left the cell cycle are in the G_0 state.

A cell cycle model was employed, that consists of a probabilistic A state and a deterministic B phase (Fig. 5.6) [9, 23, 24]. The A-state contains the cells in G_0 and G_1-pm (postmitotic) [193]. The B-phase contains the G_1-ps (pre S-phase), S, G_2 and M-phase. The number of cells in the A-state was lumped in a single parameter N_A. A transition probability was defined which determines whether a cell will progress from the A-state, past the restriction point R and enter the B-phase of the cell cycle. Once the restriction point R is passed the cell is committed to fulfill the complete cell cycle [193]. A_s indicates the start of the S-phase in which DNA synthesis and [3H]thymidine incorporation takes place. After going through mitosis in the M-phase, the division process is completed and the cell and an additional daughter cell reenter in the A-state. To track the progression through the B-phase a parameter a was defined ($0 \leq a \leq 1$), which is associated with the maturity of the cell. The cell maturity a refers, for example, to the progression in protein synthesis, which does not necessarily correspond with time for different culture conditions.

In the experiment, the cell seeded agarose construct was cultured for an initial period of 24 h followed by the 48 h loading protocol. For chondrocytes, the total length of the cell cycle can be several days [33, 101]. Therefore, as a first assumption a cell divides only once during the 72 h culture time and reentry in the cell cycle was not considered. The number of cells in the A-state (N_A) is then governed by Eq. (5.12).

$$\frac{dN_A(t)}{dt} = -K_T N_A(t),$$

(5.12)

where K_T is the transition rate constant. The cell population density at time t and age a is denoted by $n_B(t, a)$. Progression through the B-phase is described by the

A - state

B - phase

G_0 / G_1-pm

G_1-ps   S G_2 M

M

a

R
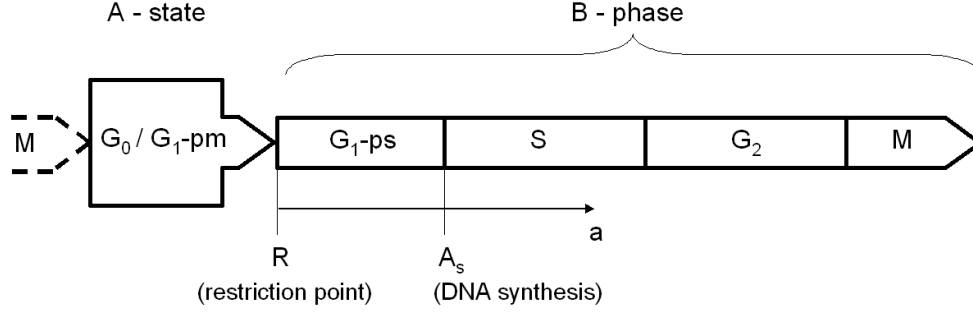(restriction point)

A_s
(DNA synthesis)

Figure 5.6: *Cell cycle model. The cell population is divided over a lumped A-state and a B-phase, where cells are distributed over the maturity axis a. Past the restriction point R a cell is committed to fulfill the complete cell cycle. A_s indicates the start of the S-phase in which DNA amplification takes place.*

balance equation Eq. (5.13):

$$\frac{\partial n_B(t,a)}{\partial t} + \frac{\partial v_B(t,a)n_B(t,a)}{\partial a} = 0, \tag{5.13}$$

where $v_B = da/dt$ [h^{-1}] is the maturation velocity. In the reference situation v_B equals $1/T_c^{ref}$, where T_c^{ref} is the reference cell cycle duration, which is not further specified since cell division was assumed to be a unique event. The boundary conditions for n_B at $a = 0$ is:

$$v_B(t,0)n_B(t,0) = K_T N_A(t) \tag{5.14}$$

It was assumed that initially all cells are in the A-state, which is consistent with low [^{3}H]thymidine incorporation during 0 - 24 h of culture and high incorporation for 24 - 48 and 48 - 72 h [32, 102]. The initial cell number $N_A(0)$ was normalized to 1. During cell cycle progression, the amount of proliferation is determined by the cell fraction that crosses A_s and enters the S-phase. Variability in proliferation can arise from both the transition probability from the A-state to B-phase, K_T, as well as from the maturation velocity v_B during the G_1-ps phase [23, 193]. In the model it was assumed that dynamic loading modulates the proliferation rate by affecting K_T and v_B.

The following analytical-numerical approach was adopted to solve Eqs. (5.12) and (5.13), for the initial unloaded $t = [0, 24]$ h and loading interval $t = [24, 72]$ h: The experimental loading protocols (Fig. 5.1a, 5.2a) can be divided in time intervals of $\Delta t^i = 1.5$ h. For each interval $i = [1, n]$ a cohort of cells N_B^i is followed that leaves the A-state and enters the B-phase during Δt^i. From Eq. (5.12) it is clear that the number of cells in the A-state decreases exponentially depending on the value of K_T^i. In the B-phase, these cells become distributed over a width $\Delta a^i = v_B^i \Delta t^i$ along the maturity axis. Therefore, the number of cells in cell cohort N_B^i is:

$$N_B^i = N_A(t^{i-1})\left(1 - e^{-K_T^i \Delta t^i}\right) \equiv \int_0^{\Delta a^i} n_B(t^i, a)da, \tag{5.15}$$

Table 5.2: *Parameter values used to evaluate the model, for the different cases presented in Figs. 5.7, 5.9, 5.11 and 5.12. Transition rate constant K_T [h^{-1}] (Eq. (5.12)) and maturation velocity v_B [$(T_c^{ref})^{-1}$] (Eq. (5.13)) for: 1) unloaded periods, 2) the first 1.5 h of a loading period and 3) loading continued after 1.5 h (Figs. 5.1a, 5.2a). For all cases $T_{A_s} = 36$ h.*

	(I)		(II)		(III)		(IV)	
	K_T	v_B	K_T	v_B	K_T	v_B	K_T	v_B
1) unloaded	0.008	1	0.011	1	0.011	1	0.011	1
2) loading $\leq$ 1.5 h	0.12	1	0.65	1	0.65	1	0.65	0.5
3) loading > 1.5 h	0.008	1	0.011	1	0	1	0.011	0.5

where $N_A(t^{i-1})$ is the number of cells in the A-state at the beginning of interval i. When a new cell cohort N_B^i is added, all previous cell cohorts progress along a with Δa^i. It was assumed that DNA duplication occurs immediately upon entry of the S-phase. Therefore, at the end of the culture period $t = T_{end}$, the cell population fraction $N_B^{prolf} = \int_{A_s}^{\infty} n_B(T_{end}, a)da$ that had crossed A_s was determined (Fig. 5.8). In the experiments [³H]thymidine incorporation was normalized with the final DNA content, therefore $P = N_B^{prolf}/(1 + N_B^{prolf})$ was used as the relative proliferation measure.

5.6   Results 2: cell cycle based proliferation

The experimental results for the continuous and intermittent loading protocols are presented in Figs. 5.1b, 5.2b [33]. In both intermittent and continuous protocols, a loading period of 1.5 h yielded the maximum proliferative response and longer loading intervals decreased proliferation. Therefore the net stimulation of proliferation was represented by an increased transition probability K_T during the first 1.5 h of every loading period. During the remaining loading period and the unloaded intervals a low reference transition probability was applied (Table 5.2, column I).

First, the start time of the S-phase in the reference situation, $T_{A_s} = A_s T_c^{ref}$, was set to 36 h. This is consistent with the sharp increase in [³H]thymidine incorporation after the first 24 h [102], while a higher T_{A_s} would not enable stimulation within the 48 h loading period. In addition this value for T_{A_s} basically limits the effective stimulation window to the first 12 h of loading (Fig. 5.8). Based only on the number of loading intervals within these 12 h, a distinction can arise between the different intermittent loading protocols, which closely corresponds to the experimental results (Fig. 5.7a). In Fig. 5.7a, the parameters have been tuned with respect to the increase in proliferation compared to the unloaded reference situation and the ratios between the different intermittent loading regimens. A high transition probability K_T in the loaded state, compared to the reference state, produces a large stimulatory effect of loading. However, if the initial stimulation (Fig. 5.8b) is chosen too high, the capacity for stimulation is exhausted and the effect of the number of subsequent loading intervals is too small (Fig. 5.8a). Unfortunately, the relatively low value for

K_T leading to the result of Fig 5.7a) results in a 35 % increase in proliferation for the single loading interval in the continuous case, which is significantly smaller than that obtained experimentally (Figs. 5.7b).

In Figs. 5.9 and 5.10 an alternative tuning approach is presented, in which the reference and loaded value for K_T were adjusted such that both I 1.5 and C 1.5 matched the experimental data (Table 5.2, column II). The downside is that the distinction between the intermittent loading protocols in Fig. 5.9a is less compared to Fig. 5.7a and does not correspond to the experimental data. From Figs. 5.7b and 5.9b it is clear that without further assumptions all continuous loading protocols coincide and the values do not decrease for longer loading periods. Therefore, in addition to only a stimulative effect of loading also an inhibitory effect was considered. Two distinct assumptions were tested.

First, after the stimulative initial 1.5 h of loading the transition probability K_T in the remaining loading period was set at zero (Table 5.2, column III). This could, for example, arise from a temporary depletion of essential molecular species. From Fig. 5.11b it is evident that proliferation is reduced for longer loading intervals. However, the effect is small compared to the experimental decrease in proliferation. A higher value for the reference transition rate K_T would give a larger capacity for inhibition during loading, but the relative stimulation of proliferation by loading would be less.

Secondly, instead of decreasing the transition probability, it was assumed that loading reduces the cell cycle progression velocity. This could for example be associated with disturbed protein synthesis. The velocity v_B during the complete loading periods was set at $0.5/T_c^{ref}$ instead of $1/T_c^{ref}$ (Table 5.2, column IV). The reduction of proliferation for C 24 agreed with the experiments (Fig. 5.12b). However, while experimentally C 24 and C 48 were similar, the computed reduction in proliferation for C 48 was disproportional. Since for C 48 the low velocity v_B was applied during the entire 48 h loading period, a large part of the reference population, as well as cells that were stimulated to enter the B-phase, did not reach the S-phase, resulting in a large decrease in proliferation.

5.7   Discussion 2: cell cycle based proliferation

A cell cycle based model was proposed for the temporal regulation of chondrocyte proliferation in response to varying intervals of dynamic compression. By incorporating the age distribution of the cell population and assuming that only the onset of loading stimulates proliferation, the model was able to represent the experimental results for the intermittent loading protocols, based on a limited number of parameters, while for the continuous loading protocols an additional inhibitory effect of further loading is required, to account for the decrease in proliferation for longer loading periods. Modeling the inhibitory effect of further loading as a decreased change of entering the cell cycle, was found to offer little room for inhibition and could not account for the experimental decrease in proliferation. This is because a large stimulation has to occur in the early phase of the loading protocol, which commits a large fraction of the cell population to the cell cycle (Fig. 5.10). Therefore, a

Figure 5.7: *Computed stimulation of proliferation by different mechanical loading regimens compared to experimental mean and standard deviation. (a): Intermittent loading. (b): Continuous loading. The parameters were tuned for the intermittent regimens I 1.5 - I 12 (Table 5.2, column I)*
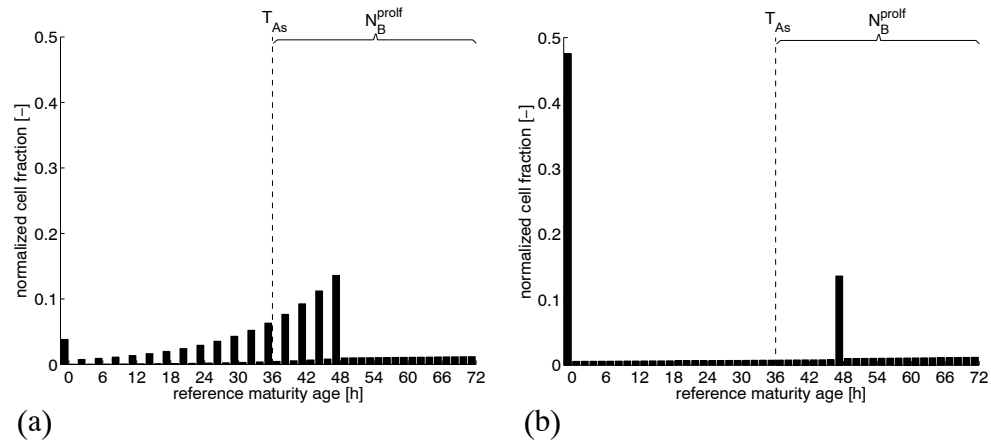
Figure 5.8: *Maturity age distribution of the cell population over the cell cycle at t = 72 h for (a): I 1.5 and (b): C 1.5 in Fig. 5.7. The fraction of cells in the A-state is given for cell age < 0. $T_{A_s} = 36$ h is the age at which the S-phase starts in the reference situation. N_B^{prolf} is the cell population fraction that has crossed T_{A_s}.*

(a)

(b)
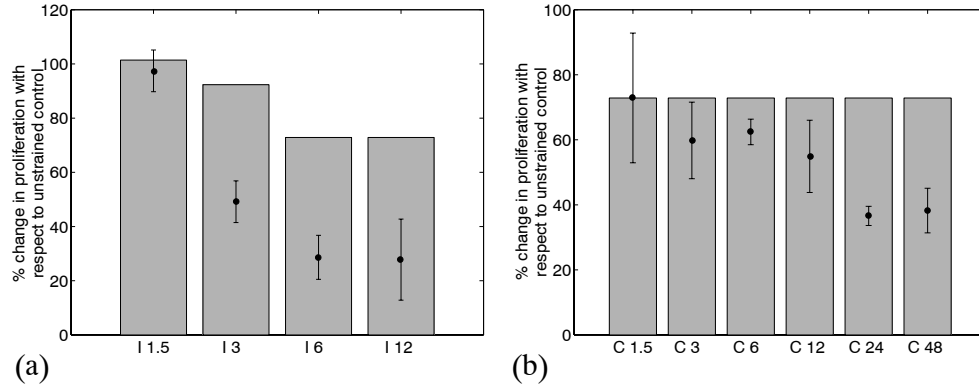
Figure 5.9: *Computed stimulation of proliferation by different mechanical loading regimens compared to experimental mean and standard deviation. (a): intermittent loading. (b): Continuous loading. The parameters were tuned for I 1.5 and C 1.5 (Table 5.2, column II).*

(a)

(b)
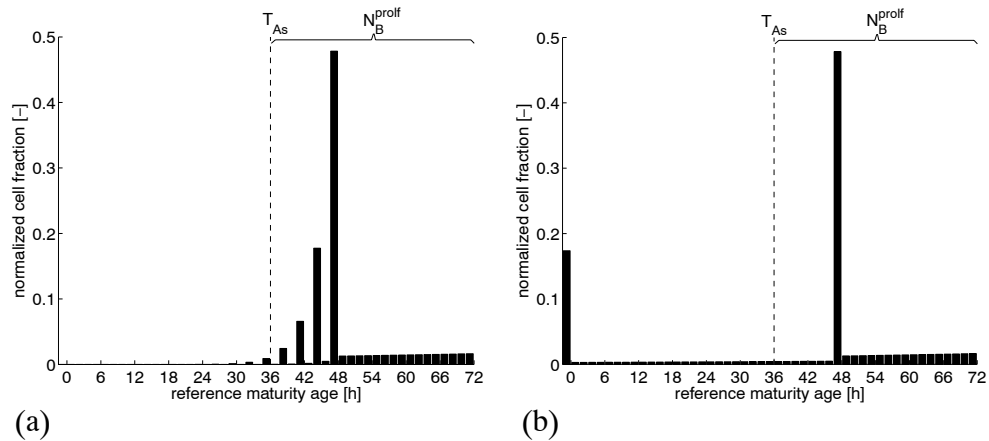
Figure 5.10: *Maturity age distribution of the cell population over the cell cycle at $t = 72$ h for (a): I 1.5 and (b): C 1.5 in Fig. 5.9. The fraction of cells in the A-state is given for cell age < 0. $T_{A_s} = 36$ h is the age at which the S-phase starts in the reference situation. N_B^{prolf} is the cell population fraction that has crossed T_{A_s}.*
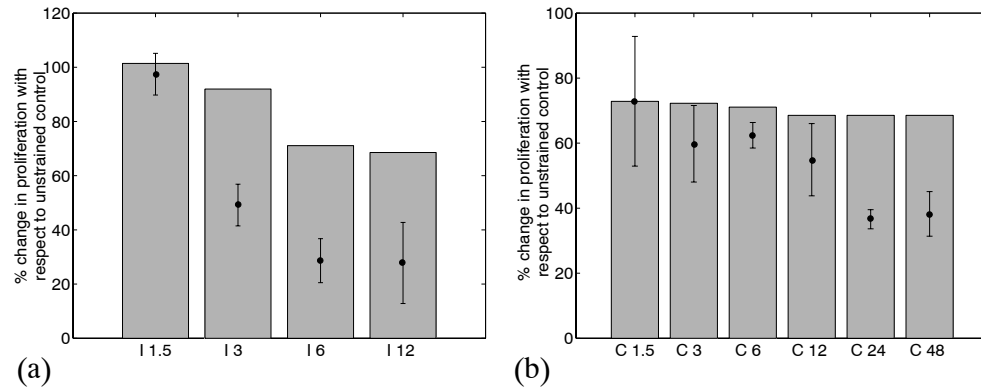
Figure 5.11: *Computed stimulation of proliferation by different mechanical loading regimens compared to experimental mean and standard deviation. (a): Intermittent loading. (b): Continuous loading. The same parameters as in Fig. 5.9 were used, but a reduced transition probability K_T from the A-state to B-phase was assumed when loading was continued after 1.5 h (Table 5.2, column III).*
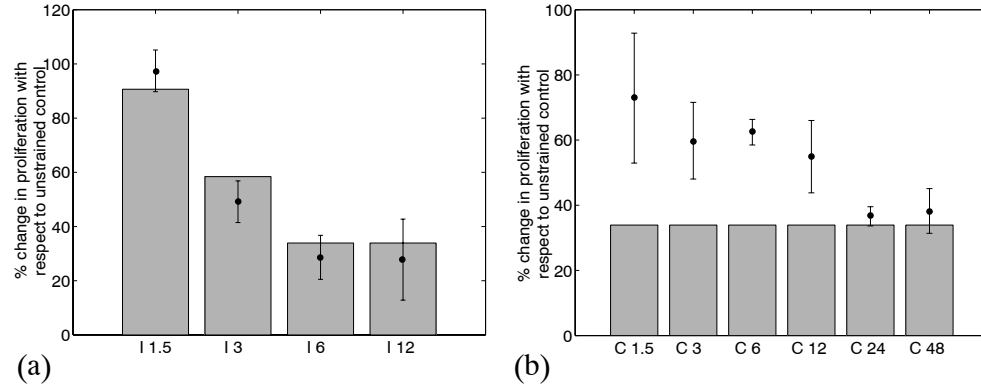

Figure 5.12: *Computed stimulation of proliferation by different mechanical loading regimens compared to experimental mean and standard deviation. (a): intermittent loading. (b): Continuous loading. The same parameters as in Fig. 5.9 were used, but during loading the maturation velocity v_B was reduced (Table 5.2, column IV).*

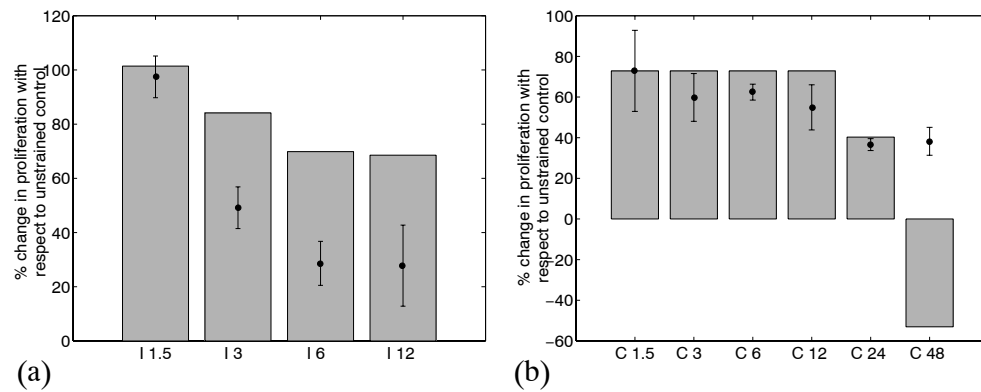reduction of the transition probability in later stages of culture cannot significantly reduce the overall proliferation. Alternatively, modeling the inhibitory effect of further loading as a decreased maturation velocity was found to be able to decrease the computed proliferation rate significantly. However, a constant lower velocity during loading resulted in a disproportional decrease in proliferation, which indicates that the reduction in velocity may depend on the duration of loading.

By 72 h the computed DNA content had increased by 25% and 33% for the unloaded cases in Fig. 5.7 and 5.9 respectively, which is between the 22% and 41% found in experiments for deep and superficial chondrocytes respectively [102]. In case cells divide only once during this period, a high 41% increase in DNA implies that a large fraction of the cell population is already involved in the cell cycle in the unloaded situation. A doubling of proliferation by dynamic loading therefore means that approximately the whole cell population is dividing, which imposes limits on the amount of stimulation possible. In addition, the extent of stimulation is limited by the delay introduced by the cell cycle, since in the unloaded reference case not all cells that are committed to the cell cycle have entered S-phase.

In the model, it was assumed that initially all cells were in the A-state, however, the actual maturity distribution is unknown and cells may have entered the B-phase during the cell isolation phase. It was also assumed that DNA multiplication occurred instantly upon entry of the S-phase, however, as DNA synthesis is in fact distributed over the S-phase the effect of loading may be more smoothened. In addition, not all cells necessarily progress along the cell cycle with the same velocity, which may lead to more dispersed results. An important model assumption was that a cell can divide only once during the 72 h culture time. However, during development, an averaged G_1-phase of 25 h and a total cell cycle duration of 36 h was determined for chondrocytes in the growthplate of mice [180].

Additional quantification is required to provide further foundations for the model assumptions. With respect to the identification of model parameters, in the unloaded reference case the transition chance is determined by the DNA increase, which can be measured directly and the unknown start of the S-phase, which needs to be estimated. For this purpose, the percentage of cells in G_0/G_1, S and G_2/M can be experimentally determined and cell cycle times can be assessed, using staining techniques with bromodeoxyuridine and propidium iodide [5, 180]. Furthermore, the mechanisms by which mechanical loading can affect cell cycle progression need to be determined. In general, integrins are involved in mechanotransduction and have been shown to regulate G_1/S transition [5]. Model validation can be provided by intermediate measurements, for example at 24 h of loading. In addition, at a longer time scale, it would be interesting to see whether multiple peaks in proliferation occur. This would support the need for a cell cycle based model, although to the contrary the absence of such peaks is not fully conclusive, due to possible desynchronization and decreased proliferation at higher cell concentrations.

5.8   General discussion

In order to predict chondrocyte proliferation in response to dynamic mechanical loading, it is necessary to incorporate the finite capacity of the cell population, in combination with the inherent time delay associated with the cell division process. It has to be stressed, that the net effect of mechanical loading is governed by these mechanisms, not only on a small time scale of days, as in the present study, but also for longer periods of culture.

Interpretation of the present experimental results is complicated, since dynamic loading modulated cell behavior within a transient proliferation phase following isolation and seeding, while information is only available at one time point after a short culture period. Therefore, the experiments have to be extended to longer periods of culture. For instance, this can confirm whether continued mechanical loading introduces a simple delay or decreases commitment to the cell cycle. Furthermore, apart from studying fundamental mechanisms, a longer culture period will reveal whether the initial response is representative for tissue engineering applications.

Two different modeling approaches were evaluated. A compartment based modeling approach can be useful to represent a balance between proliferation and proteoglycan synthesis at a large time scale, when the effect of a certain stimulation protocol is known. In order to predict the response to different intervals of mechanical stimulation, however, a more mechanistic cell cycle based approach is required. The cell cycle model supports an important role of the onset of loading. In addition, an inhibitory effect of further loading is required, which is more likely to be related to cell cycle progression velocity than to a decreased probability of commitment to the cell cycle. The mechanisms behind this inhibitory effect and the computational implementation, however, require further investigation.

Chapter 6

A computational study of culture conditions and nutrient supply in cartilage tissue engineering[1]

Abstract

Different culture conditions for cartilage tissue engineering were evaluated with respect to the supply of oxygen and glucose and the accumulation of lactate. A computational approach was adopted in which the bioreactor was modeled as a batch process and transport was considered within constructs seeded at high cell concentrations and of clinically relevant dimensions. To assess the extent to which mass transfer can be influenced theoretically, extreme cases were distinguished in which the culture medium in the bioreactor environment was assumed either completely static, or well mixed and fully oxygenated. It can be concluded that severe oxygen depletion and lactate accumulation can occur within cartilage tissue engineering bioreactors. However, the results also indicate that transport restrictions are not insurmountable, providing that the medium is well homogenized and oxygenated and the construct's surfaces are sufficiently exposed to the medium. The large variation in uptake rates of chondrocytes requires that for any specific application, the quantification of cellular utilization rates, depending on the cell source and culture conditions, is an essential starting point for optimizing culture protocols.

6.1   Introduction

Articular cartilage has a limited healing capacity under in-vivo conditions. Therefore in-vitro tissue engineering has been proposed as a way of providing suitable transplant material for clinical repair of cartilage damage. One of the most important parameters that determine the suitability of a tissue engineered (TE) construct for implantation is its mechanical functionality, i.e. the stiffness and permeability of the construct, which are related to extra cellular matrix (ECM) components such as glycosaminoglycans (GAG) and collagen II. It has been shown that the functional development of a TE cartilage construct is governed to a large extent by the bioreactor environment to which it is exposed. The main types of bioreactors that have been employed in cartilage TE studies include: Static or orbitally shaken petri dishes, mixed culture in spinner flasks, concentric cylinder bioreactors, rotating wall vessel (RVW) bioreactors and perfusion bioreactors [40, 43, 49, 51, 126, 129, 137, 153, 161, 181]. Static culture tends to produce constructs with an inhomogeneous matrix distribution, with enhanced deposition in the periphery. Mixing enhances mass transfer, increasing both the amount of GAG synthesized and the amount of GAG released to the medium [61]. Constructs cultured in RVWs displayed uniform cartilage formation and contained the highest amounts of ECM components, the lowest permeability and the highest equilibrium modulus [181]. In general perfusion through or around constructs enhances matrix synthesis [40, 129, 137], although it has also been reported that matrix production can be inhibited [126]. In addition bioreactors have been specifically designed to incorporate some form of mechanical stimulation, such as fluid shear stress, hydrostatic pressure and dynamic compression, which have been found to be beneficial for cartilage matrix biosynthesis [19, 26, 30, 98, 99, 124, 185].

Given the variability in bioreactor configurations numerical models could prove essential in enabling a comparison between results obtained in different studies. In addition establishing quantified relations between the bioreactor culture conditions and the resulting tissue properties will greatly benefit the design of optimized bioreactors and culture protocols. Numerical studies have focused on the characterization of the complex hydrodynamic environment that can occur around the construct [30, 145, 166, 185], as it is known that excessive fluid shear stress results in the formation of a fibrous capsule around the construct, while a low shear environment enhances chondrogenesis. Also at the microscopic level the local fluid-induced shear stress experienced by the chondrocytes in a porous construct has been evaluated numerically [145]. Besides the mechanical environment, the functional development of TE cartilage depends on an adequate supply of nutrients to the construct. A number of studies have investigated this issue for specific bioreactors. Fresh medium supply has been assessed by computing the flow through a porous construct in a spinner flask [166]. Also the fluid flow in combination with oxygen mass transfer to and within TE constructs has been modeled in a concentric cylinder bioreactor [185]. At the construct level nutrient diffusion, oxygen uptake, matrix biosynthesis and cell growth within TE cartilage constructs have been modeled [56, 108, 111, 129, 134]. The largest source of uncertainty in modeling studies, however, is associated with the cell behavior, both qualitatively and quantitatively. Most modeling studies

consider only one metabolite, most often, oxygen. It has been shown however that GAG synthesis is affected by both nutrient availability [125], pH [147] and oxygen [34, 64, 80, 86, 94, 103, 113, 132]. Complicated interactions exist between chondrocyte energy balance and matrix metabolism and the precise regulation mechanisms remain largely unknown [42, 87, 103–105, 110, 173].

To obtain a more complete picture of the biochemical environment of chondrocytes within a TE construct it is necessary to include in a model all the main metabolites, namely glucose, oxygen and lactate. In most cases nutrient transport has been modeled as steady state assuming constant boundary conditions, which is justified for a large medium volume. However current TE studies are essentially batch processes in which a large medium volume may not be optimal, since a balance exists between the retention of beneficial growth factors produced by the cells and the prevention of an accumulation of inhibitory waste products. Modeling the effect of a finite medium volume can therefore prove useful with respect to optimizing culture conditions. The objective of this study is to predict the distribution of the these three metabolites, which determine chondrocyte biosynthesis and survival, as a function of time, within a TE cartilage construct subjected to different culture conditions. The model is designed to compare representative bioreactor configurations, based on the same cellular behavior. Extreme cases are considered by making certain simplifying assumptions regarding mixing efficiency and bioreactor geometry. The following questions will be addressed: Firstly, does significant nutrient depletion occur at the high cell concentrations required for chondrogenesis [49]? Secondly, to what extent can mixing and perfusion influence metabolite distributions within the construct, particularly secondary mixing associated with dynamic compression experiments? Finally, do the increasing transport limitations due to matrix accumulation [17], significantly affect metabolite distributions?

6.2 Methods

A finite element approach was adopted in order to evaluate the effect of mixing and perfusion on the time dependent metabolite concentrations within TE constructs. A 4% agarose construct was considered with a high cell concentration of 40×10^6 cell cm^{-3}, a diameter of 10 mm and a thickness of 3 mm. The construct was supplied with 10 ml of medium for a 48 h period between medium exchange, equivalent to 1.9×10^6 cell ml^{-1} day^{-1} [125, 134]. Initially, modeling was restricted to diffusion alone. First, to investigate the effect of mixing, three representative basic culture configurations were considered, namely a Petri dish, with and without a loading platen, and suspended in a simple tube (Figs. 6.1a-c). For each setup, two extreme cases were considered: In the static case it was assumed that transport is governed only by diffusion and both the construct and the surrounding medium were modeled. By contrast in the mixed case, it was assumed that the medium is fully homogenized and fully oxygenated and only the construct itself was modeled, while the external medium was represented by a bulk volume. Transport of a solute in the construct
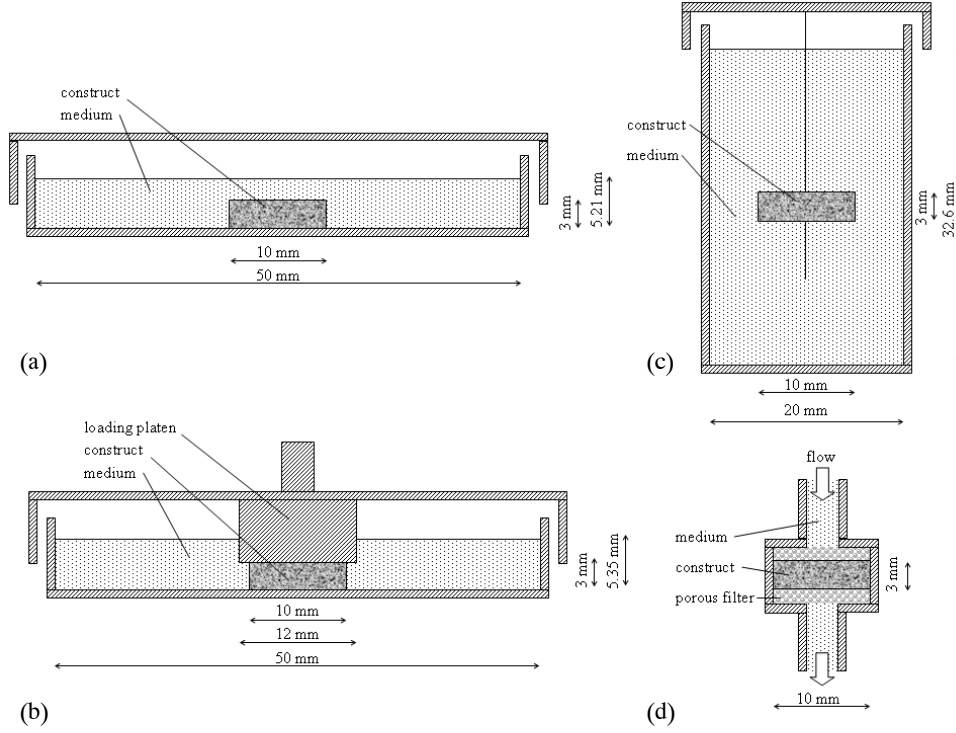
Figure 6.1: *Culture configurations. (a) Petri dish. (b) Compression setup. (c) Suspended in a tube. (d) Confined perfusion.*

and medium is described by the mass balance including Fick's law for diffusion:

$$\frac{\partial n^f c^\beta}{\partial t} - \vec{\nabla} \cdot (D\vec{\nabla} c^\beta) = q^\beta, \tag{6.1}$$

where c^β [mol m^{-3}] is the solute concentration in the fluid phase, n^f is the fluid volume fraction [-] ($n^f = 1$ in the medium), D [m^2 s^{-1}] is the effective diffusion coefficient and q^β [mol m^{-3} s^{-1}] is a source term that represents cellular utilization or production.

A much simplified model of chondrocyte metabolism was adopted. Oxygen and glucose utilization were described by the Michaelis Menten relationship [74, 86, 134, 188]. In Eq. (6.1) the source terms q^{ox} for oxygen and q^{glc} for glucose are given by:

$$q^\beta = -\frac{V^\beta c^\beta}{K_m^\beta + c^\beta}\rho^{cell}, \tag{6.2}$$

where V^β [mol cell^{-1} s^{-1}] is the maximum uptake rate, K_m^β [mol m^{-3}] is the concentration at which the half maximum rate occurs and ρ^{cell} [cell m^{-3}] the cell concentration per unit construct volume. Two assumptions were made, namely: 1) Glucose and oxygen were solely used in the energy metabolism, i.e. glycolysis

and oxidative phosphorylation and not, for example, for matrix synthesis. 2) There were no significant intermediate metabolites present and no storage in the form of glycogen occurred. Therefore the lactate production rate q^{lac} is given by the following expression:

$$q^{lac} = -2q^{glc} + \frac{1}{3}q^{ox}, \tag{6.3}$$

From the literature as summarized in Table 6.1, it is evident that there is a wide range of oxygen and glucose uptake rates for chondrocytes. For the reference situation, we use the values $V^{ox} = 6.70 \times 10^{-15}$ mol cell^{-1} h^{-1} and $V^{glc} = 6.12 \times 10^{-14}$ mol cell^{-1} h^{-1}, which were established for the same culture system for long term culture under tissue engineering conditions [132, 134]. In addition, the maximum values for the uptake parameters (Table 6.1) were used, namely, $V^{ox} = 1 \times 10^{-13}$ mol cell^{-1} h^{-1} and $V^{glc} = 4.0 \times 10^{-13}$ mol cell^{-1} h^{-1}. The constants $K_m^{ox} = 6$ μM for oxygen [74] and $K_m^{glc} = 0.35$ mM for glucose [188], represent values for chondrocytes.

The diffusion coefficients D_0 for the three metabolites in the medium were set to the values for water at 37 $^{\circ}C$ (Table 6.2). From these values the diffusion coefficients in the construct were estimated using the Mackie and Meares relation: $D_{constr}/D_0 = (n^f)^2/(2-n^f)^2 = 0.85$ for all solutes [18], based on $n^f = 0.96$ for 4% agarose [69]. The accumulation of matrix components during culture can significantly reduce diffusivity [17]. Therefore a parameter variation was carried out, setting the construct diffusion coefficients to values representative for mature cartilage, as indicated in Table (6.2). The volume fraction for cartilage in Eq. (6.1) was set to $n^f = 0.85$ [128].

The essential boundary conditions for oxygen at the free surfaces (Fig. 6.1), as well as the initial value for oxygen were set to 192 μM, based on 21% O$_2$ in air, an incubator atmosphere consisting of 5% CO$_2$, fully saturated with water (vapor pressure = 0.0618 atm) and an oxygen solubility of 10.268 μM %O$_2^{-1}$ at 37 $^{\circ}$C [86]. The initial value for glucose was set to 25 mM, based on medium containing 4.5 g l^{-1} glucose and no serum [125, 132]. The initial value for lactate is zero. In the mixed case the essential boundary conditions were adjusted by computing the solute fluxes in and out of the construct and the accompanying changes in the bulk medium concentration. The finite element package Sepran was used for all calculations [159]. Axisymmetric 6-node triangular elements were employed for the diffusion computations (Figs. 6.1a-c). The number of elements ranged from 5178 in the mixed cases to 18060 for the static flask. The transport -and source term equations were solved separately using Strang operator splitting [81]. Crank-Nicholson time integration was used for the transport term and Runge-Kutta time integration for the biokinetic source term. The numerical solution procedure for the two-dimensional axisymmetric transport and uptake was validated by comparing computed concentration profiles with the corresponding analytical solutions. This was done for the case of unsteady diffusion combined with first order reaction in a short cylinder, with constant boundary conditions and zero initial conditions [8, 37].

In case of perfusion it was assumed that the construct was placed between porous filters and was fully confined (Fig. 6.1d), such that fluid could only enter or leave the construct through the top and bottom surfaces. The construct was subjected to an external pressure difference and solute transport was evaluated. For comparison, the

Table 6.1: *Oxygen and glucose uptake rates*

Reference	Oxygen uptake rate [mol cell^{-1} h^{-1}]	Glucose uptake rate [mol cell^{-1} h^{-1}]	Remarks
Haselgrove 1993 [74]	3.7×10^{-14}	-	Chick growth cartilage
Johnson 2000 [87]	3.6×10^{-14}	-	Human articular chondrocytes, stirred suspension
Malda 2004 [111]	7.2×10^{-16}-1.4×10^{-14}	-	Bovine articular chondrocytes, 3D culture
Marcus 1973 [113]	2.2×10^{-15}-5.8×10^{-15}	3.6×10^{-13}-4.0×10^{-13} *	Rabbit articular chondrocytes, monolayer. *: Converted using 7.7 pg DNA/cell [91]
Obradovic 1999 [132]	-	6.12×10^{-14}	Bovine articular chondrocytes, 3D culture
Obradovic 2000 [134]	6.70×10^{-15}	-	Bovine articular chondrocytes, 3D culture
Nehring 1999 [129]	1×10^{-13}	-	Mini pig articular chondrocytes, 3D pellets
Stockwell 1983 [164]	3×10^{-15}-1.8×10^{-14}	-	Cartilage, various species
Tomita 2001 [173]	7.2×10^{-14}	1.9×10^{-13}	Rabbit articular chondrocytes, monolayer
Windhaber 2003 [188]	-	5.57×10^{-14}	Bovine articular chondrocytes, suspension, short term uptake

Table 6.2: *Diffusion coefficients used. References indicate direct measurements as well as ratios used to derive the values given.*

	D_0 [10^{-5} cm^2 s^{-1}]	D_{constr} [10^{-5} cm^2 s^{-1}]	D_{cart} [10^{-5} cm^2 s^{-1}]
oxygen	3.0 [74, 107]	2.6	2.2 [111]
glucose	0.92 [2, 174]	0.78	0.32 [2, 18, 115, 116]
lactate	1.4 [79]	1.2	0.69 [79]

non-perfused case with zero external pressure was computed. In both the perfused and non-perfused cases it was assumed that the external medium was fully mixed and oxygenated. In addition it was assumed that there was no delay due to the tubing and pumping system, therefore the same concentration boundary conditions were applied on the top and bottom surfaces of the construct. The confined perfusion case reduces to a quasi 1D problem. A computational method was used that has been described previously [160]. Briefly, a biphasic finite element formulation was used to derive the time varying displacement and fluid velocity field, which were subsequently used to solve the convection diffusion equations for the different solutes. The method fully accounts for finite deformation, variable fluid volume fractions and cell density. For the calculations 60, 9-node, quadrilateral elements were used. The biphasic mechanics finite elements were only used for the perfusion problem (Fig. 6.1d) and have been validated for confined compression.

For 4% agarose the aggregate modulus $Ha = 10.55$ kPa and the permeability $K = 6.62 \times 10^{-14}$ m^4 N^{-1} s^{-1} were selected [69]. A pressure $p = 2$ kPa was applied to the top surface, resulting in an overall deformation of approximately 10% in the steady state. The pressure was applied in 60 seconds. Since the mechanical properties of the construct are a function of the extracellular matrix formed, a parameter variation was carried out, in which values representative for mature cartilage were considered: $Ha = 0.5$ MPa and $K = 1 \times 10^{-15}$ m^4 N^{-1} s^{-1}, $n^f = 0.85$ [128]. In this case a pressure $p = 100$ kPa was chosen to result in approximately 10 % overall deformation of natural cartilage.

6.3   Results

The oxygen concentration within the construct and the surrounding medium after 48 h is shown in Fig. 6.2, for the case of static culture in the Petri dish, with and without loading platen and suspended in the tube. It can be observed that significant oxygen depletion occurs, with oxygen concentrations in the construct approaching zero. For the Petri dish, oxygen is almost depleted near the center of the construct (Fig. 6.2a). Application of a loading platen extents the region of oxygen depletion to a large proportion of the construct (Fig. 6.2b). For the case of culture suspended in a tube, the large diffusion distance results in a zero oxygen level throughout the entire construct (Fig. 6.2c). Compared to oxygen, more radial gradients develop for glucose in the Petri dish, due to the absence of an essential boundary condition on the top surface (Fig. 6.3a). The glucose level within the construct is the lowest for the compression setup, while the tube setup shows the smallest glucose gradients (Fig. 6.3). Glucose depletion is not evident in any of the culture conditions. A similar, though reversed, picture arises for lactate. High levels of lactate can be observed in the center region of the construct in the Petri dish. Lacate accumulation within the construct is the highest in the compression setup and the lowest in the tube setup (Fig. 6.4). The results for oxygen, glucose and lactate at 48 h in the presence or absence of perfusion are shown in Fig. 6.5. It can be seen that even without perfusion no significant differences in concentration develop within the construct, with internal
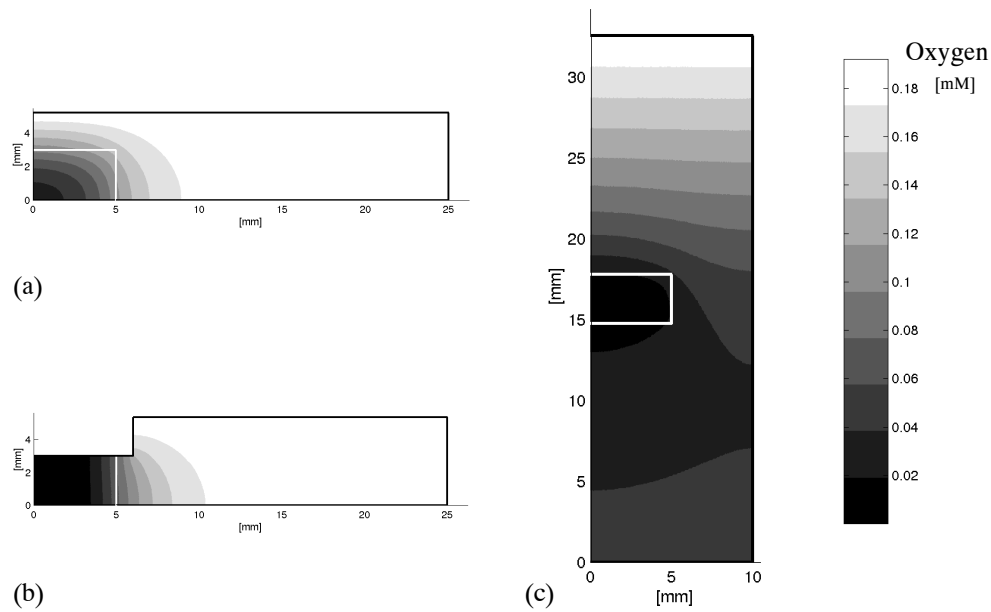
Figure 6.2: *Oxygen distribution in the static case at 48 h. Because of axisymmetry only the right half of the domain is depicted (Fig. 6.1). The construct position is indicated with a white line. (a) Petri dish. (b) Compression setup. (c) Tube.*

concentrations mainly controlled by the well-mixed bulk medium. Perfusion does not alter these results. Besides the effect of deformation due to the applied pressure gradient, the concentration profiles remain similar and fluid flow does not result in asymmetry. The same holds for perfusion in the limiting case using properties of mature cartilage (data not shown).

Fig. 6.6 shows the temporal profile of oxygen, glucose and lactate within the construct in the Petri dish. After an initial phase, the minimal glucose decreases and the maximum lactate increases at a steady rate, while oxygen decreases rapidly to an equilibrium value by 2 h. The transient behavior in the other culture setups is comparable, with the exception that in the tube it takes substantially longer (24 h) for oxygen to reach the steady state due to the longer diffusion distance from the free surface (data not shown). The results for all culture setups at 48 h are summarized in Fig. 6.7. Comparing the static to the mixed case reveals that mixing can significantly increase the oxygen and glucose levels and decrease the lactate level within the construct. This is particularly the case with the Petri dish, where mixing increases the minimal oxygen from close to zero to half the ambient level (Fig. 6.6a, Fig. 6.7a). In case of mixing, it can be observed that the minimal concentrations of oxygen and glucose are directly related to the effective surface area of the construct exposed to the surrounding medium (Fig. 6.1, Fig. 6.7a,b). The lowest values occur for the compression setup, where only the side surface is free due to the impermeable loading platen on top (Fig. 6.1b). The perfusion setup gives approximately the same
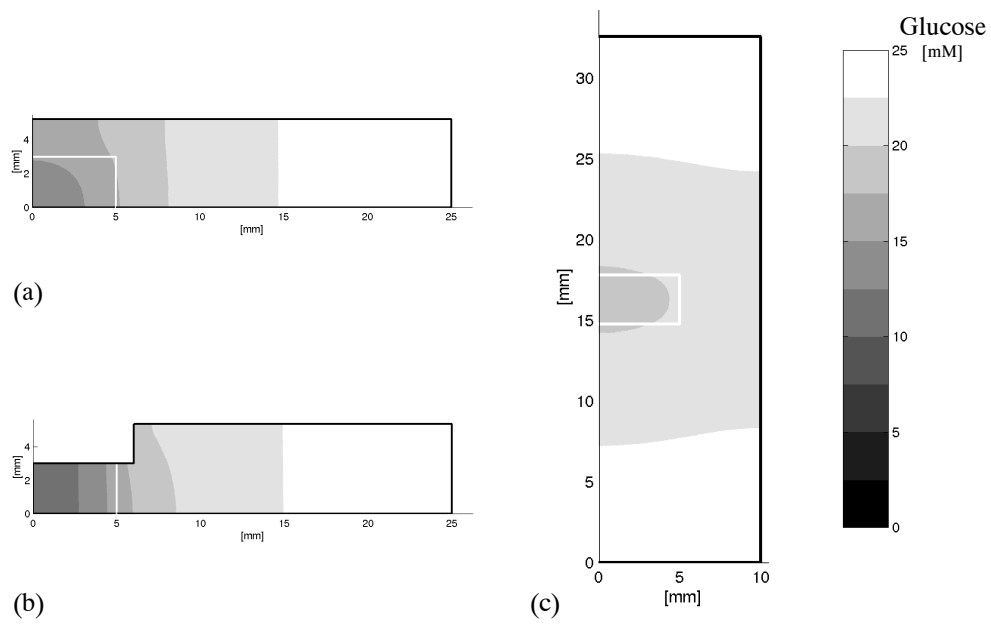
Figure 6.3: *Glucose distribution in the static case at 48 h. Because of axisymmetry only the right half of the domain is depicted (Fig. 6.1). The construct position is indicated with a white line. (a) Petri dish. (b) Compression setup. (c) Tube.*
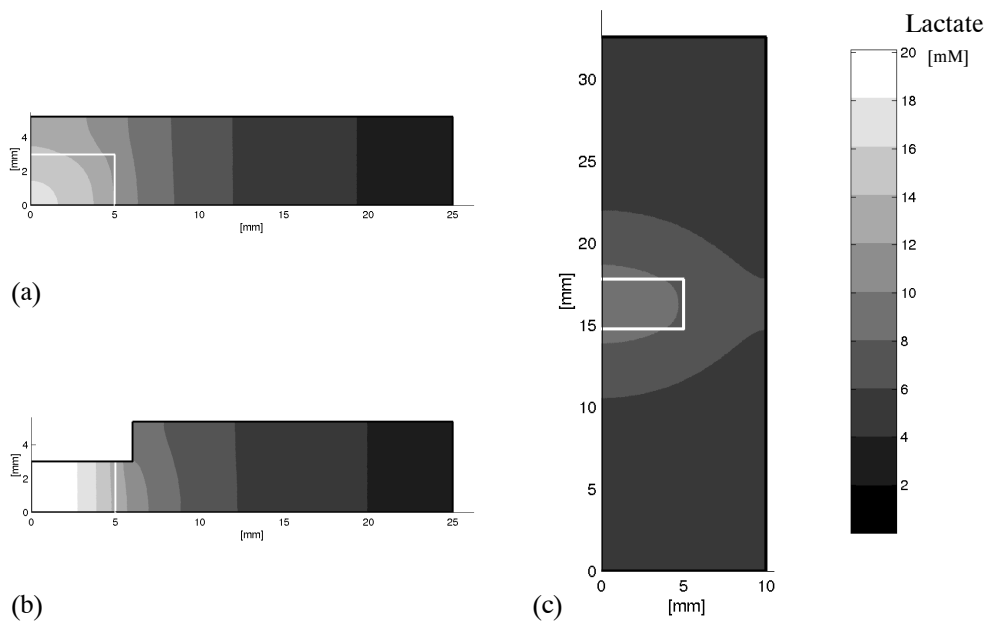
Figure 6.4: *Lactate distribution in the static case at 48 h. Because of axisymmetry only the right half of the domain is depicted (Fig. 6.1). The construct position is indicated with a white line. (a) Petri dish. (b) Compression setup. (c) Tube.*

(a)

(b)

(c)
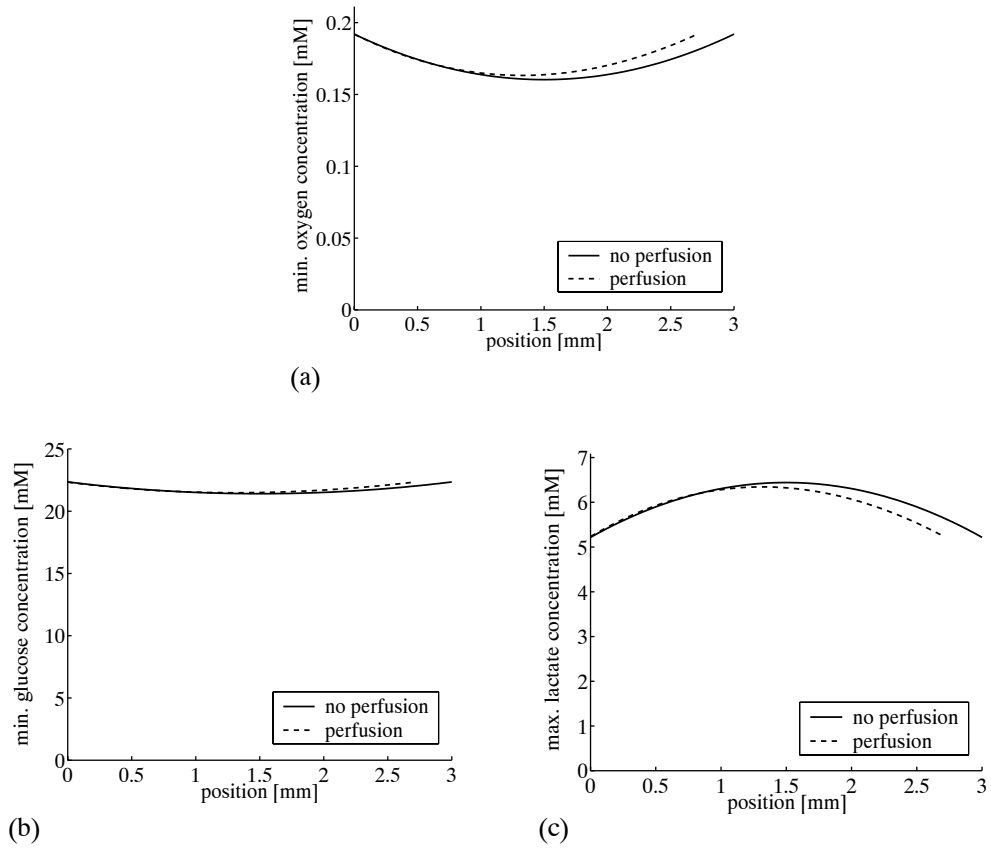
Figure 6.5: *Spatial concentration gradients over the construct thickness in the perfusion setup (Fig. 6.1d) at 48 h, for the cases with and without perfusion. (a) Oxygen. (b) Glucose. (c) Lactate. Displacement at the left side is suppressed, while the right side is free to move as a function of the external pressure.*

(a)

(b)

(c)
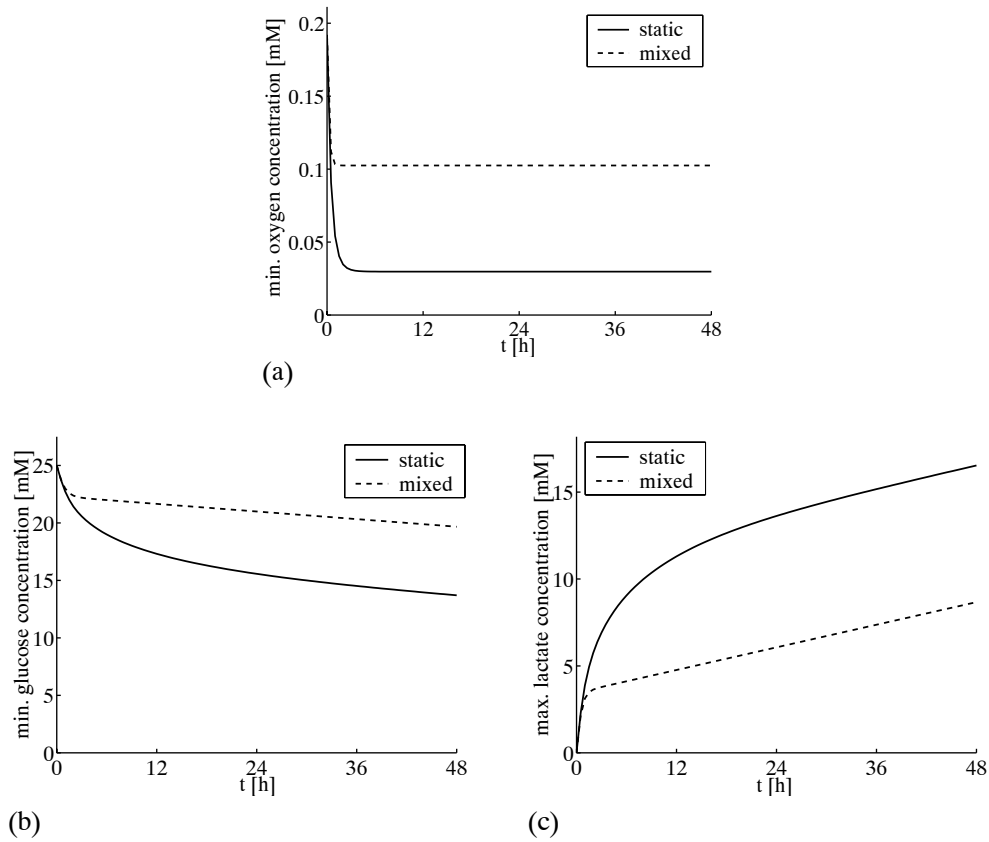
Figure 6.6: *Petri dish (Fig. 6.1a): Evolution of extreme concentration values within the construct as a function of time. Mixed and static situation. (a) Minimal oxygen. (b) Minimal glucose. (c) Maximum lactate.*

results as the tube, thus the radial confinement (Fig. 6.1d) does not appear to affect the minimal levels. The results for lactate in case of mixing show basically the same picture, only the trends are reversed (Fig. 6.7c).

Fig. 6.8 shows a selection of the results for the parameter variation of construct diffusivity. Accounting for the properties of mature cartilage results in lower oxygen and glucose levels and higher lactate levels (data not shown), for all culture setups and mixing conditions. These effects are most pronounced for the Petri dish and compression setup (Fig. 6.8). Varying the uptake rates to the maximum values results in more marked differences. In contrast to the reference situation, even the mixed cases now show severe oxygen depletion (Fig. 6.9a-c). For all mixed cases oxygen is zero at approximately 1 mm from a free surface, therefore even when all surfaces are exposed (Fig. 6.9c), a large central region of oxygen depletion is present. For the static cases the depleted region is even larger (data not shown). Varying the glucose uptake rate to the maximum value leads to severe glucose depletion within

(a)

(b)   (c)

Figure 6.7: *Concentration extremes at 48 h for all culture setups. (a) Minimal oxygen. (b) Minimal glucose. (c) Maximum lactate. Black represents the static situation, white the mixed case, except for the perfusion setup, where black and white stand for non-perfused and perfused respectively. Note that the oxygen concentration is near zero for the compression and tube setup in the static case.*

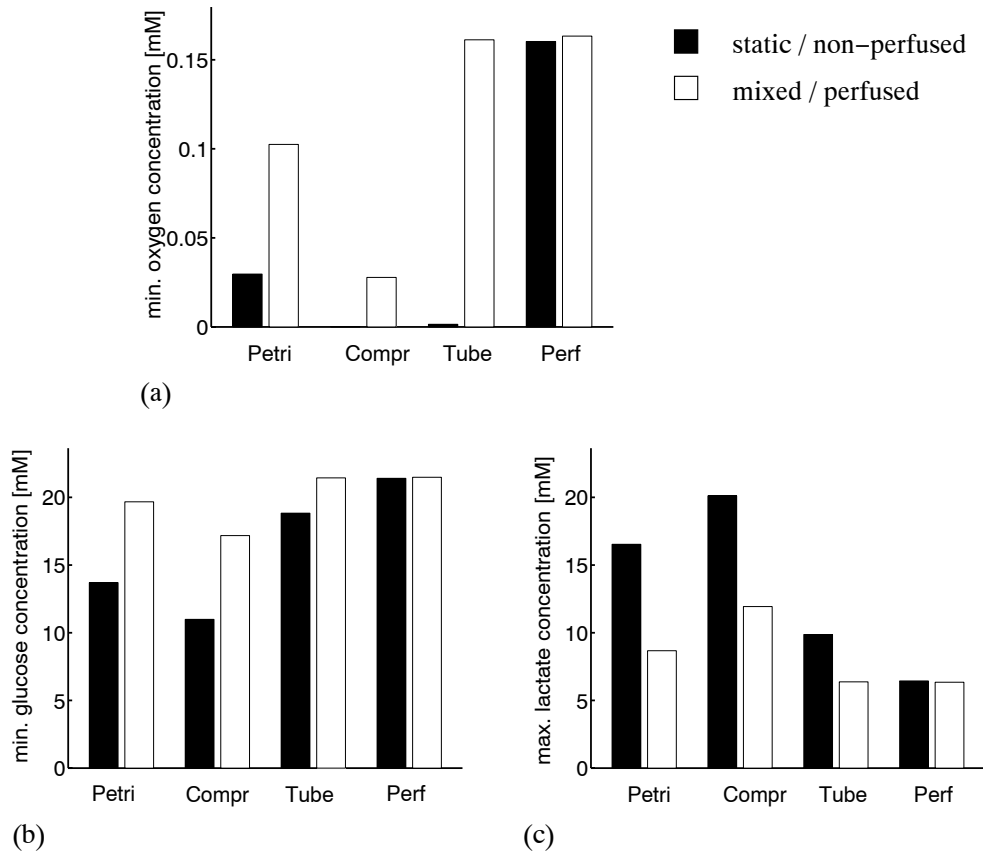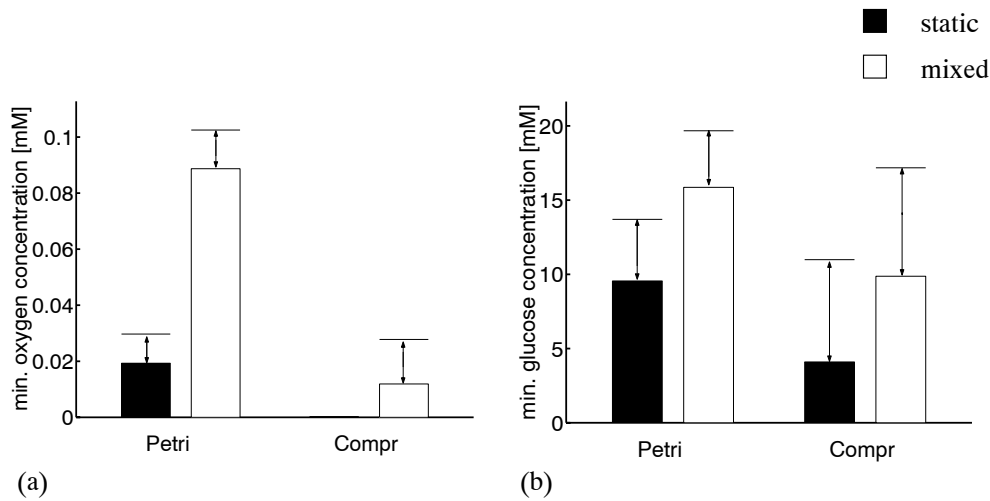**Figure 6.8:** *Parameter variation: effect of reduced construct diffusivity on minimal oxygen (a) and glucose (b) at 48 h. Results for mature cartilage in the Petri dish and compression setup. Arrows indicate the difference with the reference case. Note that the oxygen concentration is zero for the compression setup in the static case.*

the timespan considered, for all cases except the mixed tube (Fig. 6.9f). A clear difference with oxygen lies in the finite amount of glucose in the medium, which becomes relevant to the high uptake rate. As zero glucose is reached in the center of a construct, the glucose uptake becomes zero. Therefore situations with less effective surface area exposed to the medium have a net lower glucose consumption. This explains the higher boundary value and therefore larger glucose penetration depth for the mixed compression setup (Fig. 6.9d) compared to the mixed Petri dish (Fig. 6.9e).

6.4   Discussion

The mechanical functionality of tissue engineered cartilage constructs depends on cellular activity in terms of extracellular matrix synthesis, which can be related to levels of basic metabolites. Therefore, in the current study, different culture conditions were evaluated with respect to the supply of oxygen and glucose and the accumulation of lactate. A computational approach was adopted in which the bioreactor was modeled as a batch process and transport was considered within constructs seeded at high cell concentrations and of clinically relevant dimensions. To assess the extent to which mass transfer can be influenced theoretically, extreme cases were distinguished in which the culture medium in the bioreactor environment was assumed either completely static, or well mixed and fully oxygenated.

The main results of this work are that: Firstly, under static conditions severe oxygen depletion can arise within cartilage tissue engineering bioreactors. Secondly,
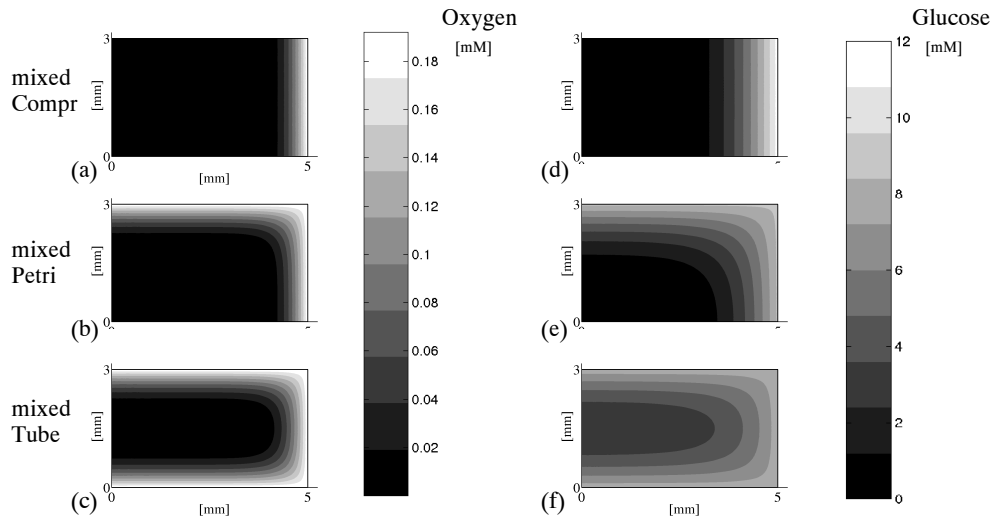
Figure 6.9: *Parameter variation: effect of increased cellular uptake on the distribution of oxygen (a-c) and glucose (d-f) at 48 h. Top: mixed compression setup (a,d). Middle: mixed Petri dish (b,e). Bottom: mixed tube (c,f).*

on the other hand, the use of high glucose medium guarantees adequate glucose supply during a 48 h period between medium refreshment. Thirdly, because of this large glucose quantity, however, significant lactate accumulation can occur. The outcomes also demonstrate that, in principle, mixing can indeed lead to a significant improvement in mass transfer compared to the static case. Depending on the culture setup different effective surface areas of the construct will be exposed to the medium, which is reflected in the metabolite concentrations within the construct (Fig. 6.7). As opposed to the static case, the results indicate that oxygen transport to the center of the construct is unlikely to be limiting, provided that the medium is well oxygenated and access to the medium is not too restricted. Also for glucose and lactate, transport to the center appears not to be limiting, provided the medium is well-mixed. Boundary values change over time due to the finite medium supply, but no significant differences occur between the center and periphery of the construct (Fig. 6.5). This is consistent with observations that by increasing the bulk medium volume, homogeneous matrix distribution could be attained in 4 mm thick alginate constructs, seeded at the same cell density as in the present study (40×10^6 cell cm^{-3}) [78].

However, these results do not imply that the supply of small metabolites is not an issue for cartilage tissue engineering in general. With respect to matrix synthesis, it has to be emphasized that not only the presence or absence of nutrients is relevant, but also the concentration level [103, 132, 134, 147, 153]. In general, for specific culture conditions, nutrient levels in the construct are determined by the ratio between the characteristic times for diffusion and uptake. For example, higher cell concentrations

have been employed in constructs of similar size, leading to lower oxygen values [134]. Furthermore, in the parameter variation study it was shown that by using maximum literature values for cellular glucose and oxygen uptake severe nutrient depletion occurred, even under optimal mixing conditions (Fig. 6.9). In addition the boundary conditions in the model for the mixed situation were based on the assumption of the limiting case of well-mixed and fully oxygenated medium. From studies using a tracer dye it was concluded that spinner flasks and RWV bioreactors closely approximated perfectly mixed conditions [50]. However, the measured oxygen level in the medium ranged from 65 - 87% of the equilibrium with the incubator atmosphere in RWV and spinner flask culture [61, 132]. In addition, depending on the local flow environment concentrations around the construct may be lower due to cellular uptake [185].

The question was posed whether mechanical stimulation experiments can be affected by mixing of the medium due to dynamic compression. The results indicate that an effect of higher oxygen and lower lactate levels cannot be excluded, while an influence of glucose seems less likely. Although in the compression setup (Fig. 6.1b) the minimal value for oxygen remains low, mixing results in higher oxygen levels in a much broader zone within the construct. Lactate levels are also reduced significantly. Glucose on the other hand is present in sufficient quantities in the construct for both mixed and static cases (Fig. 6.7).

The issue was raised whether medium refreshment around, or perfusion through the construct is more important in determining matrix synthesis [38]. For the perfusion setup in the present study it was assumed, that the medium surrounding the construct was well mixed in all cases, corresponding to medium perfusion around the construct. Under these conditions no significant gradients developed within the construct. Additional perfusion through the construct did not influence the concentration profiles (Fig. 6.5). This would indicate that with respect to small key molecules the main effect of perfusion is related to medium refreshment around the construct. The perfusion pressure applied in this study was limited, however, to avoid excessive deformation of the agarose construct. Due to the very low resulting fluid velocity of 0.05 μm s^{-1} it takes 8 h to reach the center of the construct with thickness $l = 3$ mm, while the characteristic time T_D^{glc} for the diffusion of glucose to the center is $T_D^{glc} = l^2/4D^{glc} = 0.8$ h. In principle a stiffer or more permeable construct would allow for higher flows. For PGA and PLLA/PGA scaffolds perfusion velocities ranging from 1 - 170 μm s^{-1} have been applied [40, 43, 137], which are high enough to affect the transport of even small molecules significantly.

Diffusive properties representative for cartilage were taken as a limiting case to investigate the effect of matrix accumulation during culture. For most cases it was found that the effect on solute transport is relatively limited for small solutes. However, important solutes such as growthfactors and cytokines are large molecules, for which far greater transport restrictions can arise [131]. In comparing the results for the initial construct properties and the limit of mature cartilage, it was assumed that the cellular uptake remained constant. Under tissue engineering conditions, it has been observed that the cumulative glucose utilization and lactate production was highly linear over a 5 week period, however the cell density increased by 60% implying an actual decrease in per cell uptake and production [132]. Also the per cell oxygen

consumption has been found to decrease over 41 days, which has been attributed to enhanced chondrogenic differentiation [111]. Furthermore, the matrix distribution and the cell distribution can be highly inhomogeneous, which has a large impact on computed concentration profiles [111, 134].

The results of the parameter variation of cellular uptake show that, for different culture configurations, the overall uptake can be limited by transport restrictions, as opposed to decreased cellular demand. Under conditions of nutrient limitations cellular regulation mechanisms become more important. Articular chondrocytes have been shown to display either a decrease in glycolysis as a function of decreasing oxygen [64, 103, 104] or by contrast, an increase (Pasteur effect) [94, 113, 132, 146], modulated by differences in culture conditions and associated dedifferentiation. As a first order estimation, the model assumed that glucose and oxygen uptake were uncoupled, although such regulation mechanisms can be subsequently included.

Although not the specific aim of this study, it has to be emphasized that due to the large variation in cellular uptake rates, no general guidelines can be given with respect to allowable cell concentrations. Therefore, for any specific application, the quantification of cellular utilization rates, depending on the cell source and culture conditions, is an essential starting point for optimizing culture protocols. It has been observed, for example, that chondrocytes subjected to hydrostatic pressure display a fall in glycolytic rate [105]. An open question remains however whether other types of mechanical stimulation can alter cellular uptake significantly. Such an effect would have important implications for the optimization of culture protocols, since a compromise might have to be reached between mechanical stimulation and the supply of nutrients to the center of the construct. For instance, the same number of loading cycles distributed over short intervals stimulates proliferation to a larger extent than longer consecutive loading periods [33]. In addition, it would be valuable to determine to what extent dynamic compression induces mixing in the surrounding medium, in order to evaluate implications for the use of stationary controls. Apart from mixing, improving the transport of small solute species by perfusion through the construct, requires that care must be taken to select scaffolds, which are stiff but highly permeable, in order to prevent excessive deformation.

A prerequisite for the practical application of numerical modeling as an engineering tool in cartilage tissue engineering, is the additional experimental identification of critical values, or favorable parameter domains, with respect to matrix synthesis and viability. In general, following the time course of the concentrations in the bulk medium is important, for the interpretation of measurements and the prediction of concentrations within the construct. Furthermore, combining such (on-line) measurements with relatively simple numerical models can prove useful for future bioreactor control applications [50, 191]. The type of numerical modeling employed in the current study is suited to quickly provide first order directions in the design of bioreactor setups and culture protocols. In this study the best nutrient supply was found for the mixed tube configuration. However, in order to achieve optimal functionality, mechanical stimulation could prove essential [82]. A further design criterion will therefore be to incorporate dynamic compression and to perform efficient mixing and oxygenation, while avoiding possibly excessive shear stress [40, 50, 181].

For this purpose, the present model for cellular processes within tissue engineered constructs can be combined with computational fluid dynamics for the hydrodynamic environment [30, 166, 185]. Subsequently, the predictive value of the model can be extended by establishing and incorporating regulation mechanisms of matrix metabolism and cell proliferation [56, 134].

Chapter 7

General summary and discussion

7.1   Introductory remarks

Tissue engineering as a strategy for articular cartilage repair is hampered by a lack of long term mechanical functionality. Bioreactor culture and conditioning is required to improve the functional properties of tissue engineered constructs, in order to enable appropriate clinical applications. Promoting cartilage formation is, however, a complex undertaking since in the first place the cellular environment within constructs is ill defined and secondly the cellular response to this environment is not fully determined. In this context, computational methods can be valuable to facilitate enhanced control over the development of tissue engineered cartilage.

In the present work, a general modeling framework for cartilage tissue engineering was proposed and subsequently elaborated. The aim of the approach was to provide an integration of the interactions between mechanics, transport and cell behavior, which occur simultaneously during bioreactor culture. In the following sections the findings of the specific elements of the work are summarized and discussed. Finally, recommendations for future work and conclusions are provided.

7.2   Solute transport

The first study examined the interaction between solute transport and dynamic compression. A finite element approach was adopted to describe transport due to mechanically induced fluid flow, within tissue engineered cartilage constructs (Chapter 2). An optimal frequency range for solute transport was shown to exist, since at low frequencies fluid velocities were small, while at high frequencies the fluid penetration depth in the construct was limited. In the case for which solute availability in the center of the construct was limited by diffusion and uptake, the equilibrium could be shifted by dynamic compression for large solutes but not for small solutes, such as glucose or oxygen. Therefore, compression-induced transport could only improve matrix biosynthesis when it was limited by the availability of a large solute. For an accurate description of the transport of specific large solutes, such as growth factors, however, the effect of pore size restrictions and binding need to be considered [10].

Loss of newly synthesized matrix components from the construct to the medium was dependent on the location of synthesis, i.e. whether uniform or mainly peripheral. A high percentage loss of newly synthesized matrix components was predicted, although neither proteoglycan aggregation nor hindrance by the porous scaffold material was considered. The dispersion parameter, which is related to the matrix pore size, determined the extent to which dynamic compression could result in additional loss of matrix components. Similar high loss percentages were found experimentally, for dynamic loading using a collagen scaffold with relatively large pores of 86 μm [98].

The research also examined to what extent nutrient depletion could occur during bioreactor culture. Diffusive transport combined with uptake of oxygen and glucose and production of lactate, was modeled for constructs of clinically relevant dimensions at high cell density, based on literature values (Chapter 6). Different culture configurations were evaluated, in which the bioreactor was operated as a batch process.

To assess the effect of mixing and perfusion extreme cases were considered in which the medium was assumed to be completely static or, alternatively, fully homogenized. It was shown that, in general, the use of high glucose medium guaranteed an adequate glucose level during the 48 h culture period. By contrast, under static conditions, severe oxygen depletion and significant lactate accumulation occurred within constructs. For these small metabolites, however, transport limitations were not in principle insurmountable, providing that the medium was well mixed and oxygenated and the construct was sufficiently exposed to the surrounding medium. During dynamic compression also mixing of the surrounding medium can occur, which can undoubtedly affect experimental results. Perfusion through the construct could not significantly enhance the transport of oxygen and glucose for the agarose hydrogel, since the perfusion pressure was limited in order to avoid excessive deformation of the construct, which is transfered to the cells depending on the cell-matrix interaction [100].

7.3   Tissue functionality

A high extracellular matrix content is a prerequisite for obtaining adequate mechanical properties. However, the amount of extracellular matrix alone does not fully determine the mechanical functionality of the tissue. The local, cell scale, distribution of extracellular matrix may play a role in the composition-function relationships of tissue engineered cartilage. It has been hypothesized that mechanical functionality arises when contact occurs between zones of matrix associated with individual cells [19, 122, 125, 143]. Furthermore, one of the mechanisms by which mechanical loading can enhance tissue properties may be the redistribution of matrix components, away from the cell [122, 141].

A microstructural approach was adopted to represent the evolving matrix distribution at the cellular level (Chapter 3). Matrix components produced by individual cells were assumed to diffuse outwards, while undergoing a process of binding and degradation. Predicted matrix distributions were found to agree with literature [122, 143]. Relationships between the concentration of matrix components and the local mechanical properties were assumed. Subsequently, a homogenization approach was employed to determine how the evolving matrix distribution at the cellular level, translates into the stiffness and permeability of the construct as a whole.

It was found that the overall mechanical properties of the construct were relatively insensitive to the local matrix distribution. This emphasizes the need for caution in the interpretation of functionality from histological examination and underlines the role of molecular organization in function-composition relationships. Mechanical properties can, however, be affected by a more localized matrix distribution, which can arise from the reduction in diffusivity due to matrix accumulation and the product inhibited kinetics of proteoglycan synthesis. In addition, the sensitivity to matrix distribution can be more pronounced as a result of non-linear relationships between mechanical properties and the local concentrations of matrix components.

7.4   Cell behavior

The energy metabolism of chondrocytes is closely associated with the synthesis of extra cellular matrix components. Quantification of utilization is therefore important for the design of culture protocols and bioreactors. A finite element approach was adopted to characterize the uptake of glucose and oxygen and the production of lactate in an experimental model system [77], over a wide range of cell densities (Chapter 4). It was shown that the level of glucose initially in the culture medium influenced the oxygen uptake as well as glucose utilization and lactate production. Cellular uptake rates were determined and found to be within the range reported in literature [74, 87, 111, 113, 129, 132, 134, 164, 173, 188]. Based on simple assumptions for chondrocyte metabolism, it was shown that for low glucose medium approximately all the glucose was converted into lactate, while for high glucose medium a significant fraction of glucose was stored or used in different pathways. It was also demonstrated that the oxygen uptake increased as a function of culture time. The aerobic consumption of glucose, however, could not account for the fraction of glucose that was not converted to lactate.

The main advantage of the computational approach is that it can provide spatial information, in the form of concentration gradients, which are, in general, not available experimentally. These gradients are essential for the interpretation of measurements. In addition, based on experimental data assumptions on metabolic regulation mechanisms can be evaluated quantitatively. Due to the large possible variation in uptake rate, it is necessary to start first by measuring uptake to enable numerical predictions based on specific cell types and sources and medium composition.

By applying different intervals of dynamic compression, chondrocytes have been shown to upregulate proliferation and proteoglycan synthesis in an uncoupled manner [33]. The importance of this mechanism is that when the cell response can be directed towards proliferation or proteoglycan synthesis, this potentially offers the means to control the development of tissue engineered cartilage. For the purpose of optimization and to apply loading protocols in a predictive manner, computational models can provide a valuable asset. Two modeling approaches were explored (Chapter 5). First, the cell population was divided into three compartments, an inactive compartment, one committed to proliferation and one to biosynthesis, which are in equilibrium in the unloaded situation. It was assumed that dynamic loading shifts the balance between these compartments temporarily, depending on the duration of the loading interval. The model was able to provide a reasonable overall representation of the stimulation of proliferation and biosynthesis for different loading protocols. However, for specific loading cases its predictive value was limited. Furthermore, the model could not either represent a peak in proliferation or account for the delay introduced by the cell division process.

Therefore, a subsequent cell cycle-based proliferation model was adopted. In the model a probabilistic A-state and a deterministic B-phase were distinguished. In the A-state a cell has a certain chance to pass the restriction point and enter the B-phase of the cell cycle. Once in the B-phase, the cell progresses in the cell cycle, at a

certain maturation velocity, until the cell division process is completed. Start of a loading period promotes cells to enter the B-phase of the cell cycle, while continued loading can inhibit proliferation by decreasing either the probability of entering the B-phase, or the cell cycle progression velocity. It was found that the effect of the number of loading intervals, could be represented based on an increased transition change from the A-state to the B-phase. The observed inhibition of proliferation by continued loading is more likely due to a decreased cell cycle progression velocity than to a reduced transition probability, since a large fraction of the cell population is required to have already entered the B-phase at an early stage. To represent the observed decrease in proliferation for every loading protocol, further investigations of the temporal effects of inhibition are required.

7.5   Numerical methods

An operator splitting approach was employed to uncouple, computationally, diffusive and convective solute transport and the source terms arising from cellular kinetics. By solving the linear transport equations for different solutes separately, computational efficiency is enhanced and flexibility, with respect to the number of solutes, is increased. In addition, convenient explicit (Runge-Kutta) integration methods can be used for the non-linear cellular kinetics. With respect to the balance between accuracy and computational costs, integration using the splitting scheme is fast, but requires a small time step to ensure accurate results. Furthermore, a minimal time step in relation to the element size applies for both the transient diffusion problem and the biphasic mechanics. Therefore, the use of a small time step requires also a large number of elements. Further constraints apply in the case of convective transport, since the element size and time step have to be in accordance with Peclet and Courant numbers restrictions (Chapter 2).

Accurate numerical methods are essential to describe solute transport under the influence of dynamic compression, involving a large number of load cycles. Since the main focus was on solute transport, an accurate fluid velocity field was of primary interest. For this purpose a biphasic finite element method was adopted, in which the Darcy problem was represented by a mixed formulation. The method fully accounts for finite deformation and conserves mass in each element. It was found that under influence of dynamic compression the diffusion front shifts as fluid is expressed or imbibed in the construct. In essence, the results were characterized by a diffusion process within a moving bulk of fluid, proceding from a time-varying refreshed zone. In order to represent the net effect of cyclic fluid flow on solute transport within the more central region of the construct, local mixing was introduced by means of a dispersion mechanism. However, whether such a mixing mechanism actually contributes to net solute transport is dependent on the solute diffusivity and pore size [184]. Remarkably, in other models for the transport of neutral solutes under cyclic loading, net transport was observed without the need for the introduction of a mixing mechanism [45, 121]. For both charged and neutral solutes, transport in response to dynamic loading was influenced by the fixed charge density of the tissue

[68, 192].

In the mixed finite element formulation of the Darcy problem only the divergence of the fluid flux is controlled. Therefore, for multi-dimensional flow Raviart-Thomas type elements were employed, in which the solution variables are the pressure and the normal flux through the element edges [89, 90, 120, 172]. Stabilized finite element methods can potentially enable the use of more conventional element spaces [35, 106, 120]. However, in the biphasic case this may be complicated by possibly contradictory demands of the coupled Darcy and elasticity problems, which requires further investigation. Finally, in case the aim of the biphasic calculations is to evaluate mechanical quantities rather than solute transport, the more common displacement-pressure based finite element formulation is more convenient and computationally efficient.

7.6   Perspectives and recommendations

In order to provide a value-added contribution to tissue engineering, the eventual goal of computational modeling is to quantitatively correlate culture parameters to the synthesis of functionally important matrix components, such as proteoglycans and collagen. For example, an expression based on oxygen has been used to represent GAG synthesis within cartilage constructs [134]. For the purpose of establishing relationships between medium composition and matrix synthesis, a numerical-experimental approach, as used in Chapter 4, is particularly useful. To be representative for tissue engineering applications, these studies have to be extended to prolonged culture periods and include both collagen and GAG synthesis.

In addition to matrix synthesis, chondrocyte-mediated matrix catabolism has to be considered [128, 164]. For example, for bovine articular chondrocytes, the production of matrix metalloproteinases and their inhibitors was affected by pH [147]. Furthermore, an optimum can exist between the synthesis of matrix components and retention within the construct. For example, a high oxygen tension enhanced total GAG synthesis, while proteoglycan aggregation and retention was promoted by low oxygen levels [152, 153].

From an engineering perspective, certain critical solute concentrations for optimal matrix synthesis may already be adequate for both bioreactor design and the optimization of culture protocols. However, in order to obtain sufficient predictive value, with respect to the chondrocyte response in time, it may be necessary to reach an improved quantitative understanding of the mechanisms involved in chondrocyte metabolism. For this purpose additional metabolic components need to be measured to fully elucidate to what extent certain metabolic pathways are being used. In the first place the experimental quantification of glycogen is useful.

At the lowest level chondrocyte metabolism is regulated by enzyme kinetics [103, 112, 114]. For other types of cells, computational models have been proposed, incorporating metabolic regulation based on enzyme kinetics, ADP/ATP ratio and redox state [154, 171]. This type of fundamental modeling, however, remains challenging and requires extensive experimental data.

Cell cycle models can contribute to the improved understanding of chondrocyte proliferation in response to dynamic mechanical deformation. To provide model input and validation, the cell cycle duration and the distribution of the cell population over the cell cycle can be measured [5, 180]. In addition, for tissue engineering applications, it has to be investigated whether the observed stimulatory effects of dynamic mechanical deformation extend up to longer periods of culture. A later stage of culture may provide a more clear reference configuration, since interaction with transient behavior, associated with the initial state and seeding procedure, is prevented. It is also necessary to determine whether mechanical stimulation can significantly increase cellular utilization, which in order to avoid nutrient depletion would have important implications for the optimization of loading protocols.

The modeled mechanisms for solute transport induced by dynamic compression have to be quantified by direct comparison with experimental concentration profiles. For example, a freeze-substitution method has been reported to analyze the solute distribution in cyclically-compressed cartilage explants, albeit at a low frequency of 0.001 Hz and a few loading cycles [144]. For practical applications it is not convenient to computationally evaluate solute transport at high loading frequencies for extended culture periods. Therefore it is necessary to investigate whether effective transport models can be formulated that provide a sufficient estimate, using for example a spatially varying diffusion coefficient [144], which can be based on the averaged local fluid velocity. In addition to transport within the construct, future studies of the cell response to dynamic compression will have to consider the effects of mixing in the surrounding medium, induced by movement of the loading platens.

Besides in determining global composition-function relationships, microstructural models of the cellular environment can be particularly useful in studying the development of the local matrix organization. For instance, models can be extended to incorporate fiber orientation, pre-tension and swelling, combined with kinetics of biosynthesis and mechanotransduction. Furthermore, if appropriate, scaffold degradation needs to be taken into account.

As a first step in a systematic approach, it is important to characterize the particular cell source, or even batch, by measuring utilization, for example using cells in small beads or relatively simple systems, such as those employed in Chapter 4. As a next step transport limitations have to be evaluated. Using fluorescence techniques concentration profiles can be measured in one-dimensional experimental models, which can be used to validate computational models based on uptake and diffusive transport. This provides independent confirmation of the extent to which utilization rates measured in simple systems are representative. For this purpose it is essential to have an accurate estimate of diffusive properties, since concentration profiles are determined by the ratio between the characteristic uptake and diffusion time. Subsequently, the computational models based on these systems can be used to optimize bioreactor culture conditions in three-dimensional configurations. Additional validation can be provided by measuring concentrations using probes at specific points within constructs. To avoid unnecessary transport limitations it is important in bioreactor design to incorporate (perfusion) systems that provide efficient mixing without excessive shear stresses. Providing that the culture conditions

satisfy the basic requirement of adequate nutrient supply, additional biomechanical and biochemical stimulations can be applied.

In clinical applications elaborate measurements are impractical. Therefore it is necessary to characterize the culture process experimentally, to such an extent that unexpected qualitatively divergent behavior can be excluded. If it can be assured that the process takes place within the predictive range of computational models a limited number of practical measurements suffices. In this case limited control applications are feasible. For example, measurements of medium composition as a function of time can be used to predict nutrient levels within constructs, which can serve as a criterion for medium replenishment while preserving beneficial factors as far as possible.

7.7   Conclusions

- An integrated approach is required to model the development of tissue engineered cartilage, as a function of its mechanical and biochemical environment, in bioreactor culture.

- The proposed modeling framework is well suited for this purpose. At the present stage, however, additional identification and quantification of chondrocyte behavior is necessary, with respect to utilization, biosynthesis and mechanotransduction.

- The development of functionality in tissue engineered cartilage constructs appears to be less related to the local distribution of matrix deposition, than to mechanical properties associated with the molecular organization of the matrix components.

- In the characterization of cell behavior, computational models can contribute to the interpretation of experimental results, by providing a quantitative metabolic structure, accounting for time dependency and spatial distribution.

- Short term studies can be used to identify metabolic pathways. However, longer term studies are required to determine to what extent short term cellular behavior is directive and representative for tissue engineering applications.

- In order to contribute to the optimization of mechanical stimulation protocols the present computational models need to be improved, based on fundamental studies of the cell cycle and longer term experiments.

- An adequate nutrient supply is a prerequisite for cartilage tissue engineering, which has to be ensured first so that further biomechanical stimulation can be most effective. This includes not only maintaining viability, but also conditions that favor matrix synthesis.

- The present computational models for transport and utilization, can be employed in improving bioreactor design and the optimization of culture protocols. For this purpose, criteria with respect to matrix synthesis have to be established.

- Extensive experimental characterization is required to enable control applications in bioreactor culture. Limited model-based control applications appear feasible in maintaining an optimal medium composition. Use of mechanical stimulation is presently a feed-forward process.

Acknowledgment

References

[1] B. Alberts, D. Bray, J. Lewis, M. Raff, K. Roberts, and J.D. Watson. *Molecular Biology of the Cell, 3rd ed.* Garland Publishing, New York, 1994.

[2] R.V. Allhands, P.A. Torzilli, and F.A. Kallfelz. Measurement of diffusion of uncharged molecules in articular cartilage. *Cornell Vet.*, 74:111–123, 1983.

[3] E.S. Almeida and R.L. Spilker. Mixed and penalty finite element models for the nonlinear behavior of biphasic soft tissues in finite deformation: Part I - alternate formulations. *Comp. Meth. Biomech. Biomed. Eng.*, 1(1):25–46, 1997.

[4] E.S. Almeida and R.L. Spilker. Mixed and penalty finite element models for the nonlinear behavior of biphasic soft tissues in finite deformation: Part II - nonlinear examples. *Comp. Meth. Biomech. Biomed. Eng.*, 1(2):151–170, 1997.

[5] A. Aszodi, E.B. Hunziker, C. Brakebusch, and R. Fässler. $\beta 1$ integrins regulate chondrocyte rotation, G1 progression, and cytokinesis. *Genes & Development*, 17:2465–2479, 2003.

[6] J.E. Bailey and D.F. Ollis. *Biochemical Engineering Fundamentals.* McGraw-Hill, New York, 1986.

[7] P.J. Basser, R. Schneiderman, R.A. Bank, E. Wachtel, and A. Maroudas. Mechanical properties of the collagen network in human articular cartilage as measured by osmotic stress technique. *Arch. Biochem. Biophys.*, 351(2):207–219, 1998.

[8] A. Bejan. *Heat Transfer.* Wiley, New York, 1993.

[9] S. Bernard, L. Pujo-Menjouet, and M.C. Mackey. Analysis of cell kinetics using a cell division marker: Mathematical modeling of experimental data. *Biophys. J.*, 84:3414–3424, 2003.

[10] N.R. Bhakta, A.M. Garcia, E.H. Frank, and A.J. Grodzinsky. The insulin-like growth factors (IGFs) I and II bind to articular cartilage via the IGF-binding proteins. *J. Biol. Chem.*, 275(8):5860–5866, 2000.

[11] T. Blunk, A.L. Sieminski, K.J. Gooch, D.L. Courter, A.P. Hollander, A.M. Nahir, R. Langer, G. Vunjak-Novakovic, and L.E. Freed. Differential effects of growth factors on tissue-engineered cartilage. *Tissue Eng.*, 8(1):73–84, 2002.

[12] P. Boderke, K. Schittkowski, M. Wolf, and H.P. Merkle. Modeling of diffusion and concurrent metabolism in cutaneous tissue. *J. Theor. Biol.*, 204:393–407, 2000.

[13] L.J. Bonassar, A.J. Grodzinsky, E.H. Frank, S.G. Davila, N.R. Bhaktav, and S.B. Trippel. The effect of dynamic compression on the response of articular cartilage to insulin-like growth factor-I. *J. Orthop. Res.*, 19:11–17, 2001.

[14] R.M. Bowen. Incompressible porous media models by use of the theory of mixtures. *Int. J. Eng. Sci.*, 18:1129–1148, 1980.

[15] R.G.M. Breuls, B.G. Sengers, C.W.J. Oomens, C.V.C. Bouten, and F.P.T. Baaijens. Predicting local cell deformations in engineered tissue constructs: A multilevel finite element approach. *J. Biomech. Eng.*, 124:198–207, 2002.

[16] S.J. Bryant and K.S. Anseth. Controlling the spatial distribution of ECM components in degradable PEG hydrogels for tissue engineering cartilage. *J. Biomed. Mater. Res.*, 64A:70–79, 2003.

[17] P.M. Bursac, L.E. Freed, R.J. Biron, and G. Vunjak-Novakovic. Mass transfer studies of tissue engineered cartilage. *Tissue Eng.*, 2(2):141–150, 1996.

[18] D. Burstein, M.L. Gray, A.L. Hartman, R. Gipe, and B.D. Foy. Diffusion of small solutes in cartilage as measured by nuclear magnetic resonance (NMR) spectroscopy and imaging. *J. Orthop. Res.*, 11(4):465–478, 1993.

[19] M.D. Buschmann, Y.A. Gluzband, A.J. Grodzinsky, and E.B. Hunziker. Mechanical compression modulates matrix biosynthesis in chondrocyte/agarose culture. *J. Cell Sci.*, 108:1497–1508, 1995.

[20] M.D. Buschmann and A.J. Grodzinsky. A molecular model of proteoglycan-associated electrostatic forces in cartilage mechanics. *J. Biomech. Eng.*, 117:179–192, 1995.

[21] M.D. Buschmann, Y.J. Kim, M. Wong, E. Frank, E.B. Hunziker, and A.J. Grodzinsky. Stimulation of aggrecan synthesis in cartilage explants by cyclic loading is localized to regions of high interstitial fluid flow. *Arch. Biochem. Biophys.*, 366(1):1–7, 1999.

[22] D.L. Butler, S.A. Goldstein, and F. Guilak. Functional tissue engineering: The role of biomechanics. *J. Biomech. Eng.*, 122:570–575, 2000.

[23] S.J. Cain and P.C. Chau. Transition probability cell cycle model part I - balanced growth. *J. Theor. Biol.*, 185:55–67, 1997.

[24] S.J. Cain and P.C. Chau. Transition probability cell cycle model part II - non-balanced growth. *J. Theor. Biol.*, 185:69–79, 1997.

[25] D.R. Carter, G.S. Beaupre, N.J. Giori, and J.A. Helms. Mechanobiology of skeletal regeneration. *Clin. Orthop.*, 355S:S41–S55, 1998.

[26] S.E. Carver and C.A. Heath. Influence of intermittent pressure, fluid flow, and mixing on the regenerative properties of articular chondrocytes. *Biotechnol. Bioeng.*, 65:274–281, 1999.

[27] B. Caterson, C.R. Flannery, C.E. Hughes, and C.B. Little. Mechanism involved in cartilage proteoglycan catabolism. *Matrix Biol.*, 19:333–344, 2000.

[28] S.C.N. Chang, J.A. Rowley, G. Tobias, N.G. Genes, A.K. Roy, D.J. Mooney, C.A. Vacanti, and L.J. Bonassar. Injection molding of chondrocyte/alginate constructs in the shape of facial implants. *J. Biomed. Mater. Res.*, 55:503–511, 2001.

[29] S. Chawla and S.M. Lenhart. Application of optimal control theory to bioremediation. *J. Comp. Appl. Math.*, 114:81–102, 2000.

[30] H.C. Chen, H.P. Lee, M.L. Sung, C.J. Liao, and Y.C. Hu. A novel rotating-shaft bioreactor for two-phase cultivation of tissue-engineered cartilage. *Biotechnol. Prog.*, 20(6):1802–1809, 2004.

[31] S.S. Chen, Y.H. Falcovitz, R. Schneiderman, A. Maroudas, and R.L. Sah. Depth-dependent compressive properties of normal aged human femoral head articular cartilage: Relationship to fixed charge density. *Osteoarth. Cartilage*, 9:561–569, 2001.

[32] T.T. Chowdhury. Role of nitric oxide and PGE2 in chondrocyte mechanotransduction. *Ph.D. thesis, Queen Mary University, London, UK*, 2003.

[33] T.T. Chowdhury, D.L. Bader, J.C. Shelton, and D.A. Lee. Temporal regulation of chondrocyte metabolism in agarose constructs subjected to dynamic compression. *Arch. Biochem. Biophys.*, 417:105–111, 2003.

[34] C.C. Clark, B.S. Tolin, and C.T. Brighton. The effect of oxygen tension on proteoglycan synthesis and aggregation in mammalian growth plate chondrocytes. *J. Orthop. Res.*, 9:477–484, 1991.

[35] R. Codina. A stabilized finite element method for generalized stationary incompressible flows. *Comp. Meth. Appl. Mech. Eng.*, 190:2681–2706, 2001.

[36] W.D. Comper and R.P.W. Williams. Hydrodynamics of concentrated proteoglycan solutions. *J. Biol. Chem.*, 262(28):13464–13471, 1987.

[37] J. Crank. *The Mathematics of Diffusion*. Oxford University Press, New York, 1975.

[38] E.M. Darling and K.A. Athanasiou. Articular cartilage bioreactors and bioprocesses. *Tissue Eng.*, 9(1):9–26, 2003.

[39] T. Davisson, S. Kunig, A. Chen, R. Sah, and A. Ratcliffe. Static and dynamic compression modulate matrix metabolism in tissue engineered cartilage. *J. Orthop. Res.*, 20:842–848, 2002.

[40] T. Davisson, R.L. Sah, and A. Ratcliffe. Perfusion increases cell content and matrix synthesis in chondrocyte three-dimensional cultures. *Tissue Eng.*, 8(5):807–816, 2002.

[41] M.A. Dimicco and R.L. Sah. Dependence of cartilage matrix composition on biosynthesis, diffusion, and reaction. *Transport Porous Media*, 50:57–73, 2003.

[42] C. Domm, M. Schünke, K. Christesen, and B. Kurz. Redifferentiation of dedifferentiated bovine articular chondrocytes in alginate culture under low oxygen tension. *Osteoarth. Cartilage*, 10:13–22, 2002.

[43] N.S. Dunkelman, M.P. Zimber, R.G. LeBaron, R. Pavelec, M. Kwan, and A.F. Purchio. Cartilage production by rabbit articular chondrocytes on polyglycolic acid scaffolds in a closed bioreactor system. *Biotechnol. Bioeng.*, 46:299–305, 1995.

[44] S.J. Ellis, M. Velayutham, S.S. Velan, E.F. Petersen, J.L. Zweier, P. Kuppusamy, and R.G.S. Spencer. EPR oxygen mapping (EPROM) of

engineered cartilage grown in a hollow-fiber bioreactor. *Magn. Res. Med.*, 46:819–826, 2001.

[45] S.J. Ferguson, K. Ito, and L.P. Nolte. Fluid flow and convective transport of solutes within the intervertebral disc. *J. Biomech.*, 37(2):213–221, 2004.

[46] L.E. Freed, A.P. Hollander, I. Martin, J.R. Barry, R. Langer, and G. Vunjak-Novakovic. Chondrogenesis in a cell-polymer-bioreactor system. *Exp. Cell Res.*, 240:58–65, 1998.

[47] L.E. Freed, R. Langer, I. Martin, N.R. Pellis, and G. Vunjak-Novakovic. Tissue engineering of cartilage in space. *Proc. Nat. Acad. Sci. USA*, 94:13885–13890, 1997.

[48] L.E. Freed, J.C. Marquis, G. Vunjak-Novakovic, J. Emmanual, and R. Langer. Composition of cell-polymer cartilage implants. *Biotechnol. Bioeng.*, 43:605–614, 1994.

[49] L.E. Freed, I. Martin, and G. Vunjak-Novakovic. Frontiers in tissue engineering: In vitro modulation of chondrogenesis. *Clin. Orthop.*, 367S:S46–S58, 1999.

[50] L.E. Freed and G. Vunjak-Novakovic. Tissue culture bioreactors: Chondrogenesis as a model system. In R. Lanza, R. Langer, and W. Chick, editors, *Principles of tissue engineering*, pages 151–165. Academic Press, London, 1997.

[51] L.E. Freed and G. Vunjak-Novakovic. Culture of organized cell communities. *Adv. Drug Delivery Rev.*, 33:15–30, 1998.

[52] L.E. Freed, G. Vunjak-Novakovic, J.C. Marquis, and R. Langer. Kinetics of chondrocyte growth in cell-polymer implants. *Biotechnol. Bioeng.*, 43:597–604, 1994.

[53] A.J.H. Frijns. A four-component mixture theory applied to cartilaginous tissues. *Ph.D. thesis, Eindhoven University of Technology, Eindhoven, The Netherlands*, 2000.

[54] C.J. Galban and B.R. Locke. Analysis of cell growth in a polymer scaffold using a moving boundary approach. *Biotechnol. Bioeng.*, 56:422–432, 1997.

[55] C.J. Galban and B.R. Locke. Analysis of cell growth kinetics and substrate diffusion in a polymer scaffold. *Biotechnol. Bioeng.*, 65:121–132, 1999.

[56] C.J. Galban and B.R. Locke. Effects of spatial variation of cells and nutrient and product concentrations coupled with product inhibition on cell growth in a polymer scaffold. *Biotechnol. Bioeng.*, 64:633–643, 1999.

[57] C. Gallo and G. Manzini. A mixed finite element/finite volume approach for solving biodegradation transport in groundwater. *Int. J. Num. Meth. Fluids*, 26:533–556, 1998.

[58] A.M. Garcia, E.H. Frank, P.E. Grimshaw, and A.J. Grodzinsky. Contributions of fluid convection and electrical migration to transport in cartilage: Relevance to loading. *Arch. Biochem. Biophys.*, 333:317–325, 1996.

[59] K.J. Gooch, T. Blunk, D.L. Courter, A.L. Sieminski, P.M. Bursac, G. Vunjak-Novakovic, and L.E. Freed. IGF-I and mechanical environment interact to modulate engineered cartilage development. *Biochem. Biophys. Res. Commun.*, 286:909–915, 2001.

[60] K.J. Gooch, T. Blunk, C.T. Tennant, G. Vunjak-Novakovic, R. Langer, and L.E. Freed. Mechanical forces and growth factors utilized in tissue engineering. In C.W. Patrick, A.G. Mikos, and L.V. McIntire, editors, *Frontiers in Tissue Engineering*, pages 61–82. Pergamon, Amsterdam, 1998.

[61] K.J. Gooch, J.H. Kwon, T. Blunk, R. Langer, L.E. Freed, and G. Vunjak-Novakovic. Effects of mixing intensity on tissue-engineered cartilage. *Biotechnol. Bioeng.*, 72:402–407, 2001.

[62] P. Gribbon and T.E. Hardingham. Macromolecular diffusion of biological polymers measured by confocal fluorescence recovery after photobleaching. *Biophys. J.*, 75:1032–1039, 1998.

[63] P. Gribbon, B.C. Heng, and T.E. Hardingham. The molecular basis of the solution properties of hyaluronan investigated by confocal fluorescence recovery after photobleaching. *Biophys. J.*, 77:2210–2216, 1999.

[64] M.J. Grimshaw and R.M. Mason. Bovine articular chondrocyte function in vitro depends upon oxygen tension. *Osteoarth. Cartilage*, 8:386–392, 2000.

[65] A.J. Grodzinsky, R.D. Kamm, and D.A. Lauffenburger. Quantitative aspects of tissue engineering: Basic issues in kinetics transport and mechanics. In R. Lanza, R. Langer, and W. Chick, editors, *Principles of tissue engineering*, pages 193–207. Academic Press, London, 1997.

[66] A.J. Grodzinsky, M.E. Levenston, M. Jin, and E.H. Frank. Cartilage tissue remodeling in response to mechanical forces. *Annu. Rev. Biomed. Eng.*, 2:691–713, 2000.

[67] W.Y. Gu, W.M. Lai, and V.C. Mow. A mixture theory for charged-hydrated soft tissues containing multi-electrolytes: Passive transport and swelling behaviors. *J. Biomech. Eng.*, 120:169–180, 1998.

[68] W.Y. Gu, D.N. Sun, W.M. Lai, and V.C. Mow. Analysis of the dynamic permeation experiment with implications to cartilaginous tissue engineering. *J. Biomech. Eng.*, 126:485–491, 2004.

[69] W.Y. Gu, H. Yao, C.Y. Huang, and H.S. Cheung. New insight into deformation-dependent hydraulic permeability of gels and cartilage, and dynamic behavior of agarose gels in confined compression. *J. Biomech.*, 36:593–598, 2003.

[70] W.Y. Gu, H. Yao, A.L. Vega, and D. Flagler. Diffusivity of ions in agarose gels and intervertebral disc: Effect of porosity. *Ann. Biomed. Eng.*, 32(12):1710–1717, 2004.

[71] F. Guilak and V.C. Mow. The mechanical environment of the chondrocyte: A biphasic finite element model of cell-matrix interactions in articular cartilage. *J. Biomech.*, 33:1663–1673, 2000.

[72] F. Guilak, R. Sah, and L.A. Setton. Physical regulation of cartilage metabolism. In V.C. Mow and W.C. Hayes, editors, *Basic Orthopaedic Biomechanics*, pages 179–207. Raven Press, New York, 1997.

[73] V.C. Hascall, J.D. Sandy, and C.J. Handley. Regulation of proteoglycan metabolism in articular cartilage. In C.W. Archer, B. Caterson, and

M. Benjamin, editors, *Biology of the Synovial Joint*, pages 101–120. Harwood Academic Pub., Amsterdam, 1999.

[74] J.C. Haselgrove, I.M. Shapiro, and S.F. Silverton. Computer modeling of the oxygen supply and demand of cells of the avian growth cartilage. *Am. J. Physiol.: Cell Physiol.*, 265:c497–c506, 1993.

[75] E.M. Hasler, W. Herzog, J.Z. Wu, W. Müller, and U. Wyss. Articular cartilage biomechanics: Theoretical models, material properties, and biosynthetic response. *Crit. Rev. Biomed. Eng.*, 27(6):415–488, 1999.

[76] H.K. Heywood. Chondrocyte metabolism in alginate constructs for tissue engineering. *Ph.D. thesis, Queen Mary, University of London, London, UK*, 2004.

[77] H.K. Heywood, M. Bongers, D.L. Bader, and D.A. Lee. Glucose depletion induces an upregulation of oxygen utilisation by chondrocytes. *Trans. Orthop. Res. Soc. 50th Annual Meeting, San Francisco, USA*, 2004.

[78] H.K. Heywood, P.K. Sembi, D.A. Lee, and D.L. Bader. Cellular utilization determines viability and matrix distribution profiles in chondrocyte-seeded alginate constructs. *Tissue Eng.*, 10(9/10):1467–1479, 2004.

[79] S. Holm, A. Maroudas, J.P.G. Urban, G. Selstam, and A. Nachemson. Nutrition of the intervertebral disc: Solute transport and metabolism. *Connective Tissue Research*, 8:101–119, 1981.

[80] H.A. Horner and J.P.G. Urban. Effect of nutrient supply on the viability of cells from the nucleus pulposus of the intervertebral disk. *Spine*, 26(23):2543–2549, 2001.

[81] W. Hundsdorfer and J.G. Verwer. A note on splitting errors for advection-reaction equations. *Appl. Numer. Math.*, 18:191–199, 1995.

[82] C.T. Hung, R.L. Mauck, C.C.B. Wang, E.G. Lima, and G.A. Athesian. A paradigm for functional tissue engineering of articular cartilage via applied physiologic deformational loading. *Ann. Biomed. Eng.*, 32(1):35–49, 2004.

[83] E.B. Hunziker. Articular cartilage repair: Basic science and clinical progress. a review of the current status and prospects. *Osteoarth. Cartilage*, 10:432–463, 2001.

[84] D.W. Hutmacher. Scaffolds in tissue engineering bone and cartilage. *Biomaterials*, 21:2529–2543, 2000.

[85] J.M. Huyghe and J.D. Janssen. Quadriphasic mechanics of swelling incompressible porous media. *Int. J. Eng. Sci.*, 35(8):793–802, 1997.

[86] H. Ishihara and J.P.G. Urban. Effects of low oxygen concentrations and metabolic inhibitors on proteoglycan and protein synthesis rates in the intervertebral disc. *J. Orthop. Res.*, 17:829–835, 1999.

[87] K. Johnson, A. Jung, A. Murphy, A. Andreyev, J. Dykens, and R. Terkeltaub. Mitochondrial oxidative phosphorylation is a downstream regulator of nitric oxide effects on chondrocyte matrix synthesis and mineralization. *Arthritis Rheum.*, 43(7):1560–1570, 2000.

[88] W.R. Jones, H.P. Ting-Beall, G.M. Lee, S.S. Kelley, R.M. Hochmuth, and F. Guilak. Alterations in the young's modulus and volumetric properties of chondrocytes isolated from normal and osteoarthritic human cartilage. *J. Biomech.*, 32:119–127, 1999.

[89] E.F. Kaasschieter, A.J.H. Frijns, and J.M. Huyghe. Mixed finite element modelling of cartilaginous tissues. *Math. Comp. Simul.*, 61:549–560, 2003.

[90] E.F. Kaasschieter and A.J.M. Huijben. Mixed-hybrid finite elements and streamline computation for the potential flow problem. *Num. Meth. Part. Diff. Eq.*, 8:221–266, 1992.

[91] Y-J. Kim, R.L.Y. Sah, J-Y.H. Doong, and A.J. Grodzinsky. Fluorometric assay of DNA in cartilage explants using Hoechst 33258. *Anal. Biochem.*, 174:168–176, 1988.

[92] S.M. Klisch, S.S. Chen, R.L. Sah, and A. Hoger. A growth mixture theory for cartilage with application to growth-related experiments on cartilage explants. *J. Biomech. Eng.*, 125:169–179, 2003.

[93] V. Kouznetsova, W.A.M. Brekelmans, and F.P.T. Baaijens. An approach to micro-macro modeling of heterogeneous materials. *Comp. Mech.*, 27(1):37–48, 2001.

[94] J.M. Lane, C.T. Brighton, and B.J Menkowitz. Anaerobic and aerobic metabolism in articular cartilage. *J. Rheumatol.*, 4:334–342, 1977.

[95] D. Lanser and J.G. Verwer. Analysis of operator splitting for advection-diffusion-reaction problems from air pollution modelling. *J. Comp. Appl. Math.*, 11:201–216, 1999.

[96] R.G. LeBaron and K.A. Athanasiou. Ex vivo synthesis of articular cartilage. *Biomaterials*, 21:2575–2587, 2000.

[97] H.A. Leddy and F. Guilak. Site-specific molecular diffusion in articular cartilage measured using fluorescence recovery after photobleaching. *Ann. Biomed. Eng.*, 31:753–760, 2003.

[98] C.R. Lee, A.J. Grodzinsky, and M. Spector. Biosynthetic response of passaged chondrocytes in a type II collagen scaffold to mechanical compression. *J. Biomed. Mater. Res.*, 64A:560–569, 2003.

[99] D.A. Lee and D.L. Bader. Compressive strains at physiological frequencies influence the metabolism of chondrocytes seeded in agarose. *J. Orthop. Res.*, 15:181–188, 1997.

[100] D.A. Lee, M.M. Knight, J.F. Bolton, B.D. Idowu, M.V. Kayser, and D.L. Bader. Chondrocyte deformation within compressed agarose constructs at the cellular and sub-cellular levels. *J. Biomech.*, 33:81–95, 2000.

[101] D.A. Lee, T. Noguchi, S.P. Frean, P. Lees, and D.L. Bader. The influence of mechanical loading on isolated chondrocytes seeded in agarose constructs. *Biorheology*, 37:149–161, 2000.

[102] D.A. Lee, T. Noguchi, M.M. Knight, L. O'Donnell, G. Bentley, and D.L. Bader. Response of chondrocyte subpopulations cultured within unloaded and loaded agarose. *J. Orthop. Res.*, 16:726–733, 1998.

[103] R.B. Lee and J.P.G. Urban. Evidence for a negative pasteur effect in articular cartilage. *Biochem. J.*, 321:95–102, 1997.

[104] R.B. Lee and J.P.G. Urban. Functional replacement of oxygen by other oxidants in articular cartilage. *Arthritis Rheum.*, 46(12):3190–3200, 2002.

[105] R.B. Lee, R.J. Wilkins, S. Razaq, and J.P.G. Urban. The effect of mechanical stress on cartilage energy metabolism. *Biorheology*, 39:133–143, 2002.

[106] M.E. Levenston, E.H. Frank, and A.J. Grodzinsky. Variationally derived 3-field finite element formulations for quasistatic poroelastic analysis of hydrated biological tissues. *Comp. Meth. Appl. Mech. Eng.*, 156:231–246, 1998.

[107] E.N. Lightfoot and K.A. Duca. The role of mass transfer in tissue function. In J.D. Bronzino, editor, *The Biomedical Engineering Handbook, 2nd ed.*, pages 115.1–115.15. CRC Press, London, 2000.

[108] P. Lundberg and P.W. Kuchel. Diffusion of solutes in agarose and alginate gels: 1H and 23Na PFGSE and 23Na TQF NMR studies. *Magn. Res. Med.*, 37(1):44–52, 1997.

[109] K.T.B. MacQuarrie and E.A. Sudicky. Multicomponent simulation of wastewater-derived nitrogen and carbon in shallow unconfined aquifers I. model formulation and performance. *J. Contam. Hydrol.*, 47:53–84, 2001.

[110] J. Malda, D.E. Martens, J. Tramper, C.A. van Blitterswijk, and J. Riesle. Cartilage tissue engineering: Controversy in the effect of oxygen. *Crit. Rev. Biotechnol.*, 23(3):175–194, 2003.

[111] J. Malda, J. Rouwkema, D.E. Martens, E.P. le Comte, F.K. Kooy, Tramper J., C.A. van Blitterswijk, and J. Riesle. Oxygen gradients in tissue-engineered PEGT/PBT cartilaginous constructs: Measurement and modeling. *Biotechnol. Bioeng.*, 86(1):9–18, 2004.

[112] E. Maneiro, M.A. Martin, M.C. de Andres, M.J. Lopez-Armada, J.L. Fernandez-Sueiro, P. del Hoyo, F. Galdo, J. Arenas, and F.J. Blanco. Mitochondrial respiratory activity is altered in osteoarthritic human articular chondrocytes. *Arthritis Rheum.*, 48(3):700–708, 2003.

[113] R.E. Marcus. The effect of low oxygen concentration on growth, glycolysis, and sulfate incorporation by articular chondrocytes in monolayer culture. *Arthritis Rheum.*, 16(5):646–656, 1973.

[114] R.E. Marcus and V.M. Srivastava. Effect of low oxygen tensions on glucose-metabolizing enzymes in cultured articular chondrocytes. *Proc. Soc. Exp. Biol. Med.*, 143(2):488–491, 1973.

[115] A. Maroudas. Physiochemical properties of cartilage in the light of ion exchange theory. *Biophys. J.*, 8:575–595, 1968.

[116] A. Maroudas. Biophysical chemistry of cartilaginous tissues with special reference to solute and fluid transport. *Biorheology*, 12:233–248, 1975.

[117] I. Martin, B. Obradovic, L.E. Freed, and G. Vunjak-Novakovic. Method for quantitative analysis of glycosaminoglycan distribution in cultured natural and engineered cartilage. *Ann. Biomed. Eng.*, 27:656–662, 1999.

[118] I. Martin, B. Obradovic, S. Treppo, A.J. Grodzinsky, R. Langer, L.E. Freed, and G. Vunjak-Novakovic. Modulation of the mechanical properties of tissue engineered cartilage. *Biorheology*, 37:141–147, 2000.

[119] K. Maseide and E.K. Rofstad. Mathematical modeling of chronical hypoxia in tumors considering potential doubling time and hypoxic cell lifetime. *Radiother. Oncol.*, 54:171–177, 2000.

[120] A. Masud and T.J.R. Hughes. A stabilized mixed finite element method for Darcy flow. *Comp. Meth. Appl. Mech. Eng.*, 191:4341–4370, 2002.

[121] R.L. Mauck, C.T. Hung, and G.A. Ateshian. Modeling of neutral solute transport in a dynamically loaded porous permeable gel: Implications for articular cartilage biosynthesis and tissue engineering. *J. Biomech. Eng.*, 125(5):602–614, 2003.

[122] R.L. Mauck, S.B. Nicoll, S.L. Seyhan, G.A. Athesian, and C.T. Hung. Synergetic action of growth factors and dynamic loading for articular cartilage tissue engineering. *Tissue Eng.*, 9(4):597–611, 2003.

[123] R.L. Mauck, S.L. Seyhan, G.A. Athesian, and C.T. Hung. Influence of seeding density and dynamic deformational loading on the developing structure/function relationships of chondrocyte-seeded agarose hydrogels. *Ann. Biomed. Eng.*, 30:1046–1056, 2002.

[124] R.L. Mauck, M.A. Soltz, C.C.B. Wang, D.D. Wong, P.H.G. Chao, W.B. Valhmu, C.T. Hung, and G.A. Athesian. Functional tissue engineering of articular cartilage through dynamic loading of chondrocyte-seeded agarose gels. *J. Biomech. Eng.*, 122:252–260, 2000.

[125] R.L. Mauck, C.C.B. Wang, E.S. Oswald, G.A. Athesian, and C.T. Hung. The role of cell seeding density and nutrient supply for articular cartilage tissue engineering with deformational loading. *Osteoarth. Cartilage*, 11:879–890, 2003.

[126] S. Mizuno, F. Allemann, and J. Glowacki. Effects of medium perfusion on matrix production by bovine chondrocytes in three-dimensional collagen sponges. *J. Biomed. Mater. Res.*, 56:368–375, 2001.

[127] J. Morshed and J.J. Kaluarachchi. Critical assessment of the operator-splitting technique in solving the advection-dispersion-reaction equation: 2. monod kinetics and coupled transport. *Adv. Water Resour.*, 18(2):101–110, 1995.

[128] V.C. Mow and A. Ratcliffe. Structure and function of articular cartilage and meniscus. In V.C. Mow and W.C. Hayes, editors, *Basic Orthopaedic Biomechanics*, pages 113–177. Raven Press, New York, 1997.

[129] D. Nehring, P. Adamietz, N.M. Meenen, and R. Pörtner. Perfusion cultures and modeling of oxygen uptake with three-dimensional chondrocyte pellets. *Biotechnol. Tech.*, 13:701–706, 1999.

[130] P.A. Netti, L.T. Baxter, Y. Boucher, R. Skalak, and R.K. Jain. Macro- and microscopic fluid transport in living tissues: Application to solid tumors. *Bioeng. Food Natural Products*, 43(3):818–834, 1997.

[131] E. Nimer, R. Schneiderman, and A. Maroudas. Diffusion and partition of solutes in cartilage under static load. *Biophys. Chem.*, 106:125–146, 2003.

[132] B. Obradovic, R.L. Carrier, G. Vunjak-Novakovic, and L.E. Freed. Gas exchange is essential for bioreactor cultivation of tissue engineered cartilage. *Biotechnol. Bioeng.*, 63:197–205, 1999.

[133] B. Obradovic, I. Martin, R.F. Padera, S. Treppo, L.E. Freed, and G. Vunjak-Novakovic. Integration of engineered cartilage. *J. Orthop. Res.*, 19:1089–1097, 2001.

[134] B. Obradovic, J.H. Meldon, L.E. Freed, and G. Vunjak-Novakovic. Glycosaminoglycan deposition in engineered cartilage: Experiments and mathematical model. *AIChE J.*, 46(9):1860–1871, 2000.

[135] B.P. O'Hara, J.P.G. Urban, and A. Maroudas. Influence of cyclic loading on the nutrition of articular cartilage. *Ann. Rheum. Dis.*, 49:536–539, 1990.

[136] P. Otte. Basic cell metabolism of articular cartilage. *Z. Rheumatol.*, 50:304–312, 1991.

[137] D. Pazzano, K.A. Mercier, J.M. Moran, S.S. Fong, D.D. DiBiasio, J.X. Rulfs, S.S. Kohles, and L.J. Bonassar. Comparison of chondrogenesis in static and perfused bioreactor culture. *Biotechnol. Prog.*, 16:893–896, 2000.

[138] M. Pei, G. Seidel, G. Vunjak-Novakovic, and L.E. Freed. Growth factors for sequential cellular de- and re-differentiation in tissue engineering. *Biochem. Biophys. Res. Commun.*, 294:149–154, 2002.

[139] A. Pluen, P.A. Netti, R.K. Jain, and D.A. Berk. Diffusion of macromolecules in agarose gels: Comparison of linear and globular configurations. *Biophys. J.*, 77:542–552, 1999.

[140] P.J. Prendergast, R. Huiskes, and K. Soballe. Biophysical stimuli on cells during tissue differentiation at implant interfaces. *J. Biomech.*, 30(6):539–548, 1997.

[141] T.M. Quinn, A.J. Grodzinsky, M.D. Buschmann, Y.J. Kim, and E.B. Hunziker. Mechanical compression alters proteoglycan deposition and matrix deformation around individual cells in cartilage explants. *J. Cell Sci.*, 111:573–583, 1998.

[142] T.M. Quinn, V. Morel, and J.J. Meister. Static compression of articular cartilage can reduce solute diffusivity and partitioning: Implications for the chondrocyte biological response. *J. Biomech.*, 34:1463–1469, 2001.

[143] T.M. Quinn, P. Schmid, E.B. Hunziker, and A.J. Grodzinsky. Proteoglycan deposition around chondrocytes in agarose culture: Construction of a physical and biological interface for mechanotransduction in cartilage. *Biorheology*, 39:27–37, 2002.

[144] T.M. Quinn, C. Studer, A.J. Grodzinsky, and J.J. Meister. Preservation and analysis of nonequilibrium solute concentration distributions within mechanically compressed cartilage explants. *J. Biochem. Biophys. Meth.*, 52:83–95, 2002.

[145] M.T. Raimondi, F. Boschetti, L. Falcone, G.B. Fiore, A. Remuzzi, E. Marinoni, M. Marazzi, and R. Pietrabissa. Mechanobiology of engineered cartilage cultured under a quantified fluid-dynamic environment. *Biomechan. Model Mechanobiol.*, 1:69–82, 2002.

[146] R. Rajpurohit, C.J. Koch, Z. Tao, C.M. Teixeira, and I.M. Shapiro. Adaptation of chondrocytes to low oxygen tension: Relationship between hypoxia and cellular metabolism. *J. Cell. Physiol.*, 168:424–432, 1996.

[147] S. Razaq, R.J. Wilkins, and J.P.G. Urban. The effect of extracellular pH on matrix turnover by cells of the bovine nucleus pulposus. *Eur. Spine J.*, 12:341–349, 2003.

[148] A.M. Rodriguez and C.A. Vacanti. Tissue engineering of cartilage. In C.W. Patrick, A.G. Mikos, and L.V. McIntire, editors, *Frontiers in tissue engineering*, pages 400–409. Pergamon, Amsterdam, 1998.

[149] N. Rotter, L.J. Bonassar, G. Tobias, M. Lebl, A.K. Roy, and C.A. Vacanti. Age dependence of biochemical and biomechanical properties of tissue-engineered human septal cartilage. *Biomaterials*, 23:3087–3094, 2002.

[150] R.L. Sah, S.B. Trippel, and A.J. Grodzinsky. Differential effects of serum, insulin-like growth factor-I, and fibroblast growth factor-2 on the maintenance of cartilage physical properties during long-term culture. *J. Orthop. Res.*, 14:44–52, 1996.

[151] R.L.Y. Sah, J.Y.H. Doong, A.J. Grodzinsky, A.H.K. Plaas, and J.D. Sandy. Effects of compression on the loss of newly synthesized proteoglycans and proteins from cartilage explants. *Arch. Biochem. Biophys.*, 286(1):20–29, 1991.

[152] R.L.Y. Sah, A.J. Grodzinsky, A.H.K. Plaas, and J.D. Sandy. Effects of tissue compression on the hyaluronate-binding properties of newly synthesized proteoglycans in cartilage explants. *Biochem. J.*, 167:803–808, 1990.

[153] S. Saini and T.M. Wick. Effect of low oxygen tension on tissue-engineered cartilage construct development in the concentric cylinder bioreactor. *Tissue Eng.*, 10:825–832, 2004.

[154] J.E. Salem, G.M. Saidel, W.C. Stanley, and M.E. Cabrera. Mechanistic model of myocardial energy metabolism under normal and ischemic conditions. *Ann. Biomed. Eng.*, 30(2):202–216, 2002.

[155] J.D. Sandy, J.R. O'Neill, and L.C. Ratzlaff. Acquisition of hyaluronate-binding affinity in vivo by newly synthesized cartilage proteoglycans. *Biochem. J.*, 258:875–880, 1989.

[156] J.D. Sandy and A.H.K. Plaas. Age-related changes in the kinetics of release of proteoglycans from normal rabbit cartilage explants. *J. Orthop. Res.*, 4:263–272, 1986.

[157] D. Schaefer, I. Martin, P. Shastri, R.F. Padera, R. Langer, L.E. Freed, and G. Vunjak-Novakovic. In vitro generation of osteochondral composites. *Biomaterials*, 21:2599–2606, 2000.

[158] D. Schäfer, W. Schäfer, and W. Kinzelbach. Simulation of reactive processes related to biodegradation in aquifers 1. structure of the three-dimensional reactive transport model. *J. Contam. Hydrol.*, 31:167–186, 1998.

[159] G. Segal. *SEPRAN User's Manual*. Ingenieursbureau SEPRA, Leidschendam, The Netherlands, 2003.

[160] B.G. Sengers, C.W.J. Oomens, and F.P.T. Baaijens. An integrated finite-element approach to mechanics, transport and biosynthesis in tissue engineering. *J. Biomech. Eng.*, 126(1):82–91, 2004.

[161] M. Sittinger, J. Bujia, W.W. Minuth, C. Hammer, and G.R. Burmester. Engineering of cartilage tissue using bioresorbable polymer carriers in perfusion culture. *Biomaterials*, 15(6):451–456, 1994.

[162] R.J.M. Smit, W.A.M. Brekelmans, and H.E.H. Meijer. Prediction of the mechanical behavior of non-linear heterogeneous systems by multi-level finite element modeling. *Comp. Meth. Appl. Mech. Eng.*, 155:181–192, 1998.

[163] D.K. Stangeby and C.R. Ethier. Computational analysis of coupled blood-wall arterial LDL transport. *J. Biomech. Eng.*, 124:1–8, 2002.

[164] R.A Stockwell. Metabolism of cartilage. In B.K. Hall, editor, *Cartilage, Volume 1: Structure, Function, and Biochemistry*, pages 253–280. Academic Press, Orlando, 1983.

[165] G. Strang. On the construction and comparison of difference schemes. *SIAM J. Numer. Anal.*, 5:506–517, 1968.

[166] P. Sucosky, D.F. Osorio, J.B. Brown, and G.P. Neitzel. Fluid mechanics of a spinner-flask bioreactor. *Biotechnol. Bioeng.*, 85(1):34–46, 2004.

[167] J.K. Suh. Dynamic unconfined compression of articular cartilage under a cyclic compressive load. *Biorheology*, 33(4, 5):289–304, 1996.

[168] J.K. Suh, Z. Li, and S.L.Y. Woo. Dynamic behavior of a biphasic cartilage model under cyclic compressive loading. *J. Biomech.*, 28(4):357–364, 1995.

[169] D.N. Sun, W.Y. Gu, X.E. Guo, W.M. Lai, and V.C. Mow. A mixed finite element formulation of triphasic mechano-electrochemical theory for charged, hydrated biological soft tissues. *Int. J. Numer. Meth. Eng.*, 45:1375–1402, 1999.

[170] J. Tervo, M. Vauhkonen, P.J. Vauhkonen, and J.P. Kaipio. A three-dimensional finite element model for the control of certain non-linear bioreactors. *Math. Meth. Appl. Sci.*, 23:357–377, 2000.

[171] B. Teusink, J. Passarge, C.A. Reijenga, E. Esgalhado, C.C. van der Weijden, M. Schepper, M.C. Walsh, B.M. Bakker, K. van Dam, H.V. Westerhoff, and J.L. Snoep. Can yeast glycolysis be understood in terms of in vitro kinetics of the constituent enzymes? *Eur. J. Biochem.*, 267(17):5313–5329, 2000.

[172] J.M. Thomas. Sur l'analyse numérique des méthodes d'eléments finis hybrides et mixtes. *Ph.D. thesis, Université Pierre et Marie Curie, Paris*, 1977.

[173] M. Tomita, E.F. Sato, M. Nishikawa, Y. Yamano, and M. Inoue. Nitric oxide regulates mitochondrial respiration and functions of articular chondrocytes. *Arthritis Rheum.*, 44(1):96–104, 2001.

[174] P.A. Torzilli, E. Askari, and J.T. Jenkins. Water content and solute diffusion properties in articular cartilage. In V.C. Mow, A. Ratcliffe, and S.L-Y. Woo, editors, *Biomechanics of Diarthrodial Joints*, pages 363–390. Springer, New York, 1990.

[175] S. Treppo, H. Koepp, E.C. Quan, A.A. Cole, K.E. Kuettner, and A.J. Grodzinsky. Comparison of biomechanical and biochemical properties of cartilage from human knee and ankle pairs. *J. Orthop. Res.*, 18:739–748, 2000.

[176] E. Tziampazis and A. Sambanis. Modeling of cell culture processes. *Cytotechnology*, 14:191–204, 1994.

[177] J.P.G. Urban. The chondrocyte: A cell under pressure. *Br. J. Rheumatol.*, 33:901–908, 1994.

[178] J.P.G. Urban. Present perspectives on cartilage and chondrocyte mechanobiology. *Biorheology*, 37:185–190, 2000.

[179] C.T. Vangsness, P.R. Kurzweil, and J.R. Lieberman. Restoring articular cartilage in the knee. *Am. J. Orthop.*, 33(2 Suppl.):29–34, 2004.

[180] P. Vanky, U. Brockstedt, A. Hjerpe, and B. Wikstrom. Kinetic studies on epiphyseal growth cartilage in the normal mouse. *Bone*, 4:331–339, 1998.

[181] G. Vunjak-Novakovic, I. Martin, B. Obradovic, S. Treppo, A.J. Grodzinsky, R. Langer, and L.E. Freed. Bioreactor cultivation conditions modulate the composition and mechanical properties of tissue-engineered cartilage. *J. Orthop. Res.*, 17:130–138, 1999.

[182] G. Vunjak-Novakovic, B. Obradovic, I. Martin, P.M. Bursac, and L.E. Langer, R.and Freed. Dynamic cell seeding of polymer scaffolds for cartilage tissue engineering. *Biotechnol. Prog.*, 14:193–202, 1998.

[183] H. Wang, D. Liang, R.E. Ewing, S.L. Lyons, and G. Qin. An approximation to miscible fluid flows in porous media with point sources and sinks by an eulerian-lagrangian localized adjoint method and mixed finite element methods. *SIAM J. Sci. Comp.*, 22(2):561–581, 2000.

[184] L. Wang, S.C. Cowin, S. Weinbaum, and S.P. Fritton. In response to "mixing mechanisms and net solute transport in bone" by M.L. Knothe Tate. *Ann. Biomed. Eng.*, 29:812–816, 2001.

[185] K.A. Williams, S. Saini, and T.M. Wick. Computational fluid dynamics modeling of steady-state momentum and mass transport in a bioreactor for cartilage tissue engineering. *Biotechnol. Prog.*, 18:951–963, 2002.

[186] A.K. Williamson, A.C. Chen, and R.L. Sah. Compressive properties and function-composition relationships of developing bovine articular cartilage. *J. Orthop. Res.*, 19:1113–1121, 2001.

[187] C.G. Wilson, L.J. Bonassar, and S.S. Kohles. Modeling the dynamic composition of engineered cartilage. *Arch. Biochem. Biophys.*, 408:246–254, 2002.

[188] R.A.J. Windhaber, R.J. Wilkins, and D. Meredith. Functional characterisation of glucose transport in bovine articular chondrocytes. *Pflugers Arch.*, 446:572–577, 2003.

[189] M. Wong, M. Ponticiello, V. Kovanen, and J.S. Jurvelin. Volumetric changes of articular cartilage during stress relaxation in unconfined compression. *J. Biomech.*, 33:1049–1054, 2000.

[190] J.Z. Wu, W. Herzog, and M. Epstein. Modelling of location- and time-dependent deformation of choncrocytes during cartilage loading. *J. Biomech.*, 32:563–572, 1999.

[191] Y. Xu, J. Sun, G. Mathew, A.S. Jeevarajan, and M.M. Anderson. Continuous glucose monitoring and control in a rotating wall perfused bioreactor. *Biotechnol. Bioeng.*, 87(4):473–477, 2004.

[192] H. Yao and W.Y. Gu. Physical signals and solute transport in cartilage under dynamic unconfined compression: Finite element analysis. *Ann. Biomed. Eng.*, 32(3):380–390, 2004.

[193] A. Zetterberg, O. Larsson, and K.G. Wiman. What is the restriction point? *Curr. Opin. Cell Biol.*, 7:835–842, 1995.

Dankwoord

Allereerst wil ik mijn copromotor Cees Oomens bedanken voor zijn onvoorwaardelijk positieve ondersteuning en het waar nodig geven van de juiste aanzetten. Daarnaast bedank ik mijn promotor Frank Baaijens, voor het vertrouwen in en ruimte bieden aan de eigen invulling van mijn onderzoek. I would like to thank Dan Bader especially for his accurate reading and his attention for the presentation of the results. I promise that, to the best of my abilities, from now on my writing will be in proper British English. In particular I would like to thank Hannah Heywood for the indispensable experimental contribution, providing her results at an early stage and the open discussion. David Lee has contributed valuable ideas, which have encouraged me to try my hand at what is best described as some exploratory modelling. Rene van Donkelaar heeft geholpen mijn werk in een bredere context te plaatsen en vanuit verschillende invalshoeken bruikbare suggesties aangedragen. Furthermore, I would like to thank the rest of the Imbiotor group. In between the bureaucratic obligations, there appeared to be enough time for many substantive exchanges of ideas, often in the most charming locations, which have formed the basis of my research. Tevens bedank ik Rik Kaasschieter voor het bieden van een bruikbare ingang in de meer onalledaagse mengselformuleringen. De studenten waarmee ik heb samengewerkt, Martijn Cox, Rolf Pullens en Duy Nguyen, dank ik voor hun werk dat direct en indirect veel heeft bijgedragen aan mijn onderzoek. Vanzelfsprekend bedank ik alle vrienden en collega's voor de prettige sfeer op het werk en de nodige afleiding daarbuiten. In het bijzonder geldt dit voor mijn kamergenoten, Maria, Anke, Ralf en Raoul, die bijna zeker een netto positieve invloed op de totstandkoming van dit proefschrift hebben uitgeoefend. Tenslotte, bedank ik ook mijn vader en moeder, mede omdat ze hier natuurlijk niet willen en kunnen ontbreken.

Bram Sengers,
Eindhoven, februari 2005

Curriculum vitae

Bram Sengers werd geboren op 3 september 1977 te Eindhoven. In 1995 behaalde hij het VWO diploma aan het Van Maerlant Lyceum in Eindhoven. Vervolgens studeerde hij Werktuigbouwkunde aan de Technische Universiteit Eindhoven, in de richting Werktuigkundige Medische Technologie. Als onderdeel van deze studie heeft hij in 1999 stage gelopen aan de Université Paris XII in Parijs, met als doel het ontwerp van een opstelling om cellen aan een gecontroleerde rek te onderwerpen. In 2000 is hij afgestudeerd binnen het decubitus onderzoek, met als onderwerp het ontwikkelen van een multilevel eindige elementen methode om schadecriteria voor individuele spiercellen te bepalen. In 2001 is hij begonnen aan een promotieonderzoek aan de Faculteit Biomedische Technologie van de Technische Universiteit Eindhoven, resulterend in dit proefschrift.